



Leibniz-Rechenzentrum
der Bayerischen Akademie der Wissenschaften



Technical Report

Overview of Research Projects on HLRB I

Matthias Brehm (ed.)

Dezember 2006

LRZ-Bericht 2006-05

Direktorium:

Prof. Dr. H.-G. Hegering (Vorsitzender)
Prof. Dr. A. Bode
Prof. Dr. Chr. Zenger

Leibniz-Rechenzentrum
Boltzmannstraße 1
85748 Garching

UST-ID-Nr. DE811305931

Telefon: (089) 35831-8784
Telefax: (089) 35831-9700
E-Mail: lrzpost@lrz.de
Internet: <http://www.lrz.de>

Content

Lattice Boltzmann DNS and LES of chanel turbulence with flow modifiers	1
Advanced Simulation Techniques for Turbulent Flows Using HPC	5
Large eddy simulatons of complex flows.....	9
Direct Numerical Simulation (DNS) and Large Eddy Simulation (LES) of turbulent reacting shear layers	13
Direct Numerical Simulations of Flow in Turbomachinery.....	15
Implementation and validation of LES models for partially premixed turbulent flames	19
Simulation of Jet Engine Exhaust Noise	23
Simulation of Quantum Chromodynamics on the Space-Time Lattice.....	25
Can the ⁴ He experiments serve as a database for determining the three-nucleon force?	29
The structure of the local Universe	31
3-D seismic wave propagation	35
A theoretical and experimental study of the anharmonic lattice dynamics of fluorite systems	39
Quantum chromodynamics with chiral quarks.....	43
Metal-Insulator Transitions and Realistic Modelling of Correlated Electron Systems.....	47
Predicting the structure and properties of mineral surfaces and interfaces	51
'Overlap' quarks in a 'twisted mass' sea: optimize computer power to understand the fundamental forces	55
Parallel Free-Surface and Multi-Phase Simulations in Complex Geometries using Lattice Boltzmann Method.....	57
Adsorption of DNA base molecules on solid surfaces studied from massive parallel first-principles calculations 61	
FDEM Project	65
Scalable Mesh-based Simulation on Clusters of Symmetric Multiprocessors (Project MethWerk).....	69
Simulation for the Neural Map Formation in the Primary Visual Cortex	73
Parallelization of Maximum Likelihood based Methods for the Reconstructon of a Tree of Life from Molecular Gene Sequence Alignments (Project ParBaum).....	77
Electronic Properties of DNA	81
Multi-Dimensional Quantum Dynamics of Chemical Reaction Processes	85
Reactivity of RuO ₂ : Oxidation of carbon monoxide	89
Density Functional Investigations of Complex Chemical Systems.....	93
Theoretical Studies of Structures of Vanadate Complexes in Aqueous Solution	97

Lattice Boltzmann DNS and LES of channel turbulence with flow modifiers

Research Institution:

Lehrstuhl für Strömungsmechanik,
Friedrich-Alexander Universität Erlangen-Nürnberg

Research Area:

Computational Fluid Dynamics, Turbulence Simulation and Modeling

Principal Investigator:

Dr. Kamen Beronov

Researchers:

Kamen Beronov, Nagihan Özyilmaz, Anuhar Osorio Nesme

Abstract

Several industrial applications investigated at the Institute of Fluid Mechanics (LSTM) in Erlangen have required turbulence modeling for LES or RANS simulations that cannot be calibrated with canonical flows such as developed channel or duct turbulence, nozzle flows, grid-generated turbulence, etc. but can be related on a basic modeling level to flows defined as combinations of such canonical ones: grid turbulence or converging (wedge) flow inside a plane channel. Of special interest are the stability of flow structures and the mixing properties near the flow modifier (grid, nozzle, diffuser) where turbulent shear and inhomogeneity are strongest and standard SGS or RANS models are not safe. The influence of Reynolds number and geometric parameters like blockage ratio (grid) or contraction ratio (wedge) have been investigated, also at LSTM-Erlangen. Empirical rules for the parametric dependence and spatial distribution of turbulence statistics have resulted. These need to be validated and improved. The required detailed information has been mostly lacking so far. With a lattice Boltzmann solver developed

at LSTM and optimized for large-scale simulations on the HLRB-1, a number of detailed large-size simulations were carried out. The results confirm that known empirics can be used also for "combined" flows and at lower Reynolds numbers. They also provide detailed insights into the flow structure near "turbulence generators". These qualitatively new pieces of knowledge may lead to a breakthrough in the control and optimization of a variety of existing and new designs of hydraulic and microfluidic devices such as high-throughput micromixers or injection nozzles.

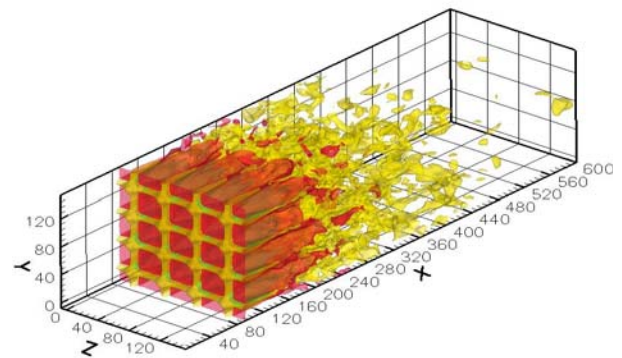


Fig. 1: streamwise velocity (instantaneous iso-surfaces) in a plane channel obstructed by a square grid

Technical background and motivation

A major part of fluid mechanics research in the last twenty years has focused on small scale devices and phenomena and the new science of microfluidics has emerged, while turbulence research has remained driven by large-scale technical applications in chemical, processing, automotive and aerospace industry, as well as by the very large-scale dynamical processes in climate and weather modeling. But a number of independent new technologies have emerged very recently, which are based on inertia-dominated flows with bulk flow Reynolds numbers (the ratio of inertial to viscous effects) of $100 < Re < 3000$ through conduits and flow-perturbing solid structures with characteristic length scales L in the 10^{-5} — 10^{-3} meter range. The present group has been working, for example, over the last three years on modeling injection nozzles ($Re : 2000$ — 5000 , $L : 10^{-5}$ — 10^{-4} m), micromixers and valves pumps ($Re : 200$ — 800 , $L : 10^{-4}$ — 10^{-3} m), stirrers with rotating fine mesh ($Re < 5000$, $L : 10^{-3}$ — 10^{-2} m). In all cases, the flow

was at least chaotic, mostly turbulent although below the accepted Reynolds number thresholds for the onset of turbulence in the respective kind of vessel or conduit. In all of these subcritical flows, turbulence is being directly induced by flow obstructions though spatially localized flow acceleration and generation of cross-flow vorticity. The considered obstructions can be classified in two kinds : (i) nozzles and expansions, and (ii) rectangular grids like those used in classical wind tunnel [1] and water channel experiments on grid-generated “nearly homogeneous” turbulence.

Although the literature both on grid-generated and on pipe and channel turbulence offers ample experimental and numerical simulation data, the engineering heuristics based on these data are not yet unambiguous concerning the model parametrization and are mostly based on flows at high Reynolds numbers. A direct use of such heuristics in the applications of interest, described above, is unreliable for several reasons : (i) The Re -range of interest is generally below that, for which the rules have been proposed. Turbulence is generated not through flow instabilities alone but mainly through vorticity injection by the designed flow obstructions. (ii) The most important part of the dynamics (dissipation, mixing, etc.) occurs near the flow obstruction, while the heuristics work for the bulk flow and not at the site of turbulence generation. (iii) There is as good as no literature on proper ways to “mix” predictions for individual “simple” flows into an estimate for a flow that has the features of several “simple” ones, for example a channel with a grid or a nozzle-like element inserted in it.

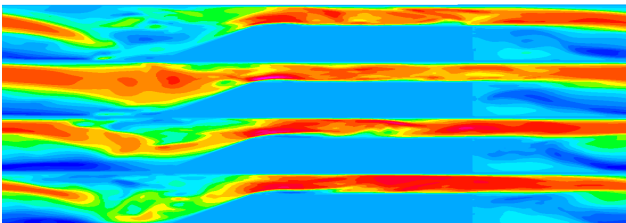


Fig. 2: streamwise velocity (snapshot in a cross-section normal to the spanwise direction) in a channel with nozzle-step obstruction — resolved LES at $Re < 2000$.

Lattice Boltzmann simulations of low- Re turbulence

Over the last ten years, lattice Boltzmann methods (LBM) have emerged as a very promising approach for detailed numerical simulation of complex flows, as they offer several beneficial features: optimal efficiency on parallel and vector computing platforms, robust treatment of very complicated boundaries, simple to implement and use, good physical foundations, assuring correct pressure computation in flow domains with multiplex branchings as well as correct and simple incorporation of meso- and macroscopic physical effects. The present group demonstrated these advantages for a number of new geometry types, including ones of interest here [2]. LBM have just come to use for simulating grid-generated turbulence, allowing for the first time, to resolve the flow at the grid as well [3].

Channel with inserted grids

The first of two types of model geometries studied under the present project is a square grid placed perpendicularly across a straight channel between two parallel walls. When a constant body force (e.g. pressure gradient) of sufficiently high amplitude is applied in the direction perpendicular to the grid, the flow through the grid is turbulent (Fig. 1). Far downstream of the grid, classical developed plane channel turbulence sets in. Taking the computational domain long enough allows to observe several transitions in flow type, starting at the grid, passing over a peak in the intensity of turbulent fluctuations near (about one mesh stride length M) downstream of the grid, then through a range of self-similar (algebraic) decay of this intensity, then through a region of growing length scale of the turbulence structures, including a “thickening” of the turbulent boundary layers in which fluctuations and dissipation are much more intensive, and reaching a developed channel flow state where the two layers associated with opposite walls merge. LBM efficacy allows to take dozens of channel heights as domain length, observe all transitions, and to apply the assumption of spatial periodicity of the flow in the direction of forcing — a customary approach for DNS and LES in plane channels.

Direct numerical simulations (DNS) carried out in this geometry under the present project, support the best hopes that heuristics for different flow kinds (grid-generated, boundary-layer and developed duct turbulence) can be combined essentially without modifications. On one hand, the development length along the streamwise

(i.e. the forcing) direction, measured between the main turbulence origin (inserted grid) and the downstream position at which standard developed channel turbulence flow type sets in. On the other hand, in the first two flow ranges mentioned earlier, at much closer downstream range from the grid, the turbulence statistics are very close to those obtained in DNS of grid-generated turbulence in the absence of walls.

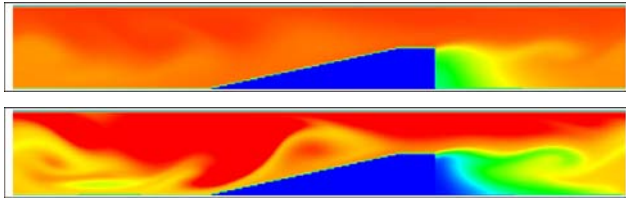


Fig. 3 : passive scalar concentration (snapshot in a cross-section) distribution in a similar channel and for similar Re — two different Schmidt numbers, same flow and time.

Channels with inserted nozzles / diffusors

Similar conclusions were obtained in DNS and LES of flows in both straight and deflecting channels with one or more (periodic sequence of) converging (nozzle-like) sections (Fig. 2): Trends known for a single nozzle (pressure drop to Reynolds number relation) and for accelerated boundary layer flow (laminarization for very strong accelerations, in this case corresponding to contraction ratio and mean flow shear rate, and generally reflected by a parameter K) were confirmed. But quantitatively, there emerged new important aspects, specifically related to factors like the presense of channel walls: The onset of turbulence is much enhanced, as measured both by a low critical Re (500-600 as opposed to 2100-2300 for plane channel flows) and by an order of magnitude lower critical K (free boundary layers laminarize at $K > 4 \cdot 10^{-6}$ and remain turbulent for $K < 2 \cdot 10^{-6}$). It can be expected, but has not been previously described by numerical simulations, that the flow convergence enhances streamwise vortices to an extent that they become self-sustained and significantly increase mixing, which is (at $Re > 100$) already strongly intensified by spanwise vorticity (Fig. 3). At the low Re considered (< 1000), the streamwise vortices fill a noticeable part of the channel cross-section and split the mean flow into fast-flow “jets” and low-speed “streaks” in the spanwise direction (complementary to the one along the mean flow and the one

perpendicular to the walls). The present DNS and large-eddy simulation (LES) show that (i) such structures emerge spontaneously from arbitrary small upstream disturbances and (ii) they remain in the flow and dominate it in its “narrow channel” part.

References

- [1] Comte-Bellot, C., and Corrsin, S. 1966 : The use of a contraction to improve the isotropy of grid-generated turbulence. *J. Fluid Mech.* 25, 657-682.
- [2] Beronov, K. N., and Durst, F. 2004 : Efficiency of lattice Boltzmann codes as moderate Reynolds number turbulence solvers. In *High Performance Computing in Science and Engineering*, Munich 2004, Springer, Berlin.
- [3] Djenidi, L. 1 2006 : Lattice-Boltzmann simulation of grid-generated turbulence. *J. Fluid Mech.* 25, 13-35.

Advanced Simulation Techniques for Turbulent Flows Using HPC

Research Institution:

Institute of Fluid Mechanics, University of Erlangen-Nürnberg

Research Area:

Computational Fluid Dynamics, Turbulence Simulation, Large Eddy Simulation, Multifield Problems (FSI, CAA)

Principal Investigator:

PD Dr.-Ing. Michael Breuer

Researchers:

PD Dr.-Ing. Michael Breuer

Dipl.-Ing. Nikola Jovicic

Abstract

The objective of this project was to evaluate the applicability of modern simulation techniques such as large eddy simulation (LES) for practically relevant high-Re turbulent flows and to investigate the influence of subgrid scale modeling and grid resolution on the quality of the predicted results.

Turbulence Simulation – A Real Challenge

Turbulence is one of the most fascinating phenomena found in fluid mechanics. Its impact on processes in nature and on technical applications is gigantic leading to strong economic consequences. Despite of three main ingredients available to tackle the problem, turbulence still belongs to the class of unsolved challenges in classical physics. These are:

the governing equations which were already derived about 150 years ago by the French engineer Navier (1785-1836) and the Irish mathematician Stokes (1819-1903),

the advanced numerical methods which were developed during the last decades to solve this

system of partial differential equations and last but not least

the existence of extremely fast supercomputers such as the SGI Altix 4700 with a peak-performance of about $2.6 \cdot 10^{13}$ floating-point-operations per second recently installed at LRZ Munich (HLRB II).

Even under these circumstances it is still out of reach to simulate turbulent flows occurring in most technical applications. An example should demonstrate that. Based on the supercomputers available up to now, turbulent flows with Reynolds number of the order $Re = O(10^4)$ can be tackled by the so-called direct numerical simulation (DNS) which means that the Navier-Stokes equations are solved numerically without any closure assumptions. Using the new HLRB II supercomputer, a first step towards $Re = O(10^5)$ might be possible, at least for flows in geometrically simple configurations. However, for engineering applications of practical relevance such as the flow around an airliner at cruise flight conditions, the characteristic Reynolds number is of the order $O(10^8)$. Unfortunately, the computational effort for DNS increases not linearly with Re but with a power of about 3. Hence to predict such a turbulent flow based on DNS, the enormous performance of present supercomputers has to grow at least 10 orders of magnitude. Consequently, the potentiality of DNS is often characterized as the 'flow over a stamp'. Nevertheless, DNS is an invaluable discovery for basic turbulence research, i.e. to achieve a deeper insight into the physics of turbulent flows and to derive and calibrate statistical turbulence models.

Very often engineers are not interested in all details of a turbulent flow delivered by DNS. Contrarily the effect of turbulence on the technically more relevant mean flow field or some integral parameters are desired. This leads to the statistical interpretation of turbulent flows. Subdividing all instantaneous flow quantities into a mean value and a fluctuating component, the Reynolds-Averaged Navier-Stokes (RANS) equations can be derived. Unfortunately, this system of equations is no longer closed. A variety of statistical turbulence models has been developed ranging from simple algebraic eddy viscosity models up to full Reynolds stress models. Despite decades of development regarding suitable RANS models, no breakthrough was achieved for a generally applicable and reliable model.

An alternative to RANS and DNS is the large-eddy simulation (LES) often described as the 'golden mean' between both concepts. The basic principle is straightforward. The large energy-carrying eddies in a turbulent flow are directly resolved by the numerical method, whereas the small eddies cannot be captured numerically and thus need to be modeled. The advantage of LES compared with RANS is obvious. In contrast to RANS only the small-scale turbulence has to be modeled for LES. These subgrid scales are assumed to be more isotropic and homogeneous and are therefore much easier to tackle. The large-scale structures, which are evidently dependent on the geometry and boundary conditions of the flow configuration under consideration are described most accurately by the solution of the governing (filtered) Navier-Stokes equations. Consequently, LES in principle overcomes the strong restriction observed for DNS. On the other hand it is a more reasonable simulation concept than RANS, especially if complex flow phenomena such as large-scale separation and reattachment, transition or vortex shedding are observed.

During the last years an increasing interest in LES can be observed. Partly this is attributed to disappointing results of RANS predictions. On the other hand the steadily increasing computer performance nowadays available strongly triggered the development of LES. Bluff-body flows are typical examples where RANS modeling generally fails and LES is definitely the better choice.

Examples should demonstrate this. The first is the sub-critical flow past a circular cylinder. Although the geometry is simple, the cylinder flow can be considered as the paradigm of complex flows, because it involves remarkably complex flow features such as thin separating shear layers, transition and large-scale vortex motion in the wake. Fig. 1 shows a snapshot of the turbulent von Karman vortex street past the cylinder at $Re=3900$ visualized by streaklines. Weightless particles released on a vertical line in front of the cylinder were integrated during the flow computation. Of course, the particles do not remain in the one plane. After transition has taken place in the free shear layers of the cylinder, they are spread out in the entire integration domain forming a complex 3-D flow structure in the wake. The predicted results were compared with experimental measurements. Regarding all flow structures investigated and all integral parameters predicted good agreement was found.

Much more challenging are the high-Re cases of $Re = 1.4 \cdot 10^5$ and 10^6 also investigated. In the first case the flow is again sub-critical, i.e. the boundary layers at the cylinder are still laminar at the separation point and transition takes place in the free shear layers followed by vortex shedding in the wake. Contrarily, at $Re = 10^6$ the super-critical stage is reached, where transition to turbulence already takes place in the attached boundary layer leading to the well-known drag crisis. Both flow regimes are reasonably predicted by LES including the drag crisis and all relevant flow features.

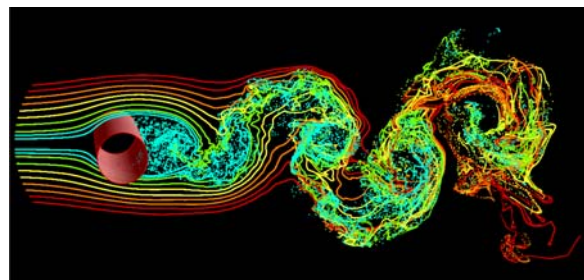


Fig. 1: Von Karman vortex street past a circular cylinder

A second example is the flow past airfoils at high angles of attack. This is again a typical case where RANS models fail to deliver reasonable results. Fig. 2 shows the instantaneous flow field around the wing ($Re = 20,000$ and $\alpha=18^\circ$) by iso-surfaces of the pressure at an arbitrarily chosen time instant. As expected, the flow at the lower side of the wing is attached and laminar. At the upper side the boundary layer separates shortly after the leading edge induced by a strong adverse pressure gradient in this region (leading-edge stall). It forms a large clockwise rotating recirculation region on the leeward side with a nearly constant pressure. Behind the trailing edge, a strong counterclockwise rotating vortex structure is visible. The development and shedding behavior of this trailing-edge vortex controls the entire flow field. It develops almost periodically in the vicinity of the trailing edge. During its initial phase, the vortex is attached to the trailing edge while vorticity is accumulated in it being fed by the corresponding shear layer. The vortex size is continuously increasing. After it has reached a certain diameter, the vortex is shed and convected downstream, while diffusion of vorticity takes place. Then a new shedding cycle begins.

The life cycle of the strong vortical structure also determines the structure and the size of the large recirculation region on the leeward side which originates from the separation at the leading edge. The separated flow forms a free shear layer, where a Kelvin-Helmholtz instability is observed and transition to turbulence takes place. No regular shedding motion of vortices generated at the leading edge is visible yielding a highly asymmetric wake as mentioned above. At a higher Re number ($Re=10^5$), a totally different flow structure was found. The flow separates shortly behind the nose but reattaches afterwards forming a closed laminar separation bubble which is extremely thin. In a zoomed animated sequence of the nose region one can observe that the size and the location of the bubble is slightly varying in time. Downstream of the bubble a turbulent boundary layer is visible at the leeward side of the airfoil. Owing to transition to turbulence, the boundary layer remains attached up to about 70% of the chord length. In the vicinity of the trailing edge a closed recirculation region is observed which is much smaller than for the low-Re case. Furthermore, no dominating trailing-edge vortex is present at $Re=10^5$. In conclusion, the high-Re case shows a typical trailing-edge stall with a laminar separation bubble, transition, and reattachment of the turbulent flow and hence completely deviates from the low-Re counterpart. These examples clearly demonstrate the power of LES placing all important flow characteristics in an unsteady 3-D and detailed manner at the disposal of the user.

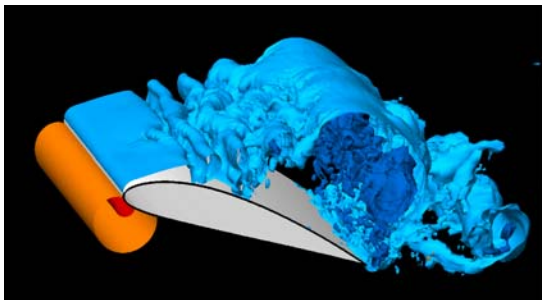


Fig. 2: Flow past an unswept wing at a high angle of attack at $Re = 20,000$ and $\alpha=18^\circ$; iso-surface of the pressure.

These applications can only give some hints on what is possible by advanced turbulence simulation strategies now and in the foreseeable future. The potential is even larger. Nowadays a tendency towards multi-physics approaches is ob-

served where the flow prediction by LES is only a part of the entire simulation. Three examples currently under investigation at LSTM Erlangen are multiphase flows, fluid-structure interaction and computational aeroacoustics. In conclusion, a fascinating area of research will remain exciting for years to come.

References

- [1] Breuer, M.: Direkte Numerische Simulation und Large-Eddy Simulation turbulenter Strömungen auf Hochleistungs-rechnern, Habilitationsschrift, Universität Erlangen-Nürnberg, Berichte aus der Strömungstechnik, ISBN: 3-8265-9958-6, Shaker Verlag, Aachen, (2002).
- [2] Breuer, M.: A Challenging Test Case for Large Eddy Simulation: High Reynolds Number Circular Cylinder Flow, Int. J. Heat & Fluid Flow, vol. 21 (5), pp. 648-654, (2000).
- [3] Breuer, M., Jovicic, N., Mazaev, K.: Comparison of DES, RANS, and LES for the Separated Flow Around a Flat Plate at High Incidence, Int. J. for Numerical Methods in Fluids, vol. 41, pp. 357-388, (2003).
- [4] Jovicic, N., Breuer, M., Jovanovic, J.: Anisotropy-Invariant Mapping of Turbulence in a Flow Past an Unswept Airfoil at High Angle of Attack, J. Fluids Engineering, vol. 128(3), pp. 559-567, (2006).

Links

<http://www.lstm.uni-erlangen.de/~breuer/>

<http://www.lstm.uni-erlangen.de/~njovicic/>

Large eddy simulations of complex flows

Research Institution:

Fachgebiet Strömungsmechanik
TU München

Research Area:

Computational Fluid Dynamics

Principal Investigator:

Univ.-Prof. Dr-Ing. R. Friedrich

Researchers:

Dipl.-Ing S. Eisenbach
M.E. Somnath Ghosh

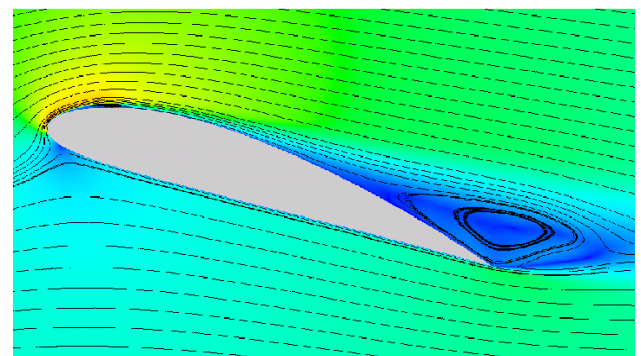
Large eddy simulations of flow around a wing of infinite span at $Re=100000$ and high angle of attack

Flow configurations with large scale separation of the flow are still challenging for large eddy simulations. Nevertheless, LES promises to provide a deeper insight into such flow phenomena than statistical approaches of solving the governing equations while remaining computationally affordable at high Reynolds numbers. With this objective in mind, we simulate the flow around a wing of infinite span at high angle of attack. The wing has a NACA 4415 profile and is positioned between an upper and lower flat plate in order to keep the computational domain as small as possible. The same configuration has been investigated experimentally at DLR Goettingen and hence the data are available for comparison with the simulation results. The computations are done in cartesian coordinates using an immersed boundary technique built into the MGLET code. The present LES results are second-order accurate. The Lagrangian formulation of the dynamic Smagorinsky model [1] is used for the subgrid scale terms. The computation typically uses 51.84 million grid points which leads to 5.9 gb of physical memory. The overall performance on the SR8000-F1 is about 220 Mflops per node.

The important flow features are shown in Fig. 1 where mean streamlines and the magnitude of the mean velocity have been plotted. It can be seen that at the present Reynolds number the flow is characterized by a small laminar separation bubble near the leading edge of the airfoil and a larger turbulent zone at the trailing edge. The laminar separation extends from $x=0.04c$ to $x=0.18c$, c being the chord length. Its maximum height is $0.007c$. The transition of the laminar boundary layer to turbulence appears in the shear layer above the separation bubble. The turbulent transport of momentum into the boundary layer finally leads to its reattachment in spite of the adverse pressure gradient on the suction side. In Fig 2 it can be

seen that the maximum production of turbulent kinetic energy occurs just after the laminar separation bubble.

Fig. 1: Streamlines and absolute value of mean



velocity

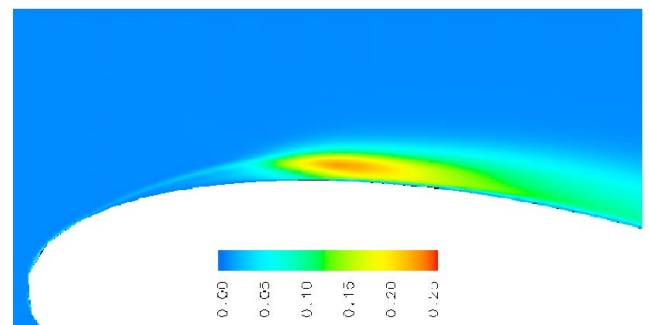


Fig. 2: Turbulent kinetic energy distribution on the suction side of the profile

Large eddy simulations of supersonic turbulent flow in axisymmetric nozzles

Compressible wall-bounded flows have been studied using DNS and LES in recent years with the aim to understand the effects of compressibility on the turbulent structure, or more clearly, on the anisotropy of the Reynolds stress tensor. It has been shown by previous studies of super-

sonic channel flow that the major compressibility effect in such flows manifests itself as an increase in Reynolds stress anisotropy with increasing Mach number. The reason for this is the decrease in the pressure-strain correlation terms in the transport equations of the Reynolds stress tensor which act as redistributing terms transferring energy from the streamwise to the spanwise and wall-normal components. The aim of this study is to investigate these effects in presence of favourable pressure gradients and dilatation. With this aim we undertake LES of fully developed, supersonic pipe flow subjected to expansion in a nozzle. The shape of the nozzle is chosen so as to have a region of nearly uniform pressure gradient and to avoid strong streamline curvatures. Streamtube equations have been used to get an area distribution for a given pressure distribution.

The LES technique used is an adaptation of the approximate deconvolution method [2] which involves single step explicit filtering of the flow variables. This technique has been shown to provide excellent predictions of the terms involving the large scales in the Reynolds stress transport equations when compared to DNS results. This has been validated by Ghosh et al. [3] who carried out DNS and LES of supersonic turbulent pipe flows using the same numerical schemes and the same LES technique as used here.

The inflow condition for the nozzle is obtained by carrying out a separate LES of a pipe flow at Mach number, $M=1.5$ and specifying inflow conditions for the nozzle simulation at each timestep using characteristic boundary conditions [4]. The nozzle wall is kept at a constant temperature. Here we present the first results from this computation. Fig 3 shows the good agreement of the centerline Mach number and centerline pressure with values calculated analytically using streamtube equations. This shows that the expanding flow remains essentially isentropic away from the walls.

The major effect of the expansion in the nozzle is the decrease of turbulence intensities along the nozzle. This is clearly shown in Fig 4 where the streamwise Reynolds stresses are plotted

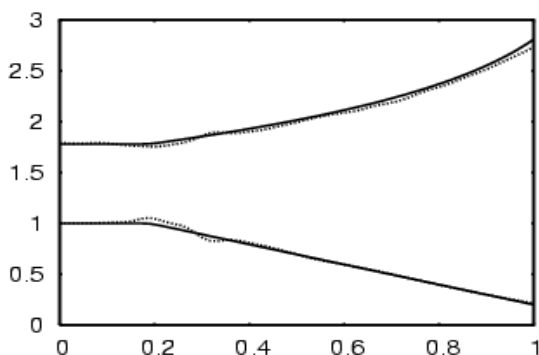
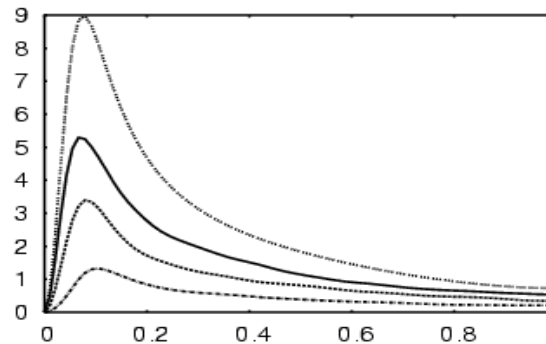
against the radius at different axial locations.

These effects need proper explanation and hence detailed DNS studies are planned in the future to validate our LES results.

x/L

Fig. 3: Centerline Mach number (upper curves) and centerline pressure (lower curves) normalized with the values at the inlet $x/L=0$ along the nozzle. Solid lines represent results from streamtube equations, dashed lines from the computations $1-r/R$

Fig. 4: Streamwise Reynolds stress normalized with the local wall shear stress at different axial locations. x/L increases from top to bottom of the figure.



Publications

- [1] Evans,G. 2003 Großstruktursimulation der abgelösten Strömung um ein angestelltes Tragflügelprofil. Dissertation TU-München
- [2] Evans, S., Eisenbach, S. and Friedrich, R. 2004 Large eddy simulation of an airfoil at $Re=20000$ using cartesian grids. High performance computing in science and engineering pp. 133-143
- [3] Eisenbach, S. and Friedrich, R. 2005 LES of Flow around an airfoil at $Re=100000$ and high angle of attack using cartesian grids. Euromech Colloquium 469 , TU Dresden
- [4] Eisenbach,S. 2006 Großstruktursimulation druckinduzierter Ablösungen. Dissertation TU München (in preparation)

References

- [1] Meneveau C., Lund T.S. and Cabot W.H. 1996 A Lagrangian dynamic subgrid-scale model of turbulence. *J . of Fluid Mech*, 319, 353-385
- [2] Mathew J., Lechner R., Foysi H., Sesterhenn J. and Friedrich R. 2003 An explicit filtering method for large eddy simulation of compressible flows. *Physics of fluids*, 15, 2279-2289
- [3] Ghosh S., Sesterhenn J., and Friedrich R. 2006 DNS and LES of compressible turbulent pipe flow with isothermal wall. *Direct and Large eddy simulations VI* , Springer
- [4] Poinso T.J. and Lele S.K. 1992 Boundary conditions fo direct simulations of compressible viscous flows. *J. of Computational Physics* ,101, 104-129

Direct Numerical Simulation (DNS) and Large Eddy Simulation (LES) of turbulent reacting shear layers

Research Institution:

Fachgebiet Strömungsmechanik,

TU München

Garching, Germany

Email: inga.mahle@aer.mw.tum.de

Research Area:

Fluid Dynamics

Researchers:

I. Mahle, J. Sesterhenn, R. Friedrich

Abstract

Hydrogen combustion presently plays an important role in transportation and power applications like rocket engines and that will remain so in the near future. In order to gain full understanding in all processes involved, it is important to investigate simple configurations, like turbulent temporally developing and reacting shear layers, that serve as generic test cases for any non-premixed combustion device working with hydrogen. In a first step, we have chosen a simple combustion model with just one global, infinitely fast chemical reaction, which enabled us to perform a high-resolution DNS.

Simulations

We simulate two gas streams with opposite flow directions, between which a turbulent shear layer develops and grows over time.

Figure 1 shows the density distribution in a vertical plane of the three-dimensional domain: The upper stream, the velocity of which is directed to the right, is air, while the lower stream is a mixture of hydrogen and nitrogen. The Mach number in this test case is low to reflect the situation in combustion chambers.

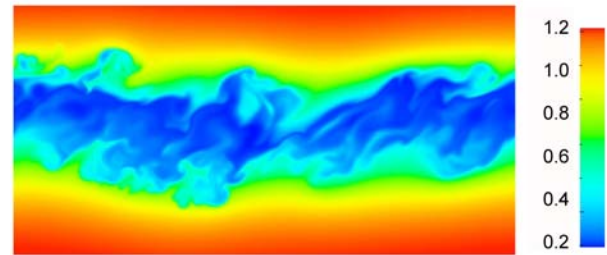


Fig. 1: Instantaneous density field in [kg/m³] of the DNS with infinitely fast chemistry, vertical cut through the domain

The use of an infinitely fast chemical reaction permits relating the chemical species to just one scalar, the so-called mixture fraction. Therefore, only the field of this non-reactive quantity has to be computed instead of the distribution of all chemical species, and a DNS with a high number of grid points, e.g. 64 million for the computation in Figure 1 can be performed. As a DNS resolves all spatial and temporal scales down to the smallest ones, the results of such a computation are of great value for many detailed statistical investigations and the development of improved subgrid-scale models for LES. Some investigations concerning DNS and LES of inert shear layers can be found in [1,2].

Since the direct numerical simulation already took as much as 82.000 CPUh on 192 processors of the Hitachi SR8000, it is too expensive to refine the combustion model as this would further increase the computational costs. When, on the other hand, the smallest scales are not resolved but modeled, as it is done in an LES, coarser grids and larger time steps can be used reducing the computational requirements drastically. Then not only infinitely fast chemical reactions [3] but also more complicated combustion models can be applied, like finite rate chemistry, which has been implemented in our LES code. We considered 9 species and 19 chemical reactions. Yet even with an LES grid that has about two orders of magnitude fewer grid points than the DNS, it is not feasible with the present computational resources to integrate the transport equations of all these species in 3D. Therefore we used a flamelet approach, which is based on the assumption that the thin turbulent flame consists of many laminar flames, the so-called flamelets. These flamelets are computed in one-dimensional space which makes it possible to apply the detailed reaction scheme.

The computation of the flamelets is done before the actual LES and the results are stored in a database. During the LES, the flamelet data, like

the species mass fractions, are recovered from this database.

One of our main objectives concerning the evaluation of the flamelet LES is to investigate the influence of detailed diffusion, namely the Soret and Dufour effects, which represent the molecular transport of species due to temperature gradients and the transport of heat due to species gradients, respectively [4,5]. Due to computational restrictions they have mostly been neglected in combustion simulations, however they are of particular importance for hydrogen chemistry. The one-dimensional nature of the flamelets permitted us to compute the flamelet database twice, one time with these thermodiffusive effects and one time without them. Then, we used these databases in two different LES simulations. Figure 2 shows an instantaneous field of the H₂O mass fraction for the computation with detailed diffusion. It is clearly visible that this simulation has a lower resolution than the DNS in figure 1. The blue spots within the turbulent shear layer are places where the flame is extinguished due to heat release, respectively its modeled equivalent, namely, high scalar dissipation rate (Figure 3) and no H₂O is produced. One of the most striking differences that we found between detailed and simplified diffusion was the value of this extinction limit. For simplified diffusion the scalar dissipation rate at which extinction occurs is more than double the value obtained with detailed diffusion. This not only has local influence, but affects mean profiles as well.

Because the interpolation of the flamelet quantities has to be done at each time step and at all grid points, we have, up to now, only been able to perform flamelet LES. Flamelet DNS is one type of computation that we are planning to perform on the next generation system at LRZ (HLRB-II). It will help us to further validate our LES results and to gain more insight into detailed diffusion effects.

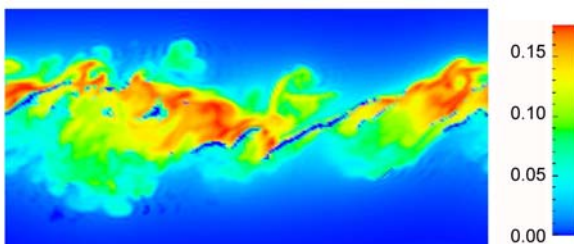


Fig. 2: Instantaneous H₂O mass fraction field of the flamelet LES with infinitely fast chemistry, vertical cut through the domain

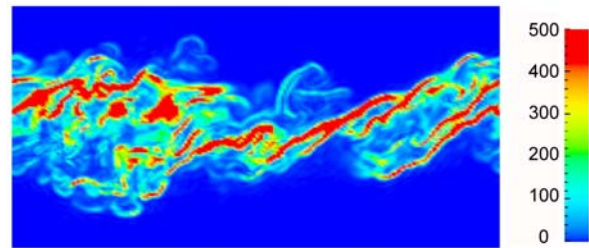


Fig. 3: Instantaneous scalar gradient field in [s⁻¹] of the flamelet LES with infinitely fast chemistry, vertical cut through the domain, values above the extinction limit (400 s⁻¹ - 11000 s⁻¹) are shown in red and are partially beyond the scale

References

- [1] Mahle I, Sesterhenn J, Friedrich R (2005) Dissipation of Active Scalars in Turbulent Temporally Evolving Shear Layers with Density Gradients Caused by Multiple Species. Appears in: Direct and Large-Eddy-Simulation-6. Poitiers, France, 12-14 September, Springer, 2005
- [2] Mahle I, Mellado J P, Sesterhenn J, Friedrich R (2005) LES of turbulent low Mach number shear layers with active scalars using explicit filtering. Appears in: iTi Conference on Turbulence. Bad Zwischenahn, Germany, 25-28 September, 2005
- [3] Mahle I, Mellado J P, Sesterhenn J, Friedrich, R (2006) LES of reacting turbulent shear layers using infinitely fast chemistry. Contribution to: Turbulence and Interaction 2006. Porquerolles, France, 29 May - 2 June, 2006
- [4] Mahle I, Sesterhenn J, Friedrich R (2005) Influence of detailed diffusion processes on turbulent mixing in temporal compressible shear layers with species and temperature gradients. In: Fourth International Symposium on Turbulence and Shear Flow Phenomena. Williamsburg, VA USA, 27-29 June, 2005, 1013—1018
- [5] Mahle I, Sesterhenn J, Friedrich R (2006) Turbulent Mixing in Shear Layers Involving Detailed Diffusion Processes. Appears in: Journal of Turbulence, 2006

Direct Numerical Simulations of Flow in Turbomachinery

Research Institution:

Institute for Hydromechanics, University of Karlsruhe

Research Area:

Computational Fluid Dynamics

Principal Investigator:

Prof. Wolfgang Rodi

Researchers:

Dr. Jan Wissink, Dr. Tamer Zaki

Abstract

A Low-Pressure Turbine (LPT) is employed, for instance, in jet engines where it supplies power to the fan and sometimes also to the first compressor stages. An LPT contains one or more stages, each consisting of one rotor-stator pair. The wakes generated by the rotor blades impinge on the stator blades causing a periodic unsteadiness. Both the low Reynolds number and the periodic unsteadiness directly influence blade-boundary layer transition, the tendency to separation, heat transfer and losses.

An overview is provided of various Direct Numerical Simulations (DNS) of transitional flows in turbine-related geometries. Two flow cases are considered: Case 1 concerns separating flow over a flat plate with oncoming turbulent free-stream fluctuations (see Fig. 1a), Case 2a concerns separating flow in a T106 turbine cascade with incoming wakes and Case 2b concerns flow around and heat transfer from a MTU turbine blade (see Fig. 1b) with incoming wakes and background fluctuations.

Computational Details

In Case 1, the computational domain, shown in Figure 1a, was chosen in accordance with experiments performed at the TU-Berlin. The Reynolds number, $Re=60000$, was based on the mean inflow velocity U_0 and the length-scale L . The free-stream turbulence – which is superposed on a uniform inflow - originates from a snapshot of a separate simulation of isotropic turbulence in a box. The size of the spanwise direction – where periodic boundary conditions are employed - is $l_z=0.08L$. The rest of the boundary conditions can be identified in Fig. 1a.

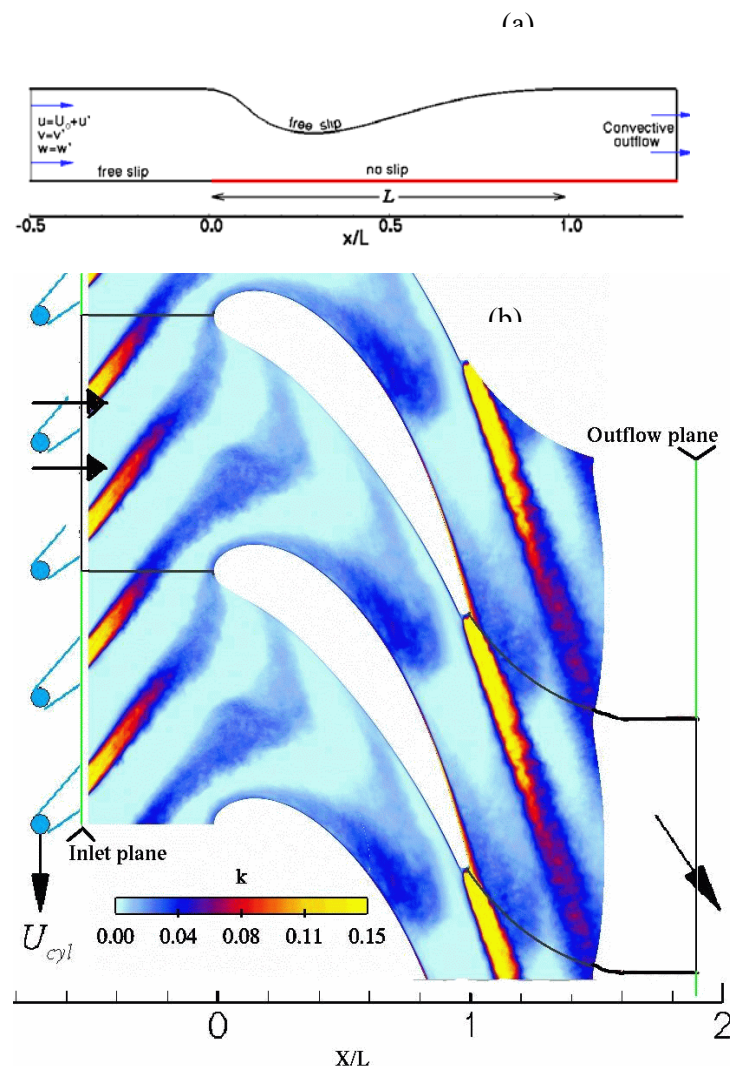


Fig. 1 : Cross-sections at midspan of the computational domain of (a): the flat plate boundary layer separation and (b) flow in a turbine cascade, where the computational domain corresponds to the region bounded by the black lines

The shape of the upper wall creates a favourable streamwise pressure gradient for $x/L < 0.3$ and

an adverse pressure gradient for $x/L > 0.3$. This adverse pressure gradient is strong enough to cause the flow to separate. More details on the computational set up can be found in Wissink and Rodi [1-3].

Fig. 1b shows a typical example of a computational domain used to calculate flow in a turbine cascade with periodically incoming wakes (Cases 2a and 2b). Along the surface of the blade a no-slip boundary condition is used.

In the spanwise direction and in the blade-normal direction both upstream and downstream of the blade a periodic boundary condition is employed. At the outflow plane, a convective outflow boundary condition is used and at the inflow plane artificial wakes were introduced, superposed on a uniform flow-field. The wake data were kindly made available by Xiauhua Wu and Paul Durbin of Stanford University. The respective Reynolds numbers for the two sets of simulations – listed in the abstract – were based on the mean inflow velocity U and the axial chord length L .

In Case 2a, simulation of flow in a T106 cascade was performed in accordance with experiments performed at the University of the Armed Forces in Munich while the simulation of flow and heat transfer in a MTU cascade (Case 2b) was performed in accordance with experiments performed by Liu and Rodi [4,5]. In the latter simulation not only wakes but also free-stream fluctuations were added at the inflow plane where the incoming flow had a temperature of $T=0.7T_0$ and the blade was assumed to have a constant temperature $T=T_0$.

More details about the computational set-up can be found in Wissink [6] and Wissink et al. [7] (T106 cascade) and Wissink and Rodi [8] (MTU cascade).

The calculations were performed on the Hitachi SR8000-F1 at Leibniz Rechenzentrum (LRZ) in München using up to 256 processors and 93.4 million grid points. To complete the simulations up to 240,000 time steps were required which took a total of 2000 clock hours of continuous running.

Brief overview of results

In Case 1, where $Re=60000$, boundary layer separation is induced by a contoured upper wall (see Fig. 1). Without free-stream disturbances, small-scale numerical noise is relied upon to

trigger a Kelvin-Helmholtz (KH) which is characterised by a roll-up of the separated boundary layer forming KH-rolls. As a result, a very large separation bubble is obtained. The KH-rolls are subject to a spanwise instability and rapidly become fully turbulent. Compared to the case without free-stream turbulence, with free-stream fluctuations this KH instability is triggered much earlier and transition is enhanced, which leads to a drastic reduction in size of the separation bubble (see Figure 2). In all cases, turbulence is observed to be produced inside the rolled up shear layer. A more detailed presentation of the results can be found in [1-3].

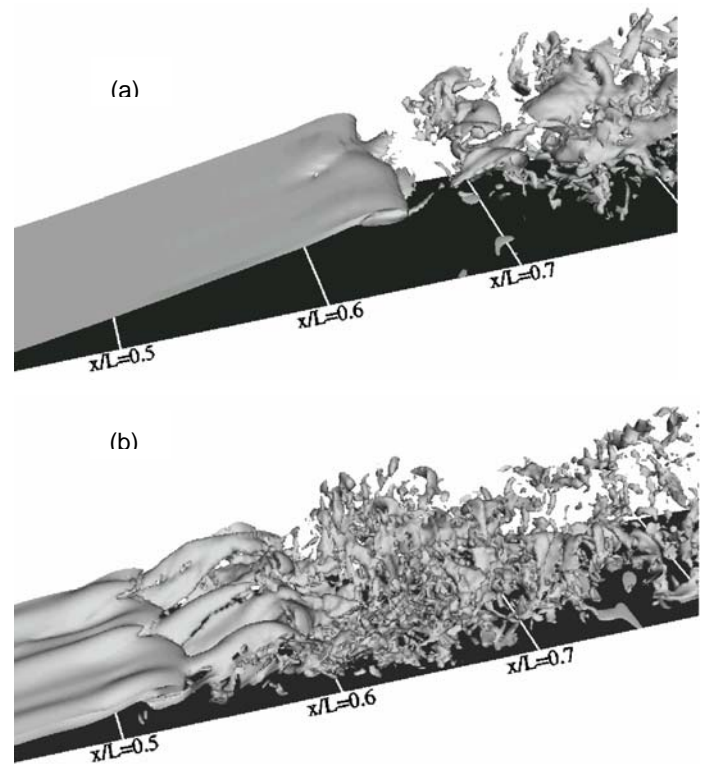


Fig. 2: Iso-surfaces of the spanwise vorticity. (a): no free-stream fluctuations, (b): with free-stream fluctuations ($Tu=7\%$ at the inflow plane)

Case 2a concerns flow in the T106 turbine cascade with periodically oncoming wakes at $Re=51800$. In this simulation, the boundary layer along the downstream half of the suction side is found to separate intermittently and subsequently rolls up due to a KH instability. This KH instability was found to be triggered by the large-scale fluctuation associated with the movement of the wake. Further transition to

turbulence is subsequently triggered by the small scale fluctuations present inside the wakes.

These fluctuations are also responsible for seeding the production of turbulent kinetic energy at the apex of the deformed wake as it travels through the passage between blades. At times when the wakes impinge separation is intermittently suppressed. See also [6,7] for a more detailed presentation of the results of Case 2a.

Case 2b concerns flow and heat transfer in a MTU cascade with oncoming wakes and background turbulence at $Re=72000$. Here, evidence of by-pass transition in the suction side boundary layer flow is observed: The free-stream fluctuations trigger low-speed and high-speed streaks in the otherwise laminar boundary layer. These streaks eventually become unstable and form turbulent spots which amalgamate downstream to form a fully turbulent boundary layer. The pressure-side boundary layer remains laminar in spite of significant fluctuations present. In agreement with the experiments, the impinging wakes cause the heat transfer coefficient to increase significantly in the transitional suction-side region close to the trailing edge and by about 30% on the pressure side. The large increase in heat transfer in the pre-transitional suction-side region observed in the experiments could not be reproduced. The discrepancy is explained by differences in spectral contents of the turbulence in the oncoming wakes. The contours of the phase-averaged fluctuating kinetic energy, shown in Figure 1b, supply a clear view of the path of the wakes as they travel through the computational domain. At the apex of the deformed wake, production of kinetic energy takes place. More results of Case 2b are presented in [1,8].

References

- [1] Wissink, J.G. and Rodi, W. 2006, Direct Numerical Simulations of transitional flow in turbomachinery. To be published in: ASME J. of Turbomachinery
- [2] Wissink J.G. and Rodi, W. 2004, DNS of a laminar separation bubble affected by free-stream disturbances. In: Direct and Large-Eddy Simulation V, (R. Friedrich, B.J. Geurts and O. Métais eds.)
- [3] Wissink J.G. and Rodi, W. 2005, DNS of separation induced transition influenced by free-stream fluctuations. In: Proceedings of the IUTAM symposium on laminar-turbulent transition, Bangalore 2004.
- [4] Liu, X. and Rodi, W. 1994, Velocity measurements in wake-induced unsteady flow in a linear turbine cascade. *Exp. in Fluids* 17, 45-58
- [5] Liu, X. and Rodi, W. 1994, Surface pressure and heat transfer measurements in a turbine cascade with unsteady oncoming wakes. *Exp. in Fluids* 17, 171-178
- [6] Wissink, J.G. 2003, DNS of separating, low Reynolds number flow in a linear turbine cascade with incoming wakes. *Int. J. of Heat and Fluid Flow* 24, 626-635.
- [7] Wissink, J.G., Rodi, W., and Hodson, H.P. 2006, The influence of disturbances carried by periodically incoming wakes on the separating flow around a turbine blade. *Int. J. of Heat and Fluid Flow* 27, 721-729.
- [8] Wissink, J.G. and Rodi, W. 2006, DNS of flow and Heat transfer in a turbine cascade with incoming wakes. Under consideration for publication in *J. Fluids Mech.*

Implementation and validation of LES models for partially premixed turbulent flames

Research Institution:

Fachgebiet Thermodynamik, TU München

Research Area:

Computational fluid dynamics - combustion

Principal Investigator:

Ludovic Durand

Researchers:

Ludovic Durand, Dr. Joern Sesterhenn

Introduction

The goal of this project is the implementation and the validation of Large eddy simulation (LES) models for the inhomogeneously premixed turbulent combustion. LES models aim at resolving the largest structures of the flow pattern due to the turbulence, and modelling the smallest structures. By inhomogeneously, one describes a mixture which can not be perfectly premixed because of technical considerations. To exploit the full potential and the precision of the LES modelling, these models are implemented in a high order scheme solver. As this solver can also compute Direct numerical simulation (DNS) calculations –computations of all turbulent scales–, the LES models will be validated versus both experimental results and DNS simulations. Considering the calculation time induced by the DNS simulations, the implementation of the combustion models for the DNS computations was started first, and preliminary results are presented here. If DNS simulations are used for the validation, no further developments in this direction (such as detailed reaction mechanisms) are planned because of the prohibitive calculation times.

Solver NSF

Cold solver

The solver called NSF has been developed by the chair for Fluids Mechanics directed by Prof. Friedrich at the Technical University of Munich. The combustion models are conjointly developed by the chairs for Fluids Mechanics and Thermodynamics in an active partnership of the project FORTVER. NSF was designed to solve turbulent compressible subsonic or hypersonic flows. The flow is described by computing transport equations and dividing the geometry in small volumes called cells. Five transport equations are solved: the pressure p , the components for the velocity u , v and w and the entropy s . These equations are written in a wave formulation, which is a particularity of this solver. It consists in formulating the Navier-Stokes equations, so that the relation between velocity and pressure fluctuations explicitly appears. This formulation is perfectly adapted to treat the hypersonic flows, and brings considerable advantages for the study of acoustics (e.g., Sesterhenn [1] for more details). The choice of the entropy for the energy equation is justified by its straightforward adaptation to the wave formulation. Nevertheless this equation makes the implementation of combustion models harder.

Combustion modelling-reactive species

The most precise way of computing the chemical reaction is to consider chemical mechanisms with reaction intermediate species and radicals. This implies the computations of numerous transport equations (more than 100), which costs too much CPU-time. For the DNS calculations, multi-species simulations with global step chemical reaction mechanisms are computed. This choice enables a better precision by taking into account the different properties of the gases (enthalpy, calorific coefficients). It is also not too prohibitive in terms of calculation time since less than 7 species are used. Models with one or two steps are implemented; the reaction rates are evaluated with the Arrhenius formulation. In the case of the two-step mechanism, the reaction coefficients are calculated with the help of genetic algorithms (e.g., Polifke and al. [2] for the global mechanism). In the case of interest, the combustion of the methane at atmospheric pressure and temperature at a lean regime ($\phi=0.6$) is modelled with two reactions.

Validation case

Geometry

The solver NFS can calculate simple geometries with structured and Cartesian grids. Considering the fact that DNS simulations were planned, the focus was set on burners with relative small turbulent Reynolds numbers. The first validation case retained is a turbulent premixed V-flame burner, which was experimented by Dinkelacker et al. (e.g., Dinkelacker [5]) at the LTT in Erlangen. This burner is composed of an inlet formed by a cylinder which includes a turbulence grid. The flame is an open flame anchored with a hot wire just after the exit of the cylinder (see Fig. 1). This burner is characterized with a turbulent Reynolds number of $Re_t = 80$ and a Mach number of $Ma = 0.006$ for the standard mass flow rate (inlet velocity $u_0 = 2$ m/s). The angle of the flame β was measured as a function of the mass flow rate and of the stoichiometric ratio.

3D-domain planned for the complete simulation

For the LES and DNS calculations at the same time very fast computers and a relative small domain are needed to limit the calculation time to a reasonable range. Also to be taken into consideration, the time step has to be smaller than 10⁻⁶ s for physical reasons (timescales of the fastest phenomena), and will be still smaller due to numerical criteria. As the central domain of the flame is mainly of interest, one can use a Cartesian grid instead of a cylindrical one. This choice makes the use of a value l_2 smaller than l_1 (see Fig. 2) possible, with an objective of reducing the number of cells. Considering the diameter $d = 40$ mm of the duct, a domain length of $l_1 = 70$ mm should offer a good compromise between the number of cells and a realistic size of the domain. The height of the domain L could be evaluated by knowing the maximal experimental flame angle $\beta < 30$. The height is chosen so that the flame exits through the top boundary, and not by the sides or the corners:

$$L = 10 + \frac{\phi/2}{\tan \beta} \approx 70 \text{ mm}$$

The width $l_2 = 15$ mm is calculated, so that three turbulent eddies could be simulated. The integral turbulent length scale was measured to be: $l_t = 5$ mm. Now the number of cells in the domain could be evaluated. The Kolmogorov length scale η could be known from the experimental turbulent Reynolds number $Re_t = 80$:

$$\eta = l_t Re_t^{-3/4} \approx 2 \times 10^{-4} \text{ m}$$

For the DNS grid it is necessary to use regular and almost cubic cells, where the side length is at most equal to the Kolmogorov length scale η . The number of cells can therefore be calculated as the ratio between the volume of the domain and the volume of a cell:

$$N_{DNS} \geq \frac{V_{Domain}}{V_{Cell}} = \frac{l_1 l_2 L}{\eta^3} \approx 9 \times 10^6 \text{ cells}$$

It is now interesting to evaluate the “final” time to reach to get a relevant simulation. This final time could be mainly evaluated with the convective and flame time scales. The following ideas (e.g., Veynante [6]) are used: it is necessary to reach a final time which is both ten times bigger than the convective time scale, and about forty times bigger than the flame time scale to get a correct solution. The convective time scale through this domain is:

$$t_c = \frac{L}{u} = \frac{70 \times 10^{-3}}{2} \equiv 3.5 \times 10^{-2} \text{ s}$$

And the flame time scale is:

$$t_f = \frac{l_f}{s_l} = \frac{0.15 \times 10^{-3}}{0.1} = 1.5 \times 10^{-3} \text{ s}$$

As a consequence, a final time of 0.3 s have to be reached.

Turbulent premixed V shaped flame

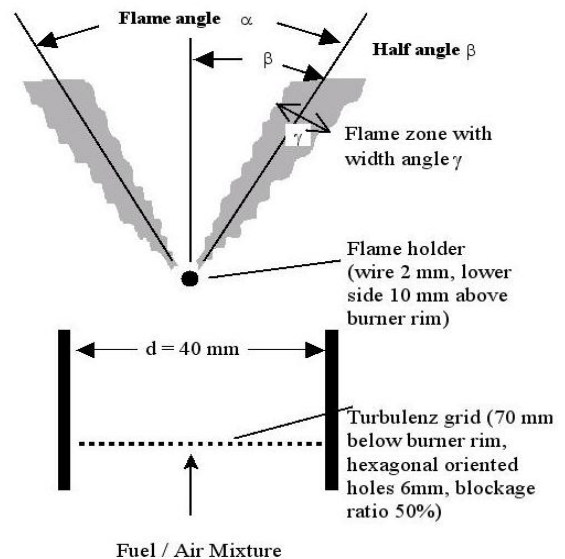


Fig. 1: Squeeze of the V-Flame burner

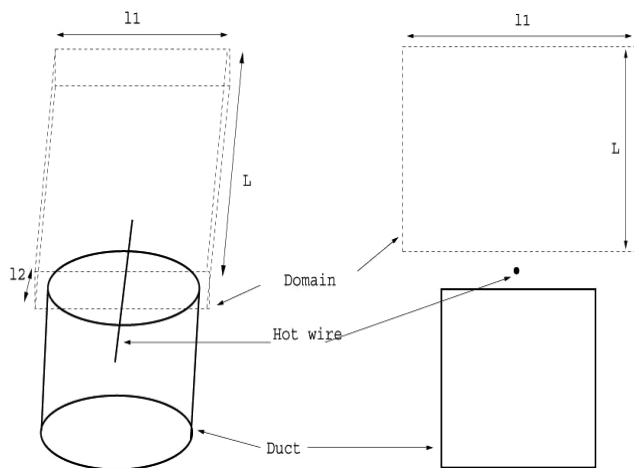


Fig. 2: 3D-domain for the complete DNS simulation

Conclusion

Unfortunately this project has been suspended. The calculation times were too large (even with the Hitachi SR8000) to produce relevant results in the specified project period.

Links

<http://www.lrz-muenchen.de/services/compute/>

Project Partners:

TU Erlangen, TU Muenchen, TU Bayreuth, TU Erlangen

References

- [1] J. Sesterhenn. A characteristic-type formulation of the Navier-Stokes equations for high order upwind schemes. In *Computers & Fluids* 30, 2001.
- [2] W. Polifke, W. Geng, and K. Doebbeling. Optimization of rate coefficients for simplified reaction mechanisms with genetic algorithms. In *Combust & Flame*, 1998.
- [3] N. Peters. *Turbulent Combustion*. Cambridge University Press, 2000.
- [4] T. Poinso, D. Veynante: *Theoretical and numerical combustion*. Edwards, 2001.
- [5] Private communication with D. Veynante, Sept. 2003.
- [6] F. Dinkelacker: Struktur turbulenter Vormischflammen . In Nr. 1.4 in *Berichte zur Energie-und Verfahrenstechnik A. Leipertz*, 2001.

Simulation of Jet Engine Exhaust Noise

Research Institution:

Institut für Strömungsmechanik und Technische Akustik

Research Area:

Computational Fluid Dynamics

Principal Investigator:

Lukasz Panek

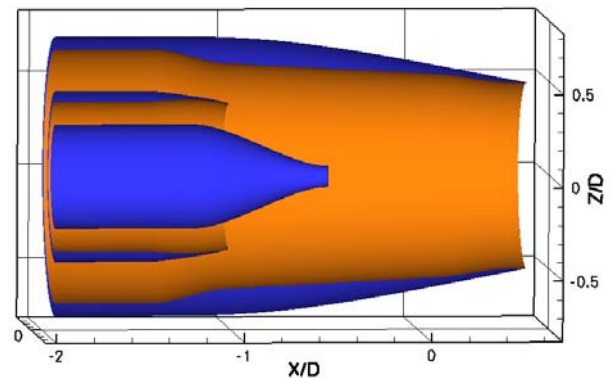
Researchers:

Jianping Yan

Karsten Tawakolian

Jet noise remains an important source of aircraft noise, especially at take-off. The reduction of jet noise due to the application of serrated exit nozzles in aero-engines is one of the subjects under investigation within the German research project FREQUENZ. The project is part of the "Luftfahrtforschungsprogramm 2003-2007" promoted by the Bundesministerium für Wirtschaft und Arbeit (BMWA). It is expected that the generation of axial vorticity by serrations attached to the trailing edge of the bypass nozzle, will influence the shear layer and flatten the radiated noise spectrum giving rise to a lower overall acoustic emission. In the present investigation, the modified and standard geometries will be compared with respect to noise generation. To obtain real simulation conditions, the nozzle is included in the computational domain. The numerical results will be validated using experimental data. The analysis is based on a 3D simulation of the mixing jet flow field under real flight conditions with the compressible ELAN3D CFD-solver of ISTA. The Detached Eddy Simulation (DES) approach in a slightly modified form was chosen to ensure numerical efficiency. The DES performs as a LES in highly resolved regions of separated flow and runs in RANS mode in

attached boundary layers using a single turbulence model implementation. Due to the turbulence-resolving capabilities of the LES-mode, this method allows the direct capturing of the sound sources. To extrapolate the sound propagation into the far field, the acoustic analogy of Ffowcs Williams and Hawkins is applied. The FWH input data is collected during the simulation at different surfaces enclosing the jet and postprocessed afterwards.



Preliminary Results

In Fig. 3 the Mach number contours obtained by RANS are shown. In the aeroengine housing, the fast and cold outer bypass flow can be clearly distinguished from the slower and hot inner stream coming from the combustion process. An overview of the developed flow field, depicted by means of iso-surfaces of the λ_2 -criterion is given in Figure 2. It can be observed, that the flow field downstream of the nozzle exit is dominated by large ring vortices, which develop quite

harmonically and are convected downstream. They remain rather undisturbed up to 2 nozzle diameters downstream and brake down hereafter into smaller structures. In Figure 4 the sound pressure levels in the jet region are depicted. Pressure fluctuations of up to 1000 Pa can be observed.

Figure 5 illustrates the mixing of the jet streams by means of stream traces. They start smoothly at the engine inlet and become increasingly chaotic when they reach the end of the potential core. The colour of the traces corresponds to the local velocity magnitude. The contours in the background depict the turbulent kinetic energy of the flow. This is the energy contained in the fluctuations of the flow. It is nearly zero in the outer region and reaches the maximum in the shear layers.

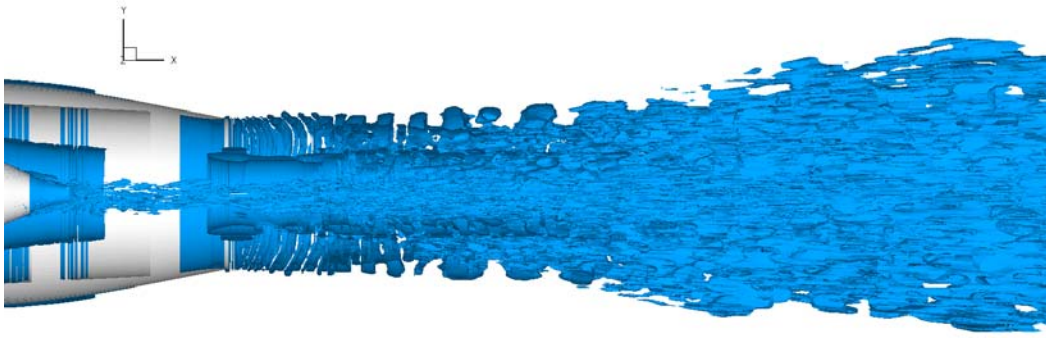


Fig. 2 Snapshot of vortex structure in the mixing jet

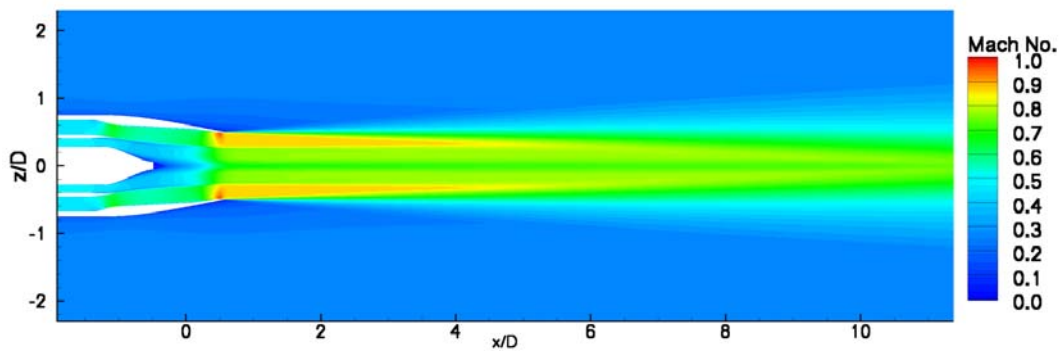


Fig. 3: Mach number contours in the coaxial jet

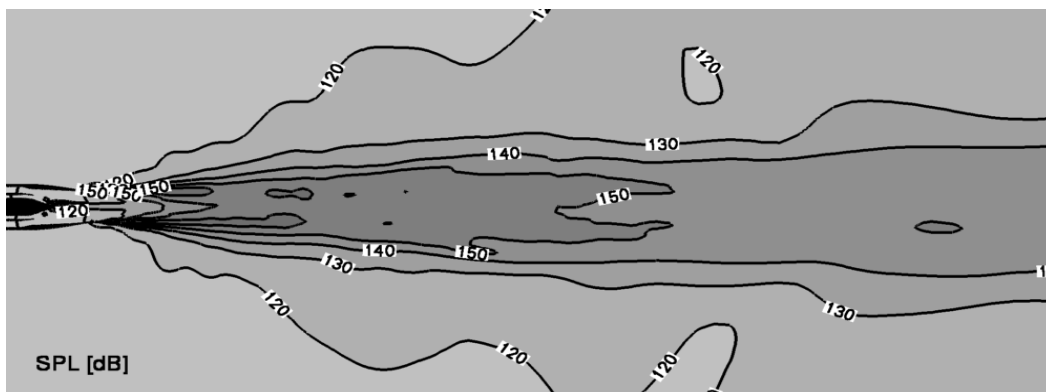
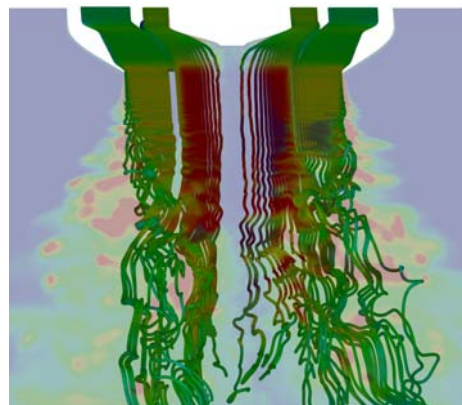


Fig. 4: Sound pressure level contours in the jet region

Fig. 5: Streamtraces coloured with velocity magnitude plotted over a contour plane showing the turbulent kinetic energy of the flow.



Simulation of Quantum Chromodynamics on the Space-Time Lattice

Research Institution:

DESY, Humboldt Univ. Berlin, Freie Univ. Berlin, ZIB Berlin, Univ. Edinburgh, Univ. Leipzig, Univ. Liverpool, LMU und TU München, Univ. Regensburg

Research Area:

Computational Physics

Principal Investigator:

Prof. Dr. Gerrit Schierholz

Researchers:

Dr. Arifa Ali Khan, Dr. Meinulf Göckeler, Dr. Philipp Hägler, Dr. Thomas Hemmert, Dr. Roger Horsley, Dr. Ernst-Michael Ilgenfritz, Prof. Dr. Karl Koller, Dr. Yoshifumi Nakamura, Dr. Holger Perlt, Dr. Dirk Pleiter, Dr. Paul Rakow, Prof. Dr. Andreas Schäfer, Dr. Arwed Schiller, Dr. Wolfram Schroers, Dr. Thomas Streuer, Dr. Hinnerk Stüben, Volker Weinberg, Dr. James Zanotti

Abstract

Quantum Chromodynamics formulated on the space-time lattice provides a framework for investigation of non-perturbative phenomena, such as hadron structure and quark confinement, which are intractable by means of analytic field theories.

The Simulation

Quantum Chromodynamics (QCD) is the fundamental theory of the strong interactions. It binds quarks and gluons, the fundamental building blocks of matter, to nucleons and mesons,

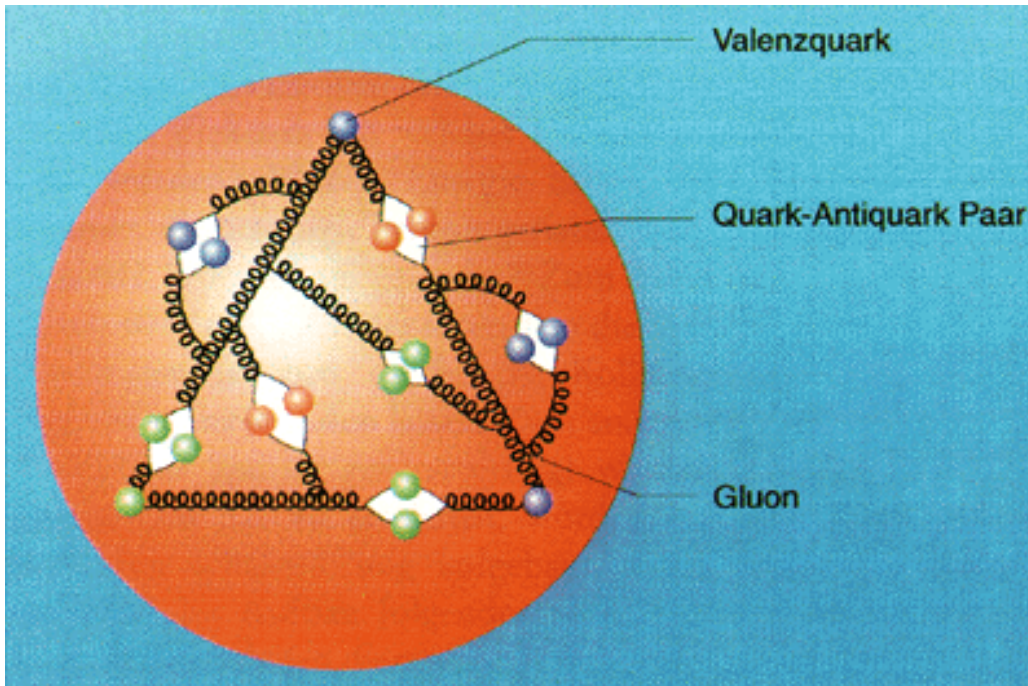
and these to nuclei. The forces are so strong that quarks do not exist in isolation. This phenomenon is called 'quark confinement'. The forces are equivalent to a weight of approximately ten tons.

Figure 1 shows a sketch of the proton. The proton can be visualized by three valence quarks (balls) bound together by the exchange of gluons (springs). The gluons strongly interact with each other, which gives rise to the confining force. In addition, gluons may transform into short-lived quark-antiquark pairs, the so-called sea quarks.

A quantitative solution of the theory requires non-perturbative techniques. Lattice field theory provides the framework for such a calculation. In this approach the theory is formulated on a discrete space-time lattice, which then may be solved from first principles and with no model assumptions by numerical simulations using well-known techniques adapted from statistical mechanics. Later on one may remove the lattice by letting the lattice spacing go to zero and the box size to infinity. The precision of the calculation is limited only by the available computing resources.

Probably the biggest challenge in theoretical particle physics is to understand the internal structure of hadrons in terms of its constituents, quarks and gluons, and in particular how quarks and gluons provide the binding (mass) and spin of the nucleon. Continuing advances in computing power and in algorithmic developments have now brought us to the point where ab initio calculations of nucleon structure are becoming possible.

Previous calculations of this kind were restricted to the quenched approximation, where effects of dynamical quark-antiquark pairs, such as the pion cloud in nucleons and mesons, have been neglected. The reason was that the inclusion of these contributions is computationally very expensive. Dynamical quarks may have a significant effect on the results. For a quantitative solution of the theory it is therefore necessary to eliminate this approximation. In this simulation we take the up and down quark-antiquark pairs into account, while the heavier strange quark has been neglected. The calculation is done for several lattice spacings and quark masses, so that the results can be extrapolated to the chiral and continuum limits.



energy x (in units of E) at a distance r from the center. The figure covers the region $0 \leq x \leq 1$ and $-1 \leq r \leq +1$ Fermi (1 Fermi = 10^{-15} cm). We see that the energetic quarks (having large fractional momentum x) are limited to a rather narrow region of $r \leq 0.3$ Fermi, while the soft (low-momentum) quarks spread

Fig. 1 : Sketch of a proton:

Nucleon Structure

A fast moving nucleon of energy E can be viewed as an ensemble of quasi-free quarks and gluons contracted to a disc due to Lorentz contraction. This is sketched in Figure 2. The quarks are located at a distance r from the center and contribute a fraction $x E$ to the total energy of the nucleon each. Gluons are not shown here.

One of the principle questions that concerned us most in this project is how the energy (mass) and spin of the nucleon is distributed among its constituents, as well as over space. In Figure 3 we show the probability distribution of finding an up quark inside the proton with fractional energy x (in units of E) at a distance r from the center. The figure covers the region $0 \leq x \leq 1$ and $-1 \leq r \leq +1$ Fermi (1 Fermi = 10^{-15} cm). We see that the energetic quarks (having large fractional momentum x) are limited to a rather narrow region of $r \leq 0.3$ Fermi, while the soft (low-momentum) quarks spread out to distances of $r = 1$ Fermi. This is to say that most of the energy of the nucleon is concentrated in a core of a fraction of a Fermi.

One of the principle questions that concerned us most in this project is how the energy (mass) and spin of the nucleon is distributed among its constituents, as well as over space. In Figure 3 we show the probability distribution of finding an up quark inside the proton with fractional

out to distances of $r = 1$ Fermi. This is to say that most of the energy of the nucleon is concentrated in a core of a fraction of a Fermi.

So far the calculations have been done at relatively heavy, unphysical quark masses, and the strange quark has been neglected completely, though its effect on the QCD vacuum is expected to be limited. The next step is to extend the simulations to realistic quark masses, including the strange quark. This will spare us uncontrolled extrapolations to the physical quark masses.

Similar pictures are obtained for the distribution of spin, which completes our view of the structure of the nucleon

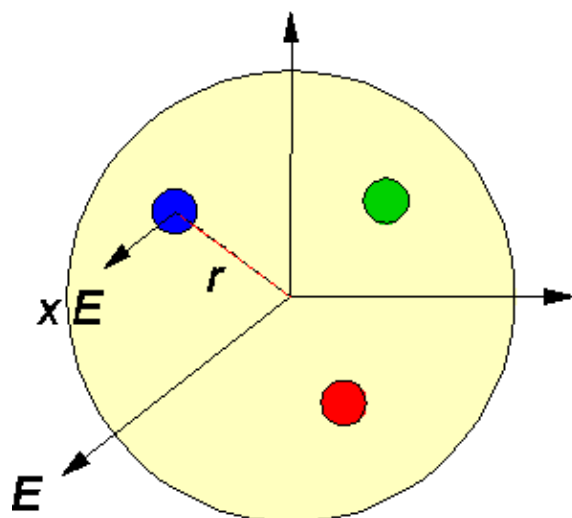


Fig. 2 : Schematic view of a fast moving proton

References

- [1] M. Göckeler et al., Phys. Rev. Lett. 92 (2004) 042002.
- [2] A. Ali Khan et al., Nucl. Phys. B689 (2004) 175.
- [3] M. Göckeler et al., Phys. Rev. D71 (2005) 034508.
- [4] M. Göckeler et al., Nucl. Phys. B717 (2005) 304.
- [5] M. Göckeler et al., Phys. Rev. D71 (2005) 114511.
- [6] M. Göckeler et al., Few. Body. Syst. 36 (2005) 111.
- [7] M. Göckeler et al., Nucl. Phys. A755 (2005) 537.
- [8] M. Göckeler et al., Phys. Rev. D72 (2005) 054507.
- [9]
- [10] M. Göckeler et al., Phys. Lett. B627 (2005) 113.
- [11] M. Göckeler et al., Phys. Lett. B639 (2006) 307.
- [12] M. Göckeler et al., Phys. Rev. D73 (2006) 015413.
- [13] M. Göckeler et al., Phys. Rev. D73 (2006) 054508.
- [14] A. Ali Khan et al., hep-lat/0603021, to appear in Phys. Rev. D.
- [15] V.M. Braun et al., hep-lat/0606012, to appear in Phys. Rev. D.

Can the ^4He experiments serve as a database for determining the three-nucleon force?

Research Institutions:

Institut für Theoretische Physik III,
University of Erlangen-Nürnberg,
Staudtstraße 7, D 91058 Erlangen, Germany

Theoretical Division,

Los Alamos National Laboratory,
Los Alamos, NM 87545, USA

Researchers:

H. M. Hofmann, G. M. Hale

Abstract

We report on microscopic calculations for the ^4He compound system in the framework of the resonating group model employing realistic nucleon-nucleon and three nucleon forces. The resulting scattering phase shifts are compared to those of a comprehensive R-matrix analysis of all data in this system, which are available in numerical form. The agreement between calculation and analysis is in most cases very good. We show one example of perfect agreement and discuss briefly implications of disagreement.

Introduction

The ^4He - system is the lightest nuclear system with several two-fragment channels, the $^3\text{H-p}$, the $^3\text{He-n}$, and the $^2\text{H-d}$ ones, and (broad) overlapping resonances, thus allowing for various elastic scatterings and reactions. Due to this, it is one of the best studied nuclear systems: more than several thousand different observables are known so far. Due to this large number of data points, an R-matrix analysis allows for a model-independent description of the system by some hundred resonance parameters.

On the other side allows the ^4He - system for theoretical studies by various methods. Since the nuclear force is not yet known from first principles, one has to rely on phenomenological approaches or recently developed effective field theories. We use the resonating group model in its refined version [1] to aim at a complete understanding of the many features of ^4He . Applying realistic two- and three- nucleon potentials, the Argonne v18 and the Urbana IX, there is no freedom left for parameters allowing to fit the data. All differences between data and calculation have to be blamed on inadequacies of the potential used. The R-matrix analysis allows for a comparison partial-wave by partial-wave between e.g. calculated scattering phase shifts and extracted ones, thus giving hints on the operator structure of the potentials needing to be improved.

Model Space and Interaction

We have performed calculations for the two-nucleon force alone and the two- and three-nucleon forces together. In the following we discuss only results for the full calculation, more details can be found in [2]. The expansion of all intrinsic and scattering wave function in the interaction region in terms of Gaussians allows to calculate each individual matrix element analytically. For the sheer number, about 10^{10} in ^4He , we need the computer. Using 70 Gaussians for $^3\text{H}/^3\text{He}$ and 8 for the deuteron, we reproduced the experimental binding energies and thresholds within 20 keV.

Comparison of Phase Shifts

In fig.: 1 we compare the calculated 0^+ phase shifts with those from the R-matrix analysis. The agreement in size and energy dependence is striking.

Therefore, there is not much room left for changes of the potentials used. The 2^- phase shifts yield the largest differences. Since the other P-wave phase shifts, 0^- and 1^- , show much smaller discrepancies, we conclude that the negative parity non-central forces need improvement. The agreement for the other partial waves is between the two cases discussed. Generally the R-matrix analysis yields a much larger J-splitting than the direct calculation.

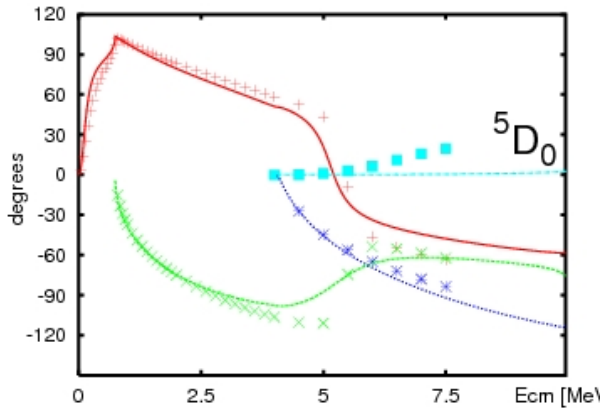


Fig. 1: Elastic 0^+ phase shifts for all physical two-fragment channels calculated for the AV18 potential together with the UIX TNF. The RRGM 1S_0 phase shifts are displayed as full lines (red) for the $t-p$ ones, as dashed lines for the $^3\text{He}-n$ ones (green), and as dotted lines for the $d-d$ ones (blue). The corresponding R-matrix results are given by + for $t-p$, by x for $^3\text{He}-n$, and by * for $d-d$.

Comparison with experiment

In fig.: 2, the differential proton-triton cross section is displayed. The full calculation reproduces the data as good as the R-matrix analysis, thus indicating that all the contributing partial waves are well given by the calculation. The overall agreement between calculation and data is good. There are some problems reproducing vector polarization data. Some tensor polarization observables demonstrate that the analysis uses other partial waves than the calculation to reproduce the data. This might be a hint for erroneous data.

Summary

In the framework of the resonating group model we have performed a rather complete scattering calculation in ^4He . In general the agreement between this direct calculation and a comprehensive R-matrix analysis is very good, thus indicating that the used potentials are already a good description of the nuclear force. It remains to be shown if new approaches, e.g. effective field theories yield better results.

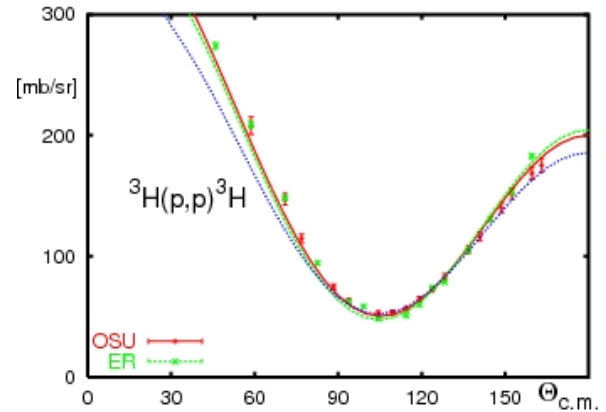


Fig. 2: Differential elastic proton-triton cross section. The R-matrix results are shown as full line (red), the results from $v18$ alone as dashed line (green), and those for $v18$ together with UIX as dotted line (blue).

References

- [1] Hofmann, H. M., 1987 : Resonating Group Calculations in Light Nuclear Systems, in Proceedings of Models and Methods in Few-Body Physics, Springer Lecture Notes in Physics, 273, 243-282
- [2] Hofmann, H. M. and Hale, G. M., 2005: Can the ^4He experiments serve as a database for determining the three-nucleon force?, arXiv:nucl-th/0512065

The structure of the local Universe

Research Institution:

Astrophysical Institute Potsdam

Research Area:

Computational Astrophysics

Principal Investigator:

Dr. Stefan Gottlöber

Researchers:

Dr. Stefan Gottlöber, Prof. Anatoly Klypin, Prof. Yehuda Hoffman, Arman Khalatyan, Prof. Andrey Kravtsov, Dr. Ewa Łokas, Prof. Gustavo Yepes, Prof. Silvio Bonometto

Abstract

We performed a series of high resolution simulations to study the formation and evolution of dark matter haloes in the local universe.

The Evolution of the Universe

Modern cosmology is based on a few key components that include the inflation (the origin of fluctuations), the expansion after inflation, the linear growth of fluctuations, and the nonlinear evolution of perturbations. The standard model of cosmological structure formation can be characterized by only five parameters that can be measured at present with high accuracy: the current rate of universal expansion, the mass density parameter, the value of the cosmological constant, the primordial baryon abundance, and the overall normalization of the power spectrum of initial density fluctuations, typically characterized by the present-day rms mass fluctuations on spheres of radius $8 h^{-1}$ Mpc. Measurements of the anisotropies of the Cosmic Microwave Background provided crucial tests for the theory. They indicate that the theory correctly predicts the structure and dynamics of the Universe. During the last years it was remarkable how well different observations agreed in the measured

values of those parameters. The standard cosmological model is compelling not just because it fits all the large-scale observations, but also because it is a natural outcome in many theories of particle physics beyond the standard model. However, there is no theoretical understanding of the cosmological constant. One can replace it by a more general Dark Energy with a still unknown equation of state. In the simplest models one additional parameter characterizes this equation of state. While successful on large scales, the standard cosmological model still faces strong challenges on small (galactic) scales. For example, it tends to over-predict the central densities of galaxies and the abundance of dwarf satellites.

Numerical Simulations

During the early inflationary phase of the evolution of the Universe, quantum fluctuations became classical perturbations in the density field whose growth can be well described by linear perturbation theory. After recombination, baryonic density fluctuations are decoupled from the radiation field and start to grow in the potential wells created by the dark matter. The density fluctuations become soon nonlinear, so that the further evolution can be studied only numerically. The first codes to handle the nonlinear evolution of density perturbations have been developed in the early eighties. In these codes, the density field is described by particles, and they could follow about 33 thousand particles. Present algorithms, like our ART code, can handle billions of particles. Since the dark matter represents 85 % of the matter, it is mainly responsible for the gravitational dynamics. Within the HLRB project we have used a version of the highly efficient parallel Adaptive Refinement Tree (ART) code that takes into account only the gravitational interaction of dark matter particles. The ART code is an N-body code, which reaches high force resolution by refining all high-density regions with an automated recursive refinement algorithm. Using Open MP directives and MPI at present we run regularly simulations on 512 processors.

Constrained Simulations

In our simulation we have reproduced the large-scale structures of the real local Universe, while keeping the initial conditions consistent with the power spectrum of a given cosmological model.

In particular, we have simulated the nearby small-scale structures within the correct large environment of the real Universe as revealed by various large-scale observational surveys.

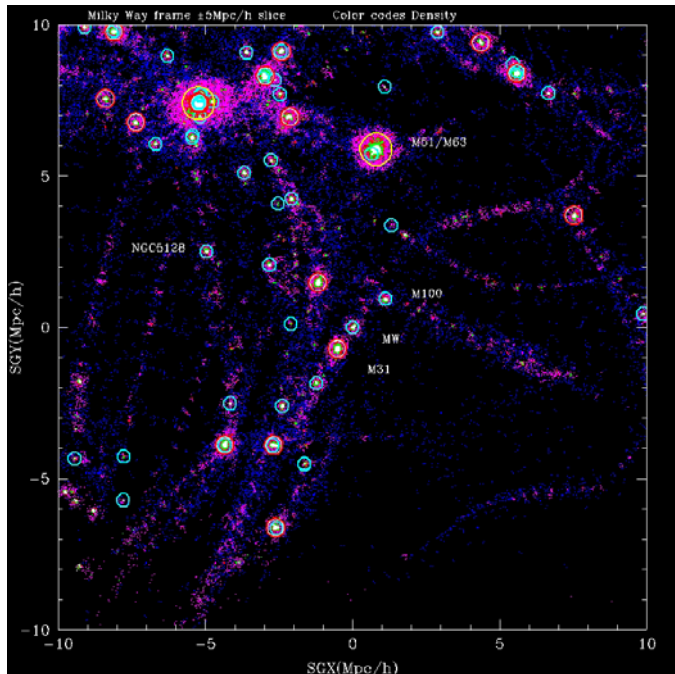


Fig. 1: Constrained simulation of the local Universe

This is done by setting the initial conditions of the simulations by constrained realizations of Gaussian fields, thereby constructing the density and velocity fields which agree both with the observed large scale structures and with the assumed theoretical model. This approach is called constrained simulation (Klypin et al 2003). Our simulation matches the observed local universe quite well, namely, we reproduced such observed structures like the Virgo cluster, the Local Supercluster, the Local Void, and the Local Group, in the approximately correct locations and embedded within the observed large-scale configuration dominated by the Great Attractor and Perseus-Pisces (Fig: 1).

With much higher mass resolution we have studied a series of voids similar to the local void. These voids contain a large number of dark matter halos, which could host dwarf galaxies. The haloes are arranged in a pattern, which looks like a miniature Universe: it has the same structural elements as the large-scale structure of the galactic distribution of the Universe. There are

filaments and voids; larger haloes are at the intersections of filaments. The only difference is that all masses are four orders of magnitude smaller. The standard model over-predicts the number of small objects in voids (Gottlöber et al 2003).

The Inner and Outer Structure of Dark Matter Halos

One of the most interesting problems of galaxy formation is the inner structure of dark matter halos, which host the galaxies. On the Hitachi and other supercomputers we have simulated the evolution of dark matter haloes in different environments, in particular within an extended filament (Fig. 2). In a series of papers based on these simulations we have studied the structure of dark matter halos of different masses (Ascasibar et al 2003, Colin et al 2004, Ascasibar et al 2004, Hoeft et al 2004, Tasitsiomi et al 2004, Wojtak et al 2005, Prada et al 2006) and recently also the influence of the environment of the halos on their properties (Avila-Reese et al. 2006)

Dark Energy

During the last 10 years many observations have shown that a substantial amount of the world contents is due to a smooth component with largely negative pressure dubbed Dark Energy. The simplest form of dark energy is a positive cosmological constant but also a slowly-evolving self-interacting scalar field could accelerate the expansion of the universe. We studied the influence of the different forms of dark energy on the large-scale structure with a series of simulations based on different equations of state of dark energy (Solevi et al 2006).

Project Partners:

New Mexico State University, Hebrew University Jerusalem, Chicago University, Copernicus-Centre Warsaw, Universidad Autónoma de Madrid, Università degli Studi di Milano—Bicocca

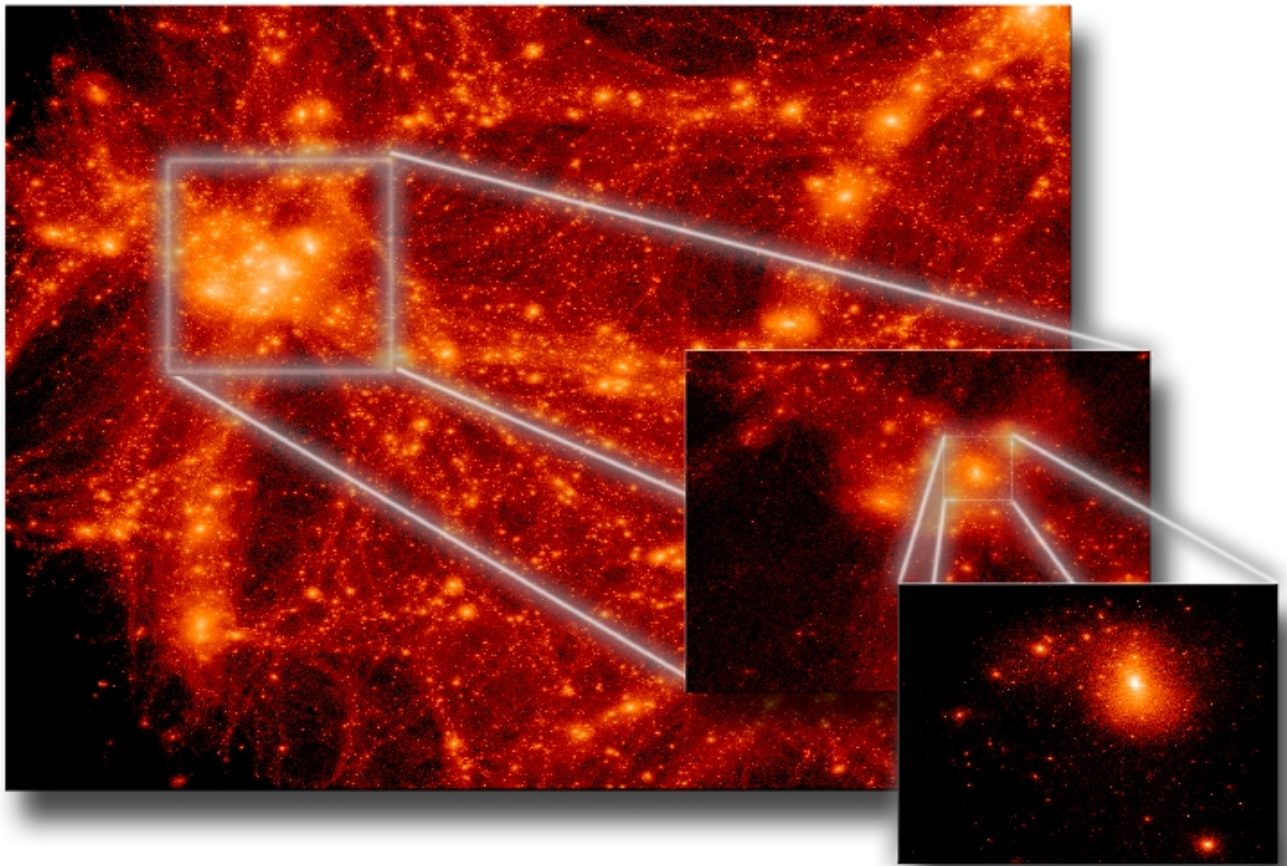


Fig. 2: High-resolution simulation of a filamentary structure with 135 million particles

References:

- [1] Klypin, Y. Hoffman, A.V. Kravtsov, S. Gottlöber, 2003: Constrained Simulations of the Real Universe: the Local Supercluster, *Astrophys. J.* 596, 19-33
- [2] S. Gottlöber, E. Łokas, A.A. Klypin, Y. Hoffman, 2003: The Structure of Voids, *MNRAS* 344, 715-724
- [3] Y. Ascasibar, G. Yepes, V. Müller, S. Gottlöber, 2003: The Radial Structure of Galaxy Groups and Clusters, *MNRAS* 346, 731-745
- [4] P. Colin, A. Klypin, O. Valenzuela, S. Gottlöber, 2004: Dwarf Dark Matter Halos, *Astrophys. J.* 612, 50-57
- [5] Y. Ascasibar, G. Yepes, S. Gottlöber, V. Müller, 2004: On the physical origin of dark matter density profiles, *MNRAS* 352, 1109-1120
- [6] M. Hoefl, J.P. Mücke, S. Gottlöber, 2004: Velocity dispersion profile in dark matter halos, *Astrophys. J.*, 602, 162-169
- [7] A. Tasitsiomi, A.V. Kravtsov, S. Gottlöber, A.A. Klypin, 2004: Density profiles of LCDM clusters, *Astrophys. J.* 607, 125-139
- [8] R. Wojtak, E.L. Łokas, S. Gottlöber, G.A. Mamon, 2005: Radial velocity moments of dark matter haloes, *MNRAS* 361, L1-L5
- [9] F. Prada, A.A. Klypin, E. Simonneau, J. Betancort-Rijo, S. Patiri, S. Gottlöber, 2006: How far do they go? The outer structure of dark matter halos, *Astrophys. J.* 645, 1001 - 10
- [10] V. Avila-Reese, P. Colin, S. Gottlöber, C. Firmani, C. Maultsby, 2005: The dependence on environment of Cold Dark Matter Halo properties, *Astrophys. J.* 634, 51 -69
- [11] P. Solevi, R. Mainini, S.A. Bonometto, A.V. Macció, A. Klypin, S. Gottlöber, 2006: Tracing the Nature of Dark Energy with Galaxy Distribution, *MNRAS* 366, 1346-1356

3-D seismic wave propagation

Research Institution:

Department of Earth and Environmental Sciences (Geophysics), Ludwig-Maximilians University, Munich

Research Area:

Geophysics - Seismology

Principal Investigator:

Prof. Dr. Heiner Igel

Researchers:

Gilbert Brietzke, Josep De La Puente, Michael Ewald, Miko Fohrmann, Heiner Igel, Gunnar Jahnke, Martin Käser, Markus Trembl, Bernhard Schuberth, Wiwit Suryanto, Mike Thorne, Haijiang Wang

Abstract

The calculation of theoretical seismograms (i.e., the numerical solution of viscoelastic, anisotropic wave propagation and earthquake rupture) is at the heart of several important problems in Earth Sciences. These include wave propagation in reservoirs, strong ground shaking following large earthquakes, global wave propagation and the structure of the earth's deep interior, wave propagation through fault zones, and the physics of earthquake rupture. In the lifetime of this project 3-D wave propagation and rupture algorithms were developed and implemented using the F90/MPI programming languages. These algorithms were applied to a variety of problems using substantial computational resources, particularly for parameter studies for wave and rupture phenomena in 3-D. Several of the algorithms are available in the software library of the EU project SPICE run by the Munich seismology group (www.spice-rtn.org).

Global wave propagation

Only recently the problem of simulating global wave propagation using numerical methods has become feasible due to the substantial computational effort required to appropriately discretize a global earth model. As the seismic method is the most important diagnostic tool to image the deep interior (i.e., seismic tomography), it is crucial to correctly predict the effects of 3-D structure on the seismic wave field radiated from earthquakes large enough to be observable everywhere ($M > 5$). Several algorithms were developed that solve numerically the elastic wave equation in spherical coordinates, both using the axi-symmetric approach (Jahnke et al., 2006, Thorne et al., 2006) and spherical sections for specific applications in regional seismology (Igel et al., 2002b). A recent example is illustrated in Fig. 1. While the long-wavelength 3-D structure of the earth's interior is fairly well constrained, there are still open questions as to what causes the velocity perturbations at depth and down to which spatial scales velocity heterogeneities exist. Therefore we investigate the effects of small-scale random velocity perturbations in the mantle.

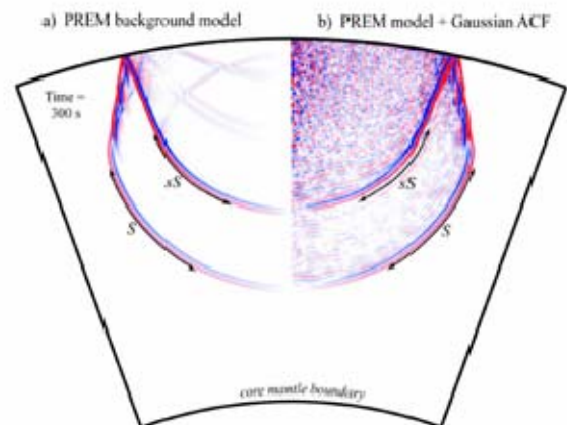


Fig. 1 : Seismic shear wave field through the upper mantle for a spherically symmetric earth model (left) and a model with random velocity perturbations (right) with the resulting scattering behaviour (Jahnke et al., 2006).

Our simulations show that – in case such perturbations exist – neglecting them may lead to erroneous images when applying tomographic methods. This study also illustrates the benefits using the axisymmetric approach allowing the calculations to be carried out in a 2-D computational domain. Thus much higher wave frequencies can be achieved.

Earthquake scenarios, shaking hazard

As reliable deterministic earthquake prediction is not in sight, the simulation of realistic earthquake scenarios is one of the most important tools to assess the seismic hazard of active regions. The ground motion observed at the surface after large earthquakes predominantly depends on (1) the source depth; (2) the magnitude; (3) the source mechanism (the orientation and size of the slip on the fault plane); and (4) the structure of the Earth's crust. One of the key factors in shaking hazard is the local seismic velocity structure. Low seismic velocities near the surface (e.g. sedimentary basins as in Los Angeles, Mexico City, the Cologne area) may amplify the ground motion up to ten-fold and thereby increase the hazard even for moderate earthquake magnitudes or distant large earthquakes. This is an inherent 3-D effect and can only be properly modelled with the use of 3-D modelling techniques. In Fig. 2. snapshots from the first 3-D simulations of earthquake scenarios in the Cologne basin are shown (Ewald et al., 2006). In a recent study we calculated a data base with solutions for single subfaults in the Los Angeles Basin. From such a data base arbitrary finite-fault scenarios can be synthesised (Wang et al., 2006). This allows the investigation of source related variations of strong ground motions following large earthquakes.

Waves in fault zones and dynamic rupture

The detailed structure of fault zones (FZs) plays an important role in problems related to fault mechanics, earthquake rupture, wave propagation and seismic hazard. FZs are thought to consist of a O(10-100)m wide region of decreased seismic velocity but structural details such as their depth extent, lateral and vertical variations etc. are elusive. The small spatial scales involved make such structures difficult to image with ray-theoretical methods such as tomography. We performed numerical calculations of wave propagation in various 3-D FZ geometries and analyzed the waveforms, spectra and envelopes of the synthetic seismograms. The main results are that (1) moderate changes of the shape of FZ or (2) small-scale heterogeneities or (3) depth-dependent properties do not strongly affect the observed FZ waves. In contrast, strong effects are to be expected from (4) breaks in the continuity of FZ structure (e.g. offsets), which may at some point allow imaging such features at depth (Jahnke et al., 2002; Igel et al, 2002a,

Fohrmann et al., 2004). Recent investigations demonstrated the effects of a bi-material interface on the dynamics of rupture propagation both in 2-D and 3-D settings (Brietzke et al., 2006ab).

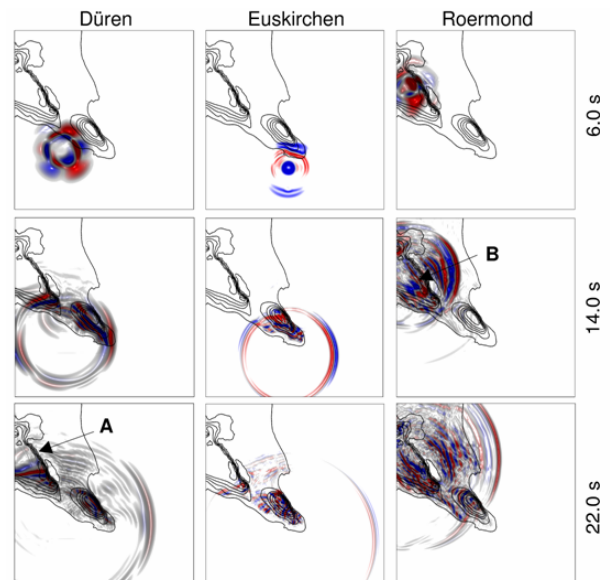


Fig. 2 : Snapshots of the seismic wave field at the surface of a 140 km x 140 km x 60 km model of the Cologne Basin, Germany, for three different epicentres of historical earthquakes (Ewald et al., 2006). Note the strong effects of the sedimentary basin (contour map shows basin depth).

Rotational ground motions

Standard seismometers record the three components of translational ground motions. However, there are three more components (i.e., rotations) that should be observed. This was so far difficult due to the lack of accuracy of rotation sensors. Recently, ring laser technology was used to record earthquake-induced rotational ground motions and the consistency and accuracy of these observations could be demonstrated by comparing with theoretical predictions calculated with 3-D modelling tools (Igel et al., 2005; Cochard et al. 2006, Suryanto et al., 2006a). Furthermore, we could demonstrate – again with support from sophisticated 3-D modelling – that these additional observations allow the recovery of structural information on the subsurface (Suryanto et al., 2006b). These results have opened new routes into the potential use of such observations in earthquake engineering, earthquake seismology and tomography.

References (Highlights)

- [1] Brietzke, G. B., and Y. Ben-Zion, Examining tendencies of inplane rupture to migrate to material interfaces, *Geophys. J. Int.*, 167, 0, doi:10.1111/j.1365-246X.2006.03137.x, 2006a.
- [2] Brietzke, G. B., Cochard, A., and Igel, H., Dynamic Rupture Along Bimaterial Interfaces in 3D, *Geophys. Res. Lett.*, submitted, 2006b.
- [3] Cochard, A., Igel, H., Flaws, A., Schuberth, B., Wassermann, J., Suryanto, W., Rotational motions in seismology, in “*Earthquake source asymmetry, structural media and rotation effects*” eds. Teisseyre et al., Springer Verlag, 391-413, 2006.
- [4] Ewald, M., Igel, H., Hinzen, K.-G., Scherbaum, F., Basin-related effects on ground motion for earthquake scenarios in the Lower Rhine Embayment, *Geophys. J. Int.*, 166, 197-212, 2006.
- [5] Fohrmann, M., Igel, H., Jahnke, G., Ben-Zion, Y.: Guided waves from sources outside faults: an indication for shallow fault zone structure? *Pure Appl. Geophys.*, 161, 1-13, 2004.
- [6] Igel, H., G. Jahnke, and Y. Ben-Zion, Numerical simulation of fault zone trapped waves: accuracy and 3-D effects, *Pure Appl. Geophys.*, 159, 2067-2083, 2002a.
- [7] Igel, H., Nissen-Meyer, T., Jahnke, G., 2002b. Wave propagation in 3-D spherical section: effects of subduction zones, *Phys. Earth. Planet. Int.*, 132, pp. 219-234.
- [8] Igel, H., Schreiber, K.U., Flaws, A., Schuberth, B., Velikosevtsev, A., Cochard, A., Rotational motions induced by the M8.1 Tokachi-oki earthquake, September 25, 2003, *Geophys. Res. Lett.*, Vol 32, L08309, doi:10.1029/2004GL022336, 2005.
- [9] Jahnke, G., H. Igel and Y. Ben-Zion, 2002, Three-dimensional calculations of fault zone guided waves in various irregular structures, *Geophys. J. Int.*, 151, 416-426.
- [10] Suryanto, W., Igel, H., Cochard, A., Schreiber, U., Velikosevtsev, A., Schuberth, B., Love-wave dispersion from collocated measurements of rotation and translations, *Geophys. Res. Lett.*, submitted, 2006a.
- [11] Suryanto, W., Wassermann, J., Igel, H., Cochard, A., Vollmer, D., Scherbaum, F., A. Velikosevtsev, U. Schreiber, First comparison of seismic array derived rotations with direct ring laser measurements of rotational ground motion, *Bull. Seismo. Soc. Amer.*, 2006b, in print.
- [12] Thorne, M., T. Lay, E. Garnero, G. Jahnke, H. Igel, 3-D Seismic Imaging of the D" region beneath the Cocos Plate, *Geophysical J. Int.*, in print.
- [13] Wang, H., Igel, H., Cochard, A., Ewald, M., Numerical Green's Functions for Sub-Faults in 3-D: Application to the Newport-Inglewood Fault, Los Angeles Basin, *Geophys. J. Int.*, submitted, 2006.

Links

<http://www.geophysik.uni-muenchen.de>

<http://www.spice-rtn.org>

<http://konwihl.in.tum.de>

<http://www.erdbeben-in-bayern.de>

<http://elite.geophysik.uni-muenchen.de>

<http://www.rotational-seismology.org>

Main Project Partners:

University of Southern California, Los Angeles, CA.

SCRIPPS Institution of Oceanography, La Jolla, CA.

Institut de Physique du Globe, Paris.

Arizona State University, Tempe, AZ.

University of Tokyo, Japan.

A theoretical and experimental study of the anharmonic lattice dynamics of fluorite systems

Research Institution:

Forschungszentrum Jülich, 52425 Jülich, Germany

Institut Laue-Langevin, F-38042 Grenoble, France

Universität Regensburg, D-93040 Regensburg, Germany

Research Area:

Solid State Physics

Principal Investigator:

Dr. Karin Schmalzl

Researchers:

Prof. Dr. D. Strauch

As early as 1839, M. Faraday had studied crystals with the fluorite structure. He observed an anomalously high electrical conductivity in the solid material comparable to that of a molten salt, stemming from the mobility of the fluorine ions.[1] As this ionic conduction is a strongly temperature dependent and intrinsically anharmonic process, we have chosen fluorite systems like CaF_2 [2] and BaF_2 [3] as model systems to study the phenomenon of anharmonicity which is still difficult to predict reliably, in contrast to the harmonic properties which give very good results in many cases. CaF_2 is also widely used as a crystalline lens material for high-precision VUV optics, and BaF_2 represents an alternative material. The knowledge of volume- and temperature-dependent effects inducing stress and strain in this material is important. The technological importance asks for a good theoretical characterization of the fluorites.

In the harmonic approximation, the inter-ionic potential can be described by a parabola. In this approximation, the excitations of lattice waves (phonons) possess an infinite lifetime, and the lifetime is inverse to the width of the excitation peaks in the spectra. In contrast, anharmonic interactions (like is needed for hopping over potential barriers) show a finite lifetime and a non-vanishing peak width.

We have thus focused on the thermal motion of the atoms by investigating the temperature and volume dependence of the lattice dynamics.

Methods

The electronic, ground-state and lattice-dynamical properties have been determined within the framework of density functional theory using different computer program packages like Abinit, VASP or WIEN97 (see links below) within their common and well tested approximations (LDA and GGA). The parameter-free approach of this method constitutes a method equivalent to experiment.

From the experimental side we have used inelastic neutron scattering. Neutrons penetrate the whole of a crystal, interact with the atomic nuclei, and leave it with either gain or loss of momentum and of kinetic energy allowing conclusions about the arrangement and motion of the atoms in the system investigated.

The experiments have been performed with the three-axis spectrometers IN1, IN3, and IN8 at

Abstract

We contrast the results from density-functional calculations for solid-state systems with results from neutron-scattering experiments. In this article we report lattice-dynamical properties of the fluorite system CaF_2 . It is found that in CaF_2 the harmonic properties are reproduced quite well and that an important part of the anharmonic effects can be understood from the volume dependence of the energies and from the energy dependence of the channels for anharmonic decay.

Introduction

Anharmonic properties of materials affect our everyday life, e. g., in the form of the omnipresent thermal conductivity or thermal expansion appearing when warming up materials.

the Institut Laue-Langevin in Grenoble, France (see link below).

Results

Inelastic neutron scattering experiments have been performed on CaF_2 between 10 K and 1273 K. All phonon modes soften with increasing temperature, and a broadening of all excitation peaks occur. Figure 1 shows the temperature evolution of a selected but typical INS spectrum.

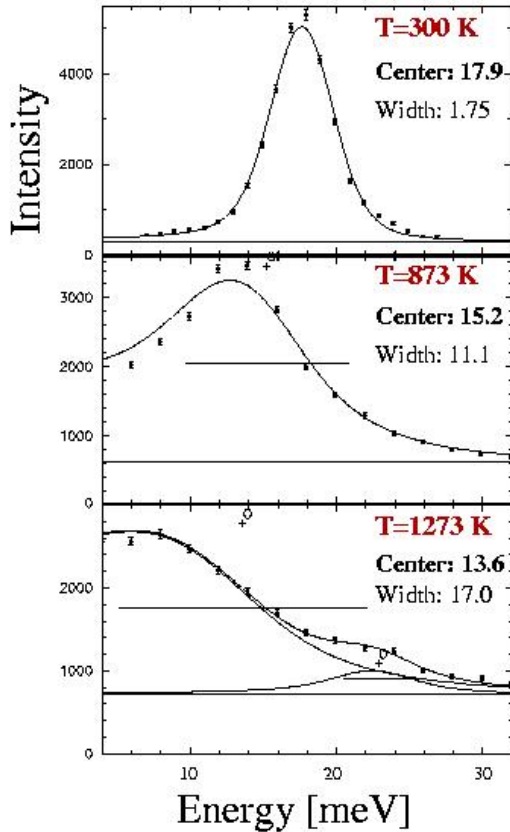


Fig. 1: Temperature dependence of selected raw data at the Brillouin-zone boundary (X point) fitted by a damped harmonic oscillator convoluted with the calculated instrumental resolution.

In parallel, electronic and harmonic lattice-dynamical properties have been calculated from ab-initio density-functional methods. Results for all modes along the [001] direction are shown in fig. 2 demonstrating the good agreement between theory and experiment.

Raising the temperature, the anharmonicity causes a down-shift in frequency and a broadening of the width of the lines in the spectra. The X'_2 mode at the Brillouin-zone boundary (X) is the lowest-energy mode (see fig. 2) and stands

out in so far as it has the largest shift in frequency with temperature. The width of all modes increases (except for the optical Γ_5 modes), and the width is larger for the optical than for the acoustic modes.

While anharmonic ab-initio methods are still under development, we have been able to calculate single anharmonic processes. To lowest order, there are three processes contributing to the anharmonic line shift: (1) thermal expansion, (2) coupling to thermal fluctuations, and (3) two-phonon decay. Process (1) can be investigated by calculating the phonon frequencies for various lattice volumes. In this way the process of thermal expansion can be separated from the other anharmonic phonon-phonon processes occurring and observed in an experiment.

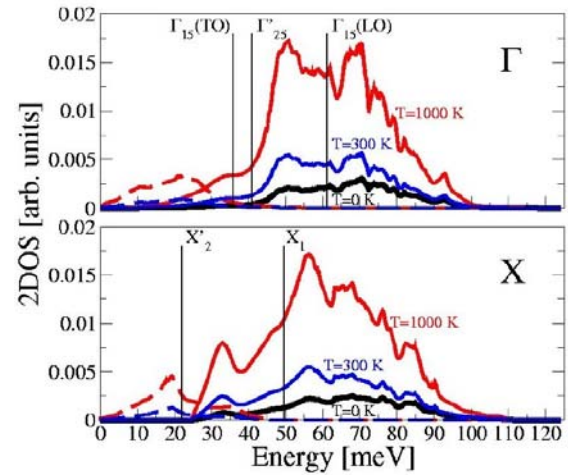


Fig. 2: Phonon dispersion curves (i.e., energy-momentum relations) for lattice waves along the [001] direction from experiment at $T = 10$ K (data points) and from ab-initio theory (black lines).

From the theoretical volume dependence of the phonon frequencies, a critical softening of the lowest-frequency X'_2 mode at the Brillouin-zone boundary is found, which is hard to be observed in the experiment, where the mode softens and becomes unobservable because of the increasingly large line width (see fig 1).

Comparing the experimental and theoretical results, it is found that the shift of the X'_2 mode can be explained by just thermal expansion. This holds for all X-point modes, while for the zone-

centre (Γ) the shift is overestimated, and the processes (2) and (3) have to be taken into account.

Only process (3) contributes to the line width. The process of two-phonon decay is proportional to (the square of) the coupling constants and the two-phonon density of states (2DOS) which is shown in fig 3. Assuming a constant coupling constant, the phonon width is proportional to the 2DOS taken at the phonon energy (indicated by vertical lines in fig. 3). Actually, this turns out to be a good approximation for the modes at the Γ and X points except for the X'_2 mode. Thus a detailed theory of the coupling constant is necessary here.

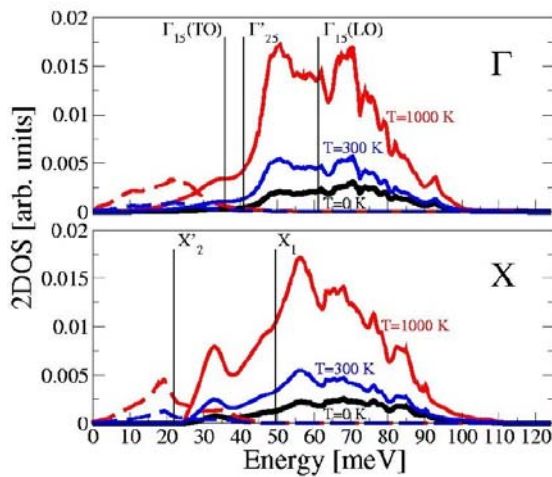


Fig. 3: Two-phonon combined density of states at the Brillouin-zone center (Γ) and -zone boundary (X): Contributions of the summation processes (full lines) and difference processes (broken lines) are shown. The vertical lines show the optical modes at Γ and the lowest and highest mode at X .

Summarizing, the harmonic properties of CaF_2 are quite well understood on the grounds of the density functional theory. Among the anharmonic properties, the process of thermal expansion seems to reproduce the phonon line shift of most of the X-point modes quite well, while the calculation of the line shift of the other modes as well as of the line widths needs the explicit knowledge of the anharmonic coupling constants, which are not available so far and the calculation of which poses a challenge for the future.

This report is largely taken from the ILL Annual Report 2003.

References

- [1] M. Faraday, Experimental Researches in Electricity, Vol. 1 (London 1839).
- [2] Schmalzl, K., D. Strauch, and H. Schober, 2003 : Lattice-dynamical and ground-state properties of CaF_2 studied by inelastic neutron scattering and density-functional methods. Phys. Rev. B, 68, 144301.
- [3] Schmalzl, K., 2006: Volume and pressure dependence of ground-state and lattice-dynamical properties of BaF_2 from density-functional methods. Submitted to Phys. Rev. B.

Links

<http://www.abinit.org>

<http://cms.mpi.univie.ac.at/vasp>

<http://www.ill.fr>

Quantum chromodynamics with chiral quarks

Research Institution:

Institute for Theoretical Physics
University of Regensburg
93040 Regensburg, Germany

Research Area:

Particle Physics

Principal Investigator:

Prof. Dr. Andreas Schäfer

Researchers:

Tommy Burch, Christof Gatttringer, Leonid Glozman, Meinulf Göckeler, Christian Hagen, Peter Hasenfratz, Dieter Hierl, Christian B. Lang, Ferenc Niedermayer, Stefan Solbrig, Tilo Wettig

Abstract

We have calculated properties of excited hadrons, e.g. excited states of the proton, the nucleon and the pion. Our results allow to reach conclusions about their internal structure, for example, whether some state is rather a 3-quark state like the proton or rather a 'molecule' consisting of, e.g., a proton and a pion.

Hadron Resonances

Normal nuclear matter is composed of neutrons and protons, which in first approximation can be thought of as three quark states bound together by gluonic interactions. The interaction creating such bound states is rather special, as it leads to 'confinement', meaning that quarks and gluons cannot be isolated. The detailed microscopic mechanisms leading to confinement are still not understood in detail and major experimental facilities, like the planned European research

center FAIR in Darmstadt address this problem already at present or will do so in the near future.

One way to investigate confinement is to study the excitation spectrum of hadrons. The ground states are predominantly 3-quark states (called baryons) like the proton and quark-antiquark states (called mesons) like the pion. In principle the spectrum of hadrons should be as characteristic for QCD as the level scheme of atomic hydrogen is for the Coulomb potential. In practice, however, it is far more difficult to establish the link between observed excited states and the underlying fundamental interaction. Presently, this can only be achieved by massively parallel numerical computations, an activity which has evolved into a major research field of its own, called Lattice-QCD.

Lattice QCD

In quantum field theory, the value of a field at every space-time point is treated as an independent variable. Therefore, in principle, one has to solve a problem with infinitely many degrees of freedom, which is only possible for a few, very special observables. In lattice QCD a volume of space-time, large enough to fit in, e.g., a proton, is replaced by a lattice of space-time points, fine enough to study the internal structure of, e.g., the proton with the resolution of interest. Thus one is left with a very high-dimensional problem. Different approaches use different discretizations of the QCD interaction. Several of these violate a specific symmetry QCD has in the continuum theory, the 'chiral symmetry'. Only in recent years, with the advent of Tflop computing, it became possible to use formulations which preserve chiral symmetry also in the discretized lattice formulation. Presently, a very intense discussion goes on, as to which chiral formulation and concrete algorithmic implementation is optimal for such studies. The understanding in the international community is, however, that while this development will certainly still need quite a number of years, in the end chiral fermions will become the standard in lattice QCD.

In our project we used and compared two variants of approximately chiral fermions, as it was unclear, which one would be more efficient. It turned out that both performed quite comparably in most respects, though for specific applications either one or the other is more suitable. Let

us stress that the development of well-performing (the efficiency reached on the Hitachi and Altix is above 20 percent) simulation codes for dynamical chiral fermions constitutes by itself a major break-through in our field.

The spectrum of hadron resonances

Without going into detail let us simply state that lattice-QCD is especially efficient in calculating the lowest mass eigenstate for a given set of quantum numbers. In recent years it became also possible to extract the masses of typically the lowest two to four excited states. Their signals are exponentially suppressed, but we and others have optimized techniques to still extract signals. These make it relatively straight-forward to study the nature of hadron resonances. A hadron is a complicated many particle quantum state which can be thought of as a superposition of many different Fock-states. On the lattice one introduces different combinations of quarks/antiquark fields (called sources and sinks) in different regions of the lattice and studies specific correlators, which provide the mass eigenvalues. The general approach is to study such correlations for a set of specifically chosen sources. If one obtains the correct mass eigenvalues of a resonance one can conclude that the offered sources permit a sufficiently large overlap with the physical wave function of that state. If not, then one can conclude that this is not the case. For example many meson resonances are assumed to have a large component with two quark-antiquark pairs rather than only one. On the lattice one can suppress such pairs (by using the so-called quenched approximation) and study which hadron states are affected. Fig.1 to 4 give some examples.

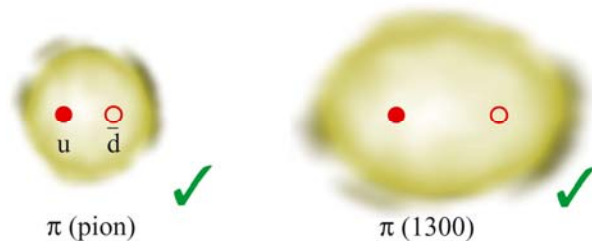


Fig.2 : Illustration of the result presented in Fig.1. The excited pion state is predominantly a quark-antiquark state and thus well reproduced when additional quark-antiquark pairs are suppressed.

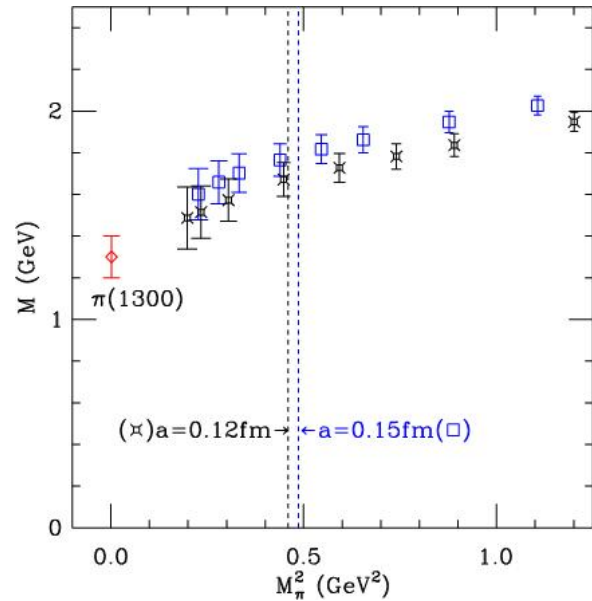


Fig. 1 : The first excited pion state. The physical mass is indicated by the leftmost point. Its value is roughly 1300 MeV, which is the usual mass unit in particle physics. With decreasing ground state pion mass (i.e., quark mass) our simulation points seem to converge nicely towards this point. The lattice constant is denoted by 'a'. The finer lattice gives an even better extrapolated result. This successful description of the pion resonance in the quenched approximation gives a clear indication that it is predominantly a simple quark-antiquark state.

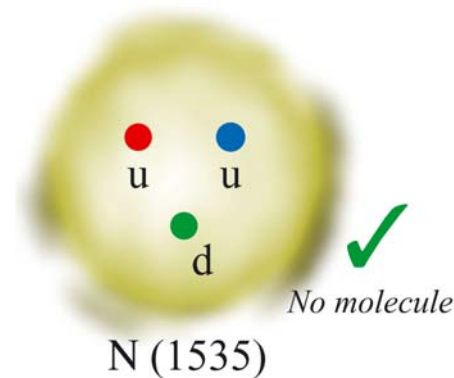


Fig. 2 : The excited nucleon states with negative parity (the usual proton has positive parity). One finds in the quenched approximation two nearly degenerate states which can be identified with the two resonances $N(1535)$ and $N(1600)$. This basically rules out the much discussed possibility that one of them is a pure molecule-like bound state of two hadrons. (Though their wave functions can still contain substantial molecule-like components.)

Results

To understand the figure 1 one has to know that the required computer time increases drastically if quark masses (respectively the mass of the normal pion, which is tied to the quark masses by a simple relation) are decreased and if the lattice is made finer. Therefore, calculations are performed with unphysically large quark masses and for different lattice constants 'a' and then one extrapolates to the physical masses and to $a=0$. Finally positive or negative parity characterizes states which are symmetric respectively anti-symmetric under space inversion.

References

- [1] T. Burch et. al., 2006: Excited hadrons on the lattice: Baryons, Physical Review D74, 014504
- [2] T. Burch et. al., 2006: Excited hadrons on the lattice: Mesons, Physical Review D73, 094505
- [3] A. Hasenfratz et al.: First results in QCD with 2+1 light flavours using the fixed-point action, hep-lat/0610096

Project Partners:

Institut für Physik, FB Theoretische Physik,
Universität Graz, A-8010 Graz, Austria

Institut für Theoretische Physik, Universität
Bern, CH-3012 Bern, Switzerland

Links

<http://homepages.uni-regensburg.de/~sca14496/schaefer.html>

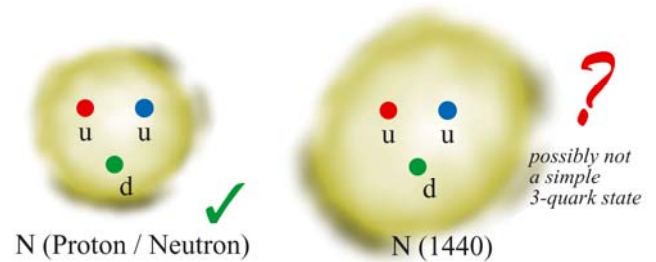


Fig. 3 : The excited nucleon states of positive parity. The ground state is reproduced very nicely, but the excited states come out substantially too high, indicating that the $N(1440)$ is possibly not a normal 3 quark bound state. (This was already strongly suspected.)

Metal-Insulator Transitions and Realistic Modelling of Correlated Electron Systems

Research Institution:

Theoretical Physics III, Center for Electronic Correlations and Magnetism, Institute for Physics, University of Augsburg

Research Area:

Physics

Principal Investigator:

Dieter Vollhardt

Researchers:

Georg Keller, Xinguo Ren

Scientific Collaborators:

Karsten Held (Physics Department, Princeton University), Volker Eyert (Institute for Physics, University of Augsburg), Vladimir I. Anisimov (Institute of Metal Physics, Ekaterinburg)

Introduction

The calculation of physical properties of electronic systems by controlled approximations is one of the most important challenges of modern theoretical solid-state physics. In particular, the physics of transition-metal oxides - a singularly important group of materials both from the point of view of fundamental research and technological applications - may only be understood by explicit consideration of the strong effective interaction between the conduction electrons in these systems. The investigation of electronic many-particle systems is made especially complicated by quantum statistics, and by the fact that the phenomena of interest (e.g., metal insulator transitions and ferromagnetism) usually require the application of non-perturbative theoretical techniques.

One of the most famous examples of a cooperative electronic phenomenon of this type is the

transition between a paramagnetic metal and a paramagnetic insulator induced by the Coulomb interaction between the electrons, referred to as Mott-Hubbard metal-insulator transition. The question concerning the nature of this transition poses one of the fundamental theoretical problems in condensed matter physics.^{1,2} Correlation-induced metal-insulator transitions (MIT) are found, for example, in transition metal oxides with partially filled bands near the Fermi level. For such systems band theory typically predicts metallic behavior. The most famous example is V_2O_3 doped with Cr.³⁻⁵

While at low temperatures V_2O_3 is an antiferromagnetic insulator with monoclinic crystal symmetry, it has a corundum structure with a small trigonal distortion in the high-temperature paramagnetic phase. The first-order transitions from the high-temperature paramagnetic phases into the low-temperature antiferromagnetic phase are naturally explained by the fact that the transition is accompanied by a change in crystal symmetry. By contrast, the crystal symmetry across the MIT in the paramagnetic phase remains intact, since only the ratio of the c/a axes changes discontinuously. This is usually taken as an indication for the predominantly electronic origin of this MIT, caused by strong correlations.

In the last decade, a new approach for treating electronic lattice models, the dynamical mean-field theory (DMFT), has led to new analytical and numerical opportunities to study correlated electronic systems.^{6,7} This theory, introduced by the work of Metzner and Vollhardt in 1989, is exact in the limit of infinite dimensions ($d=\infty$).⁸ In this limit, the problem is reduced to a single-impurity Anderson model with self-consistency condition,⁹⁻¹¹ allowing for a solution by quantum Monte-Carlo (QMC) simulations without a sign problem for one-band models (for multi-band models, see Ref. 12), i.e., down to temperatures $T \sim 10^{-2}W$ (W : bandwidth).

Recently, the LDA+DMFT, a new computation scheme that merges electronic band structure calculations and the dynamical mean field theory, was developed.¹³⁻¹⁸ Starting from conventional band structure calculations in the local density approximation (LDA) the correlations are taken into account by a Hubbard interaction term and a Hund's rule coupling term. The resulting DMFT equations are solved numerically with a parallelized auxiliary-field quantum Monte-Carlo algorithm. This scheme makes

possible the investigation of real systems close to a Mott-Hubbard transition such as the MIT in V_2O_3 discussed above. In this report, results on the correlation-induced metal-insulator transition and dynamic properties of multi-band Hubbard-type models at low temperatures obtained within the DMFT are presented. Calculations at experimentally relevant temperatures were made possible by the increased computer power of the Hitachi SR8000-F1. Here we report some of the results obtained during the allocation period 2001-2003.

Results

In a first step, LDA calculations were performed for paramagnetic *metallic* V_2O_3 and paramagnetic *insulating* $(V_{0.962}Cr_{0.038})_2O_3$, respectively.¹⁹ The LDA results for corundum V_2O_3 and $(V_{0.962}Cr_{0.038})_2O_3$ are very similar. In particular, the changes in crystal and electronic structure occurring at the transition are insufficiently reflected by the LDA calculations and the experimentally observed insulating gap is *missing* in the LDA DOS. It is generally believed that this insulating gap is due to strong Coulomb interactions which are not adequately accounted for by the LDA. This is where our LDA+DMFT(QMC) scheme sets in. Using this approach we can show explicitly that the insulating gap is indeed caused by electronic correlations. The spectra obtained by LDA+DMFT(QMC) imply that the critical value of U for the MIT is about 5 eV.¹⁹ Indeed, at $U=4.5$ eV one observes pronounced quasiparticle peaks at the Fermi energy, i.e., characteristic metallic behavior, even for the crystal structure of $(V_{0.962}Cr_{0.038})_2O_3$, while at $U=5.5$ eV the form of the calculated spectral function is typical for an insulator for both sets of crystal structure parameters.

Whereas for computations at $T=1100$ K (which were done on a workstation) we only observe metallic-like and insulating-like behavior with a rapid but smooth crossover between these two phases, calculations done on the Hitachi SR8000-F1 at lower temperatures show more pronounced differences between the metallic and insulating phase; the smooth crossover is replaced by a sharp first order metal-insulator transition.^{20,21} To compare with the photoemission spectrum of V_2O_3 by Schramme *et al.*,²² and Kim *et al.*,²³ the LDA+DMFT(QMC) spectra are multiplied with the Fermi function at $T=1100$ K and Gauss-broadened by 0.05 eV to account for the experimental resolution. In contrast to the

LDA results, the theoretical results¹⁹ for $U=5$ eV are seen to be in good agreement with experiment, see Fig. 1. We also note that the DOS is highly asymmetric with respect to the Fermi energy due to the orbital degrees of freedom. This is in striking contrast to the result obtained with a one-band model. The comparison (not shown) between our results, the data of Müller *et al.*²⁴ obtained by X-ray absorption measurements, and LDA shows that, in contrast with LDA, our results not only describe the different bandwidths above *and* below the Fermi energy (≈ 6 eV and $\approx 2-3$ eV, respectively) correctly, but even resolve the two-peak structure above the Fermi energy.

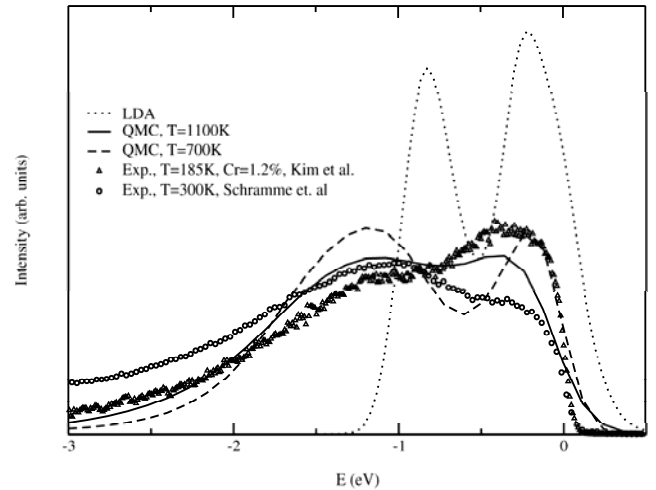


Fig. 1: Comparison of the LDA+DMFT(QMC) spectra¹⁹ with the LDA spectrum and the photoemission experiments on metallic V_2O_3 by Schramme *et al.*²² (pure sample) and Kim *et al.*²³ (Cr-doped sample).

Particularly interesting are the spin and the orbital degrees of freedom in V_2O_3 . We find that for $U \geq 3$ eV the squared local magnetic moment $\langle m_z^2 \rangle$ saturates at a value of 4, i.e., there are *two* electrons with the same spin direction in the $(a_{1g}, e_{g1,\pi}, e_{g2,\sigma})$ orbitals.¹⁹ Thus, we conclude that the spin state of V_2O_3 is $S=1$ throughout the Mott-Hubbard transition region. Our $S=1$ result agrees with the measurements of Park *et al.*²⁵ and also with the data for the high-temperature susceptibility. Thus LDA+DMFT (QMC) provides a remarkably accurate microscopic theory of the strongly correlated electrons in the paramagnetic phase of V_2O_3 .¹⁹

Acknowledgements

We gratefully acknowledge support by the Leibniz-Rechenzentrum through HLRB-project *h0531* and by the Deutsche Forschungsgemeinschaft through Sonderforschungsbereich 484.

References

- [1] N. F. Mott, *Rev. Mod. Phys.* **40**, 677 (1968); *Metal-Insulator Transitions* (Taylor & Francis, London, 1990).
- [2] F. Gebhard, *The Mott Metal-Insulator Transition* (Springer, Berlin, 1997).
- [3] D. B. McWhan and J. P. Remeika, *Phys. Rev. B* **2**, 3734 (1970).
- [4] D. B. McWhan *et al.*, *Phys. Rev. B* **7**, 1920 (1973).
- [5] T. M. Rice and D. B. McWhan, *IBM J. Res. Develop.* 251 (May 1970).
- [6] D. Vollhardt, *Investigation of correlated electron systems using the limit of high dimensions*, in: *Correlated Electron Systems*, ed. by V. J. Emery, World Scientific, Singapore, 1993.
- [7] A. Georges, G. Kotliar, W. Krauth and M. Rozenberg, *Rev. Mod. Phys.* **68**, 13 (1996).
- [8] W. Metzner and D. Vollhardt, *Phys. Rev. Lett.* **62**, 324 (1989).
- [9] M. Jarrell, *Phys. Rev. Lett.* **69**, 168 (1992).
- [10] M. Jarrell and T. Pruschke, *Z. Phys. B* **90**, 187 (1993).
- [11] A. Georges and G. Kotliar, *Phys. Rev. B* **45**, 6479 (1992).
- [12] One limitation of QMC is that it is very difficult to deal with the spin-flip term of the Hund's rule coupling because of a *minus-sign problem* which arises in a Hubbard-Stratonovich decoupling of this spin-flip term, see K. Held, Ph.D. thesis Universität Augsburg 1999 (Shaker Verlag, Aachen, 1999).
- [13] V. I. Anisimov, A. I. Poteryaev, M. A. Korotin, A. O. Anokhin, and G. Kotliar, *J. Phys.: Cond. Matt.* **9**, 7359 (1997).
- [14] A. I. Lichtenstein and M. I. Katsnelson, *Phys. Rev. B* **57**, 6884 (1998).
- [15] M. B. Zöfl, Th. Pruschke, J. Keller, A. I. Poteryaev, I. A. Nekrasov, and V. I. Anisimov, *Phys. Rev. B* **61**, 12810 (2000).
- [16] A. Nekrasov, K. Held, N. Blümer, A. I. Poteryaev, V. I. Anisimov, and D. Vollhardt, *Europhys. J. B* **18**, 55 (2000).
- [17] K. Held, I. A. Nekrasov, N. Blümer, V. I. Anisimov, and D. Vollhardt, *Int. J. Mod. Phys. B* **15**, 2611 (2001).
- [18] For an introduction into LDA+DMFT, see K. Held, I.A. Nekrasov, G. Keller, V. Eyert, N. Blümer, A.K. McMahan, R.T. Scalettar, T. Pruschke, V.I. Anisimov, D. Vollhardt, *Quantum Simulations of Complex Many-Body Systems: From Theory to Algorithms*, eds. J. Grotendorst, D. Marx and A. Muramatsu, NIC Series Vol. 10 (NIC Directors, Forschungszentrum Jülich, 2002), p. 175.
- [19] K. Held, G. Keller, V. Eyert, D. Vollhardt, and V. I. Anisimov, *Phys. Rev. Lett.* **86**, 5345 (2001).
- [20] M. J. Rozenberg, *Phys. Rev. B* **55**, R4855 (1997).
- [21] G. Moeller, Q. Si, G. Kotliar, M. J. Rozenberg, and D. S. Fisher, *Phys. Rev. Lett.* **74**, 2082 (1995); J. Schlipf, M. Jarrell, P. G. J. van Dongen, N. Blümer, S. Kehrein, Th. Pruschke, and D. Vollhardt, *Phys. Rev. Lett.* **82**, 4890 (1999); M. J. Rozenberg, R. Chitra and G. Kotliar, *Phys. Rev. Lett.* **83**, 3498 (1999); R. Bulla, *Phys. Rev. Lett.* **83**, 136 (1999).
- [22] M. Schramme, Ph.D. thesis, Universität Augsburg, 2000; M. Schramme *et al.*, unpublished.
- [23] H.-D. Kim, J.-H. Park, J. W. Allen, A. Sekiyama, A. Yamasaki, K. Kadono, S. Suga, Y. Saitoh, T. Muro, and P. Metcalf, *condmat/0108044*.
- [24] O. Müller, J. P. Urbach, E. Goering, T. Weber, R. Barth, H. Schuler, M. Klemm, S. Horn, and M. L. denBoer, *Phys. Rev. B* **56**, 15056 (1997).
- [25] J.-H. Park, L.H. Tjeng, A. Tanaka, J.W. Allen, C.T. Chen, P. Metcalf, J.M. Honig, F.M.F. de Groot, and S.A. Sawatzky, *Phys. Rev. B* **61**, 11 506 (2000).

Predicting the structure and properties of mineral surfaces and interfaces

Research Institution:

Department of Earth and Environmental Sciences, LMU

Research Area:

Physics - Solid State

Principal Investigator:

Dr. Rossitza Pentcheva

Researchers:

Prof. Dr. Wolfgang Moritz, Dr. Rossitza Pentcheva, Katrin Otte, Narasimham Mulakaluri

gain a microscopic understanding of the mechanisms of charge accommodation as well as structural and electronic relaxations at complex mineral surfaces and interfaces employing large scale density functional theory (DFT) calculations. Magnetite is important not only in paleomagnetism and mineralogy but is also a prospective material for the development of spintronic devices. The surface phase diagram of $\text{Fe}_3\text{O}_4(001)$ compiled in the framework of ab initio thermodynamics revealed that the origin of the experimentally observed surface reconstruction is a Jahn-Teller distortion instead of ordering of surface defects as simple electrostatic arguments would suggest. In the project extension we are studying the role of water adsorption on the surface stoichiometry and structure which is a fundamental process both in nature and technology. Further topics of intensive investigation include charge ordering phenomena at iron oxide or perovskite interfaces leading to novel magnetic phases or conductivity distinct from the bulk behavior.

Introduction

A multitude of important reactions both in nature and industry (e.g. catalysis) take place at mineral surfaces, some examples being the adsorption and dissociation of water, the adsorption and reduction of heavy metals, or ammonia synthesis to mention only a few. In order to understand and control the reactivity of these surfaces and/or tailor their electronic and magnetic properties, it is indispensable to know the surface structure and morphology at ambient conditions. To this end a major problem in modern surface science is that the vast majority of experimental techniques is restricted to UHV (ultra

Abstract

The surfaces and interfaces of transition metal oxides represent a natural disruption of the bulk charge neutrality and a multitude of unexpected properties have been observed that differ substantially from the ones of the corresponding bulk materials. The goal of project h0721 is to

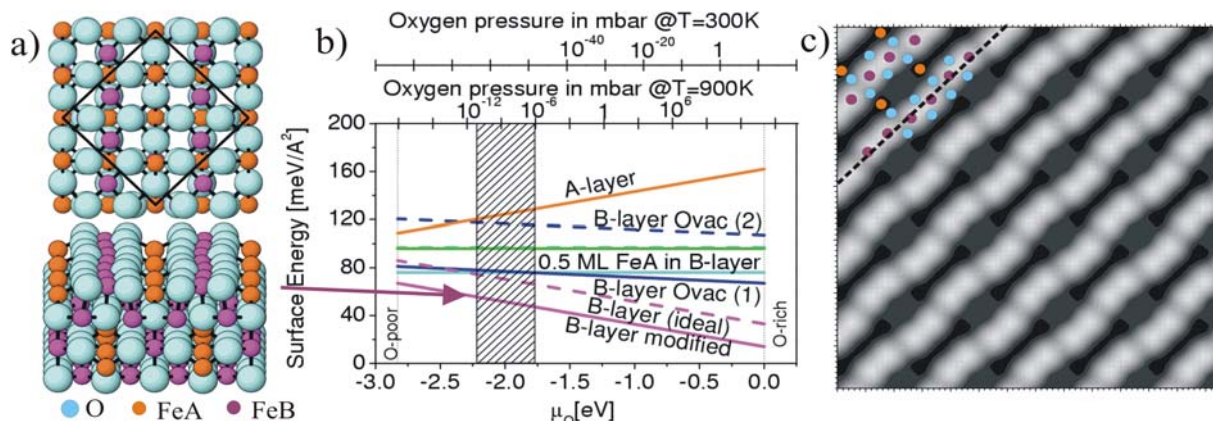


Fig. 1 : a) Jahn-Teller distorted modified bulk termination of $\text{Fe}_3\text{O}_4(001)$ predicted as lowest energy configuration over a broad range of oxygen pressures from the calculated surface phase diagram (b) · (c) STM-simulation of the surface layer

high vacuum). Furthermore, the insulating nature of most of the oxides limits the use of imaging techniques like scanning tunneling microscopy. Quantitative diffraction analyses for oxide surfaces are scarce and by far less satisfactory than for metal or semiconductor surfaces.

Method and Optimization of wien2k on SR8000

On the side of theoretical modeling, density-functional theory (DFT) has established in the past decades as a powerful tool to predict the properties and stability of technologically relevant materials. Last but not least this was recognized by the Nobel Prize for Chemistry given to Walter Kohn in 1998 for the development of DFT. However, this approach is restricted to $T=0$ and $p=0$. Only recently it has become possible to extend the predictive power of DFT to finite pressures and temperatures by combining DFT with concepts from thermodynamics in the framework of *ab initio atomistic thermodynamics*. The large system sizes necessary to model the complex structure of mineral surfaces makes DFT calculations extremely computationally demanding. Such calculations have only recently become feasible through the implementation of fine-grain parallelization schemes. After porting and optimizing the MPI parallel version of the WIEN2k code in collaboration with the Leibniz Rechenzentrum Munich on the Hitachi SR8000, we were able to achieve a performance of 5 GFlops per node (640 MFlops per CPU). This amounts to 42% of the theoretical peak performance of the machine and is a very good result for this type of code making it one of the best performing codes on SR8000.

Surface termination and Properties of $\text{Fe}_3\text{O}_4(001)$

Magnetite is one of the most important minerals in geophysics and mineralogy as it stores information on the earth magnetic field, and plays a role in the orientation of microorganisms and birds. Of technological relevance is the *half-metallic* behavior predicted for the bulk material i.e. it possesses a 100% spin polarization. This property coupled with the high magnetic ordering temperature of 858 K makes magnetite a prospective material for spintronics applications. Still, at surfaces and interfaces the properties may differ substantially from the bulk and are dependent on the surface structure. The surface

termination of magnetite(001) has been subject of a controversial debate in the literature. We performed systematic DFT-calculations employing the full-potential linearized augmented-plane wave method as implemented in the WIEN2k code for a variety of stoichiometric and non-stoichiometric terminations, including a full structural optimization of each system. The surface is modeled by supercells containing on the average 100 atoms and 1000 electrons resulting in matrix dimensions for the generalized eigenvalue problem of 18000×18000 .

It is typically assumed that the excess charges at a polar surface can be compensated by surface reconstructions. The latter are commonly understood as the ordering of surface vacancies. Contrary to this, the surface phase diagram of $\text{Fe}_3\text{O}_4(001)$ compiled in the framework *ab initio atomistic thermodynamics* [cf. Fig. 1b] reveals that a modified bulk termination which was hitherto ignored on the basis of simple electrostatic arguments is the most stable termination over a broad range of oxygen pressures. The results indicate a novel stabilization mechanism at polar oxide surfaces, where the surface periodicity is achieved by a *wave-like* distortion of the surface layer instead of an ordering of defects. This unusual stabilization mechanism is accompanied by dramatic changes in the electronic properties e.g. a *half-metal to metal* transition from bulk to the surface which may be relevant for future applications. Experimental results obtained by scientists in Munich, Aachen and Konstanz support the theoretically predicted model. The close collaboration between theory and experiment plays an important role in this project, e.g. the structural information from DFT is used as a starting point for quantitative diffraction analyses and vice versa. Current and future investigations include the influence of correlation effects beyond the generalized gradient approximation (GGA) as well as the adsorption of water and the impact of a humid atmosphere on the surface stability and electronic properties of oxide surfaces.

Correlated electron behavior at oxide surfaces and interfaces can lead to intriguing possibilities to compensate charge mismatch and polarity that do not exist at semiconductor interfaces. Novel charge and magnetic ordered phases evolving at oxide interfaces pose both fundamental questions and open new possibilities for technological applications. The recent resource extension at LRZ (e.g. the newly installed SGI ALTIX

4700) will be invaluable to tackle these numerically intensive and challenging problems.

References

- [1] R. Pentcheva, F. Wendler, H.L. Meyerheim, W. Moritz, N. Jedrecy, and M. Scheffler 2005 : Jahn-Teller stabilization of a "polar" metal oxide surface: Fe₃O₄(001). Phys. Rev. Lett. **94**, 126101.
- [2] R. Pentcheva 2006 : M. Fonin, R. Pentcheva, Yu. S. Dedkov, M. Sperrlich, D.V. Vyalikh, M. Scheffler, U. Rüdiger, and G. Güntherodt 2005 : Surface Electronic Structure of the Fe₃O₄(100): Evidence of a Half-Metal to Metal Transition. Phys. Rev. B **72**, 104436.
- [3] R. Pentcheva, F. Wagner, W. Moritz, und M. Scheffler 2005 : Structure, Energetics and Properties of Fe₃O₄(001) from First Principles in "High Performance Computing in Science and Engineering", p. 375, Springer Verlag.
- [4] R. Pentcheva 2006 : Predicting the Stability and Properties of Mineral Surfaces at Ambient Pressures. InSiDE (Innovatives Supercomputing in Deutschland) 4, 14.
- [5] M. Fonin, Yu.S. Dedkov, R. Pentcheva, U. Rüdiger and G. Güntherodt 2006 : Magnetite: A Search for the Half-Metallic State, submitted to Journal of Physics: Condensed Matter, Special Issue; Half-Metallic Ferromagnets
- [6] R. Pentcheva, J. Rundgren, W. Moritz, S. Frank, D. Schrupp, und M. Scheffler, 2006 : A Combined DFT/LEED-approach for complex oxide surface structure determination: Fe₃O₄(001). in preparation.

Links

<http://www.krist.geo.uni-muenchen.de/ober/pentche.html>

Project Partners:

Leibniz Rechenzentrum

Prof. M. Scheffler, FHI Berlin

Prof. W.E. Pickett, UC Davis

Prof. J. Rustad, UC Davis

Prof. G Güntherodt, RWTH Aachen

Prof. U. Rüdiger, Uni Konstanz

'Overlap' quarks in a 'twisted mass' sea: optimize computer power to understand the fundamental forces

Research Institution:

Humboldt Univ. Berlin, NIC/DESY Zeuthen, Freie Univ. Berlin, Muenster Univ., Wuppertal Univ., University of Milan "Bicocca", University of Rome "Tor Vergata", ECT*.

Research Area:

High-Energy Physics

Principal Investigator:

Dr. Cecilia Tarantino

Researchers:

Dr. Andrea Shindler, Dr. Thomas Chiarappa, Dr. Kei-Ichi Nagai, Dr. Mauro Papinutto, Prof. Giancarlo Rossi, Dr. Luigi Scorzato, Dr. Carsten Urbach, Dr. Urs Wenger, Dr. Ines Wetzorke, Dr. Stefan Schaefer, Dr. Federico Farchioni, Dr. Cecilia Tarantino.

Introduction

We have a quite good theory of fundamental interactions, which unifies all known forces (except gravity) and stood against experimental tests for the last 37 years. It is called the Standard Model and can explain an amazing variety of natural phenomena. However, the Standard Model involves about 20 free parameters which must be determined by matching experiments with theoretical predictions. As far as we can see, these parameters show no clear pattern although this is difficult to say because we do not know them very precisely. If we could know them better, we would probably be able to un-

derstand what is the idea behind them, or even find a limit of the model. However, in order to do this, we need to link precise experimental results to those fundamental parameters. In other words, we need to compute precisely how something that we can measure depends directly on those parameters. Such computations are very hard, because Quantum Mechanics forces us to take into account all possible ways in which the elementary constituents can interact with each other. There are two main methods to perform them: the first one consists in assuming that our universe is not so different from a very simple one (in which particles do not interact and evolution is trivial) and systematically compute the deviations (or perturbations) from that. This is called the 'perturbative' approach which works well for some processes. However, there are many phenomena where the perturbative approach cannot work: the most evident example is the proton (or the neutron). Such particles are build up of more elementary objects called 'quarks' and the quarks are bound together by the so called 'strong force' or 'QCD' (Quantum Chromo Dynamics), which is one of the two main building blocks of the Standard Model. The behaviour of quarks inside the proton is very far from the very simple model without interaction, and the lack of a good description of particles like the proton is the main reason why the parameters of the standard model cannot be determined precisely. Here comes the second approach. The idea is to describe the space-time by a four dimensional lattice (three dimensions for space and one for time). In this set up elementary particles are described by complex waves in the lattice. In order to compute the physical quantities that we wish, we have to sample these waves in all the possible ways which are allowed by the Standard Model (or at least those which have a significant probability). This task can be automatized and given to a computer. The idea is not new and it goes back to the early days of the Standard Model and is called the 'lattice' approach. However, a naive application of this idea is a too hard task for any conceivable computer. In the past 30 years much progress have been made in the various aspects which are crucial to perform realistic simulations. Important 'non-perturbative' phenomena (i.e. which cannot be explained in the perturbative approach) have been qualitatively explained, such as confinement of quarks in the proton. But it is only in recent years that lattice methods reached the maturity to aim at precise computation with good control over all systematic ef-

fects. One of the crucial steps, in order to achieve this, is the choice of the 'discretization' of light quarks, which I explain below.

The way to represent a wave on a discrete lattice is not unique. A given choice is called 'discretization' and it is very important to select carefully the optimal one. A requirement which is hard to fulfill is a discretization of quarks that allows them to be very light. In fact the so called 'up' and 'down' quarks which build up the proton and the neutron happen to be almost massless and (by special relativity) move almost at the speed of light. However, if we try to produce a wave on the lattice which describes a massless quark, we get also many other unphysical waves, which also move at the speed of light but exists only on the lattice and are therefore unwanted lattice artifacts (to make a rough picture, imagine to color the lattice vertices with white if they can be reached with an even number of steps from the origine, and with black if this number is odd. Then imagine a wave with opposite phases in white and black points. Such waves only make sense in a discrete lattice, have no physical meaning and should be suppressed, in order to do correct computations). The safest way to eliminate such unwanted modes is to introduce a (fake) fifth space dimension together with a potential well, which is devised to trap only physical modes in the four physical dimension. This is called the 'overlap' discretization, which is theoretically very clean but also very expensive. An alternative is to give explicitly a mass to the unwanted unphysical modes, however this simple procedure necessarily disturbs also the properties of the physical modes at small energies. One way to disturb less the physical waves is to play with the sign of the masses of the unphysical waves. Different choices of sign of the unphysical masses can improve different physical quantities. This procedure is called 'twisted mass' discretization, whose symmetry properties are only approximate, but simulations are cheaper. In this project we use the overlap discretization to represent the quarks which build the proton (so called 'valence quarks') and the twisted mass discretization to represent the quarks which populate the quantum vacuum (so called 'sea' quarks). In fact for valence quarks exact symmetry properties are more crucial than for sea quarks. However it is the sea quarks that constitute by far the most expensive part of the computational cost. In this way we can optimize the computational resources.

Also thanks to the Hitachi SR8000 at LRZ, we have already produced a large amounts of 'snapshots' of the vacuum which include the effect of twisted mass sea quarks. This is the essential background which is needed to compute all other physical interactions. We have also performed various tests of some properties of overlap valence quarks. In particular, the interaction between quarks and gluons is local, as it should be in Relativistic Quantum Mechanics and the effects which do not conserve probability (this is also required by Quantum Mechanic) are under control.

Parallel Free-Surface and Multi-Phase Simulations in Complex Geometries using Lattice Boltzmann Method

Research Institution:

Institute of Computer Applications in Civil Engineering, Technical University of Braunschweig

Research Area:

Enviromental Sciences

Principal Investigator:

Prof. Dr. Manfred Krafczyk

Dr. Jonas Tölke

Researchers:

Dr. Jonas Tölke, Benjamin Ahrenholz, Jannis Linxweiler, Sören Freudiger, Sebastian Geller, Björn Nachtwey, Christoph van Treeck

Abstract

This project focused on the design, development, implementation and optimization of methods, algorithms and software for very-large scale simulations of free surface and multi-phase flows based on the generalized lattice Boltzmann (GLBM) method. Parallel solvers based on hierarchical grids and cache optimized algorithms have been developed to simulate multi-component-multi-phase and turbulent transient flows in arbitrarily complex threedimensional geometries.

The first subproject is concerned with the accurate and reliable prediction of transport of contaminants and nutrients in porous media (soils) on different scales (DFG-Project MUSKAT, *Multi Scale Transport in soils* and FIMOTUM, *First principle based transport in unsaturated media*). The second subproject investigates air-water flow in research waste water batch reactors (SFB 411, Prof. Wilderer,

Fundamental Studies of Aerobic Biological Wastewater Treatment). The third subproject is concerned with the the simulation of free surface flows for different engineering applications.

Multiphase flows

Multiphase flow in a bioreactor:

The flow geometries are obtained from polydisperse sphere packings generated by molecular dynamics type simulations delivering locations of spheres which are mapped onto the computational grid for the fluid simulation. These carrier-bodies are covered with a biofilm that is supposed to eliminate toxic substances in the waste water.

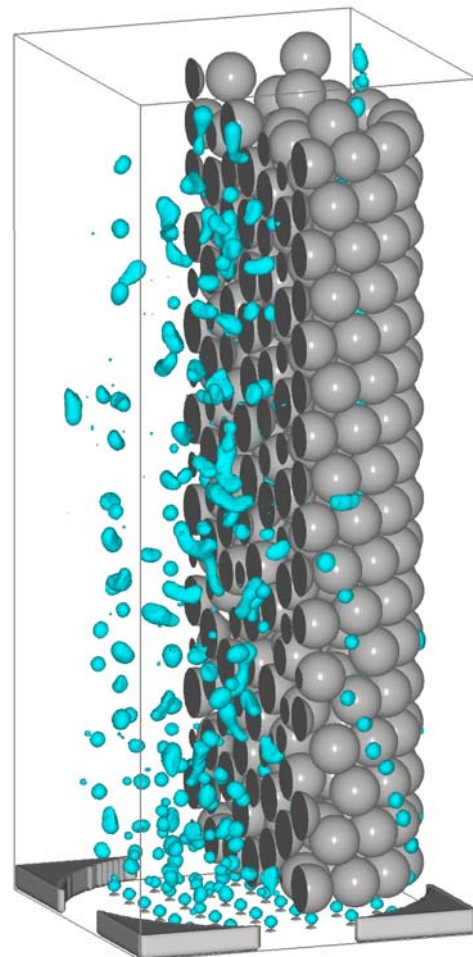


Fig. 1 : Distribution of air phase in a bioreactor

The biofilm growth rate (and thus the cleaning performance of the batch reactor) on these spheres critically depends on the available integral air concentration in the wastewater

ambience which itself depends on the geometry and positioning of air inlet nozzles of the reactor. We generated different sphere packings and setups to homogenize and optimize integral air concentrations in a laboratory scale batch reactor containing up to 5.000 mineralic spheres with diameters around 6 mm. For this multiphase system we computed the fully transient 3D problem on grids of up to 50 million nodes. In Fig. 1 the distribution of the air phase during the aerobic phase is shown. (Tölke et al., 2002)

Multiphase flow in soils:

The goal of MUSKAT/FIMOTUM is to predict appropriate material functions for multiphase transport in porous media (unsaturated soils) based on the pore space geometry and the physical properties of the two-fluid system. To reach this goal, direct numerical simulations on the microscale of the two-phase system based on artificially generated as well as reconstructed porous media are performed. The flow geometry is obtained directly from x-ray tomography with a typical resolution of 10 micrometers.

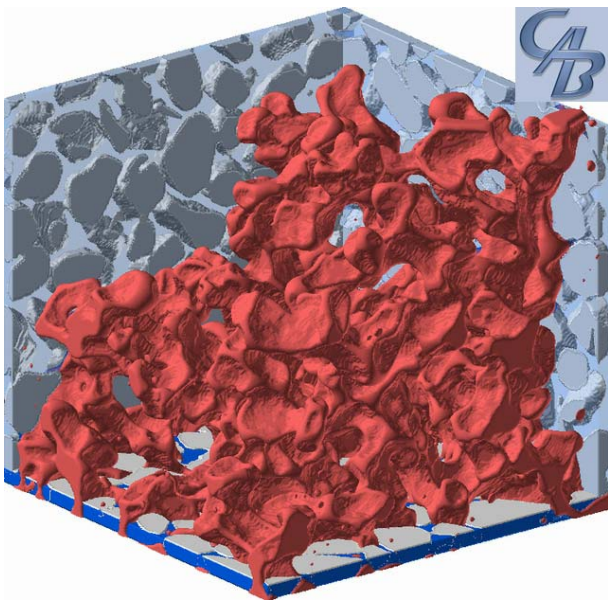


Fig. 2 : Distribution of air phase in a porous medium

To obtain on the one hand a representative elementary volume of the porous medium including the multiphase dynamics and on the other hand a sufficient resolution large grids up to 1000^3 nodes are needed. Although the flow in such porous systems is typically laminar, the sheer complexity of the three dimensional pore space in combination with the formation of interfaces makes multi-phase pore scale simulations extremely demanding. In Fig. 2 the distribution of the air phase in a porous medium during a drainage simulation is shown. (Ahrenholz et al., 2006)

Free Surface Flows

Free surface flows are characterized by a geometrically changing fluid domain by the motion of the fluid and appropriate boundary conditions at the free surface. They require a different treatment than multiphase flows to obtain a good parallel performance due to the load balancing problem. Applications are the simulation and optimization of flows over spillway weirs and the effects generated by obstacles in rivers and channels. In Fig. 3 the flooding of a bridge is shown.

Future Work

The future work focuses on the development, implementation and optimization of methods using *adaptive* hierarchical grids based on the LB-method. By using adaptive refinement and coarsening we are confident to substantially improve the predictive capability of multi-phase and free surface simulations.

Usually high-end supercomputers such as the HLRB-System are utilized to extend our knowledge in terms of basic research which is the goal of the present project line.

In the future the computing power of the HLRB2-system will be also used to predict flooding and wave impact events (e.g. Tsunamis) by faster than real-time simulations of a coupled system of a 2D shallow water and a 3D free surface kinetic model. The geometric and topographic input is obtained automatically from a GIS-system. This approach is expected to improve our abilities to predict the possible impact of flow related natural catastrophes on civil infrastructure and to support the design of evacuation and support activities.

References

- [1] M. Schulz, J. Tölke, M. Krafczyk, E. Rank: Parallel single- and multiphase CFD-applications using lattice Boltzmann methods. Transactions of the first joint HLRB and KONWIHR status and result workshop, October 10-11, 2002, Munich, Germany. Berlin: Springer. 91-103 (2003)
- [2] J. Tölke, S. Freudiger, M. Krafczyk (2006): An adaptive scheme for LBE Multiphase Flow simulations on hierarchical grids, Computers & Fluids, Volume 35(8-9): 820-830
- [3] J. Tölke, M. Krafczyk, M. Schulz, E. Rank (2002): Lattice Boltzmann Simulations of binary fluid flow through porous media, Philosophical Transactions of the Royal Society of London, Series A Mathematical, Physical and Engineering sciences, 360 (1792): 535-545.
- [4] B. Ahrenholz, J. Tölke, M. Krafczyk (2006): Second-order accurate Lattice Boltzmann flow simulations in reconstructed porous media, accepted for publ. in International Journal of Computational Fluid Dynamics.
- [5] S. Geller, M. Krafczyk, J. Tölke, S. Turek, J. Hron (2006): Benchmark computations based on Lattice-Boltzmann, Finite Element and Finite Volume Methods for laminar Flows, Computers & Fluids, Volume 35(8-9): 888-897

Links

<http://www.cab.bau.tu-bs.de>

<http://www.lrz-muenchen.de/services/compute/>

Project Partners:

Leibniz Rechenzentrum München

Lehrstuhl für Bauinformatik, TU München

Institut für terrestrische Ökologie, ETH Zürich

Institut für Wasserbau, Universität Stuttgart

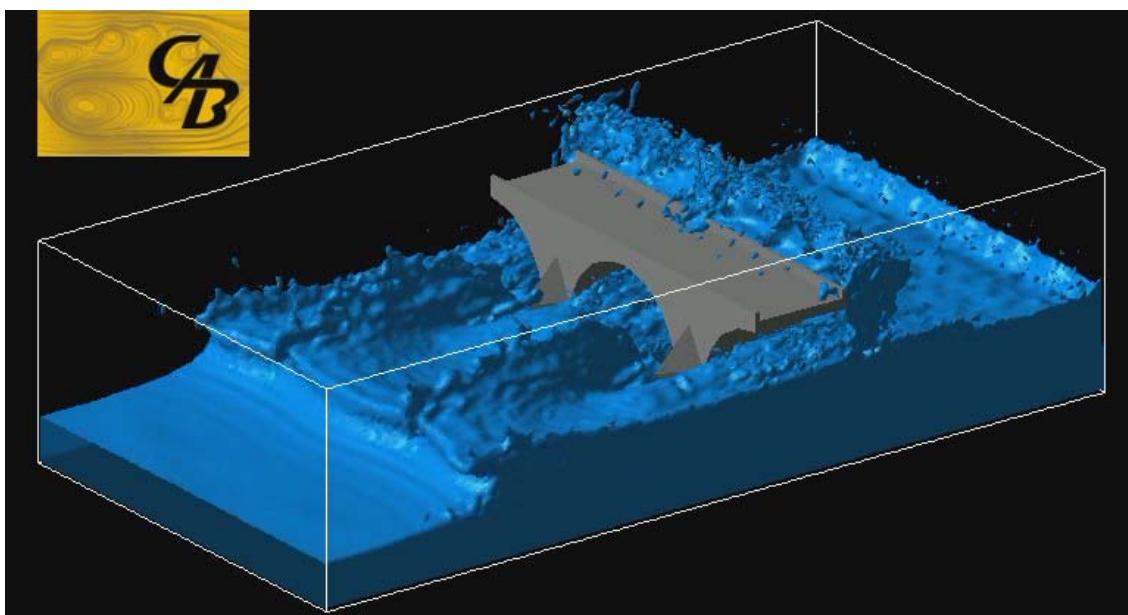


Fig. 3 : Flooding of a bridge

Adsorption of DNA base molecules on solid surfaces studied from massive parallel first-principles calculations

Research Institutions:

Theoretische Physik, Universität Paderborn and Institut für Festkörperteorie und Theoretische Optik, Universität Jena

Research Area:

Computational Materials Science

Principal Investigator:

Prof. Dr. Wolf Gero Schmidt

Researchers:

Dr. Patrick Hahn, Dr. Kaori Seino, Martin Preuss, Andreas Hermann, Frank Groth, Frank Ortmann

Abstract

Possible bonding scenarios for the adsorption of organic molecules on solid surfaces were studied using first-principles calculations. The adsorption of uracil on Si(001) and the adsorption of adenine on Cu(110) and graphite(0001) surfaces serve as prototypical examples to highlight relevant molecule-substrate interactions and their consequences for the properties of the adsystem. Covalent bonds formed during organic reactions with semiconductor surfaces significantly modify the structural and electronic properties of both the adsorbed molecules and the substrate. Organic molecule adsorption on metals may be driven by mutual polarisation that leads to substantial charge transfer and re-hybridisation, despite small adsorption energies. Subtle effects related to the lowering of the kinetic energy of the valence electrons as well as dispersion forces,

finally, govern the interaction between the organic molecules and chemically inert substrates such as graphite.

Motivation

Organic molecules are very promising building blocks for electronic devices due to the possibility of tailoring molecules with particular properties, the tunability of their characteristics, and the efficiency and flexibility of deposition methods. Self-organisation of organic molecules appears as one of the most promising approaches to the further miniaturisation of electronic devices. This so-called

bottom-up approach contrasts with the exponentially increasing fabrication costs of further down-scaling the lithographic processes in the top-down approach for device manufacturing. The latter approach already has led to atomic dimensions (the gate oxide thickness of the presently produced transistors of the 65 nm generation amounts to only 1.2 nm, i.e., about 4-5 atomic layers!) and is bound to lead soon to fundamental physical limits. The rich variety of living structures that are all based on different combinations of a few molecular building blocks, i.e., amino acids, proves the usefulness and robustness of the bottom-up approach for producing complex structures. However, we are only beginning to understand how the mechanisms of molecular recognition and self-assembly could be exploited for actual device production. In order to investigate the molecular self-organisation, suitable model systems need to be found that allow studying the molecular interactions reproducibly and with high accuracy. Surface adsorbed molecules are an obvious choice. They are accessible to sophisticated surface analysis tools such as scanning tunnelling microscopy (STM) as well as electron diffraction techniques, infrared and other optical spectroscopies. However, suitable substrates must be chosen that ensure that the molecule-molecule interactions are not completely masked by the interactions between the substrate and the molecules. In this context, metal substrates or graphite are often used as static checkerboards for the molecules. In particular in the latter case, the substrate induced perturbations of the molecular properties are minimal and the molecule seems to swim freely on the substrate, as illustrated in Fig. 1 for the case of adenine adsorbed on graphite (0001) [1].

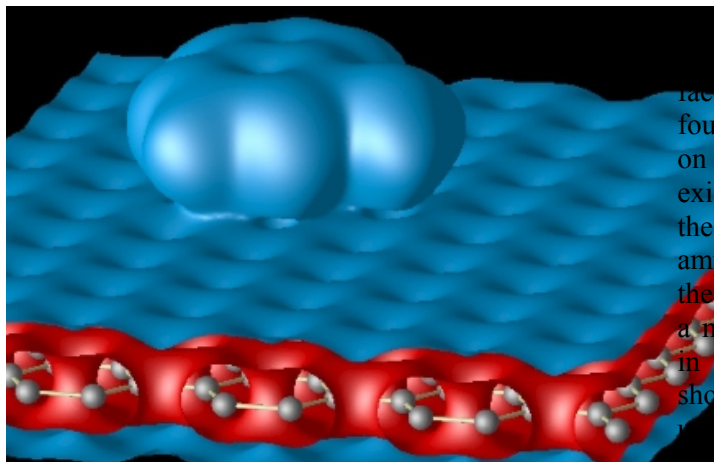


Fig. 1: Isosurfaces of the calculated total valence charge density of adenine adsorbed on graphite(0001). The positions of the carbon atoms in the uppermost graphene sheet are indicated.

Results

The adsorption of uracil on Si(001), investigated experimentally by STM and high-resolution electron energy-loss spectroscopy leads to what can be considered a prototypical interface between a polyfunctional organic molecule and a semiconductor surface. The (001) surface of silicon is the starting point for the fabrication of most microelectronic devices. Uracil is a small molecule featuring one C=C double bond, two N-H and two carbonyl groups and may thus bond to the surface in various ways. In addition, its tautomerism and electrostatic effects have been found to be important for the interface formation [2]. From accurate first-principles calculations [2], we find that the electronic properties of the uracil/Si(001) interface depend strongly on the details of the chemical bonding and adsorption geometry. Dative-bonded interfaces are characterised by a high density of states in the energy region of the fundamental gap and a very strong reduction of the ionisation energy. The formation of covalent bonds at the interface accompanied by a transfer of protons from the molecule to the semiconductor surface leads to an electronically passivated surface with an ionisation energy close to the value of the clean surface.

The interaction of large and complex organic molecules with metal surfaces gives rise to fascinating phenomena of molecular recognition and self-assembly that are basically not understood. Already the interaction of single polyfunctional molecules with metal substrates raises

number of interesting questions. The complex interplay and mutual influence between the surface-molecule bonds and intra-molecular bonds found already for simple hydrocarbons adsorbed on metals may be substantially enhanced by the existence of various functional groups. Using the adsorption of adenine on Cu(110) as an example, we have shown that at least in this case the interaction of a polyfunctional molecule with a metal substrate can seemingly be rationalised in a simple and intuitive picture [3]. Fig. 2 shows that the charge density redistribution upon adenine adsorption on Cu(110) cannot be interpreted in terms of covalent interactions. However, the bonding can to a large extent be explained in terms of an attractive interaction due to image charges induced in the metal substrate plus a repulsive contribution from the strain effects resulting from the molecular and substrate deformations.

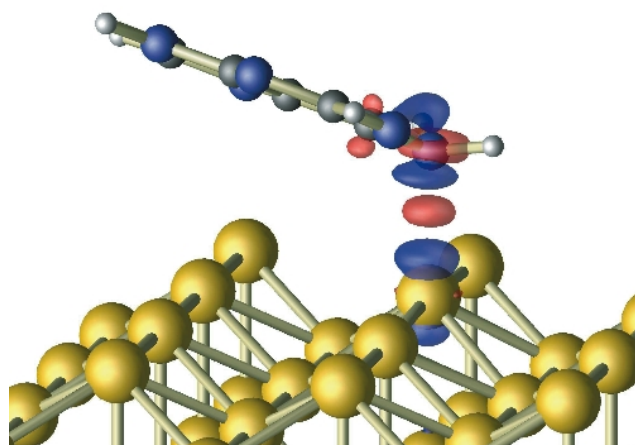


Fig. 2: Total charge density difference plot. Regions of electron accumulation/depletion are displayed in blue/red. Note that within the N-Cu bond center a charge depletion occurs, in contrast to the behaviour typical for covalent bonds.

It seems very likely that the combination of attractive image forces with repulsive deformation energies is characteristic for many more organic molecules adsorbed on metal surfaces. Thus a weak bond does not imply a weak interaction, but a small resulting net energy gain. Due to the very weak, mainly dispersive, interactions between ad molecules and substrate, molecular adsorption on inert surfaces provide an excellent model to probe single molecules and intermo-

molecular interactions. On the other hand, the accurate description of the molecule-substrate interactions is particularly challenging in this case, because dispersive interactions have to be taken into account. Using a modified version of the London dispersion formula, we studied numerically the adsorption of adenine on graphite [1]. Remarkably, we found an attractive interaction not only from van-der-Waals forces, but also due to the lowering of the kinetic energy of the molecular valence electrons upon adsorption. Fig. 3 shows the calculated total-energy surface seen by adenine adsorbed on graphite, which was shown on the cover page of the Physical Review Letters.

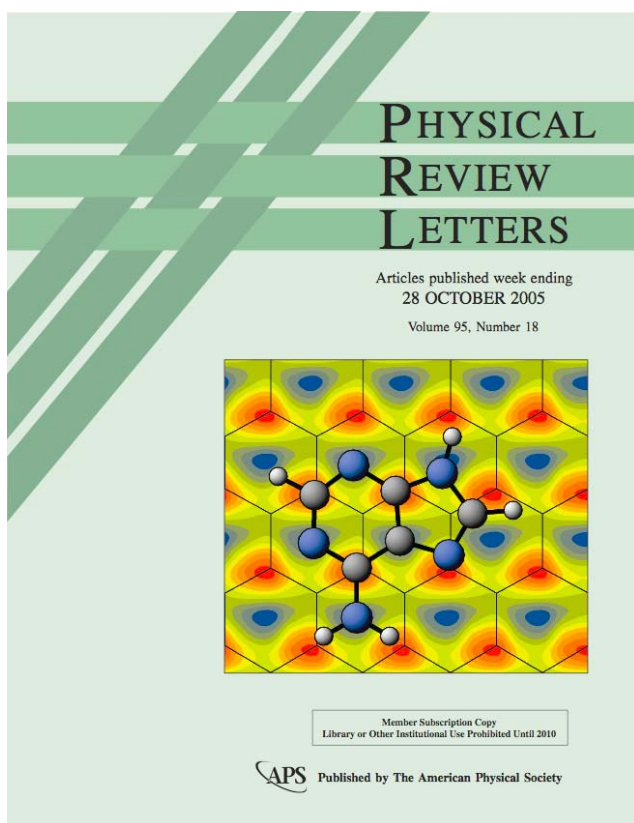


Fig. 3: Calculated potential energy surface as seen by adenine gliding on a graphite surface.

Acknowledgment

We thank Prof. Friedhelm Bechstedt for numerous, extremely helpful discussions. Generous grants of computer time from the Leibniz-Rechenzentrum München (HLRB), the Höchstleistungsrechenzentrum Stuttgart (HLRS) and the Paderborn Center for Parallel Computing (PC²) are gratefully acknowledged.

References

- [1] F Ortmann, WG Schmidt, F Bechstedt, Phys. Rev. Lett **95**, 186101 (2005); selected for Virtual Journal of Biological Physics Research 10(9) (2005).
- [2] K Seino, WG Schmidt, F Bechstedt, Phys. Rev. B **69**, 245309 (2004).
- [3] M Preuss, WG Schmidt, F Bechstedt Preuss PRL Phys. Rev. Lett **94**, 236102 (2005); selected for Virtual Journal of Nanoscale Science & Technology **11(25)** (2005).

Links

<http://www.phys.uni-paderborn.de/~wgs/>

FDEM Project

Research Institution:

RZ at University of Karlsruhe

Research Area:

Computer Science

Principal Investigator:

Prof. Dr. Willi Schönauer

Researchers

Dr. Torsten Adolph

consistency order q . This is an unprecedented generalization of the finite difference method. For practical reasons we use only the orders $q=2, 4, 6$. The unique property of FDEM is the computation of the discretization error estimate from the difference of formulas of order $q+2$ and q . For arbitrary nonlinear systems of PDEs the differential operator is

$$Pu \equiv P(t, x, y, z, u, u_t, u_x, u_y, u_z, u_{xx}, u_{yy}, u_{zz}, u_{xy}, u_{xz}, u_{yz}) = 0.$$

For a system of m PDEs u and Pu have m components. The linearization with the Newton-Raphson method and discretization including the error estimate leads to the error equation, part of which is the Newton correction. The FDEM code is efficiently parallelized with MPI.

The computers

We consider as a realistic case for the characterization of a computer the vector triad with data from memory

$$a_i = b_i + c_i * d_i$$

That needs 3 loads and 1 store per cycle and arithmetic unit, so it measures the memory bandwidth, for data from cache it measures the cache bandwidth, see [3]. Fig. 1 gives the characteristics of the measured computers that were accessible to us until June 2001. For the comparison we want to have a computer with total theoretical peak performance of 24 000 MFLOPS. Where we do not meet this value we give a correction factor for the measurements.

The comparison

The model problem were the Navier-Stokes equations in velocity-vorticity form, see[1], that contain the Reynolds number Re . For large value of Re the equations are critical. We introduced forcing terms so that the exact solution is of sugar loaf form. The 2-D rectangular grid on a 4x1 domain is 256x128 nodes, 64770 linear triangles and 98304 unknowns. Case 1 is for $Re=1$, here BICGstab2 converges, Case 2 is for $Re=10\ 000$, here we need full LU preconditioning with fill-in of the sparse matrix. Fig. 2 shows the results of the measurements. Although we have selected computers with the same theoretic

Abstract

This is a short report on the paper "The Same PDE Code on Many Different Parallel Computers" [1]. The idea was to run a complicated partial differential equation (PDE) solver code on many different supercomputers with the same theoretical peak performance and then to look for a formula that allows to extrapolate from the measurement of one computer for this code to an other computer by only measuring the vector triad of the other computer.

The FDEM

The FDEM (Finite Difference Element Method) program package [2] is a black-box solver for arbitrary nonlinear systems of elliptic and parabolic (eventually hyperbolic) PDEs developed at the University of Karlsruhe with a grant of the German Ministry of Research (BMBF). We select from the element list of an unstructured FEM mesh appropriate nodes and generate from these nodes difference formulas of arbitrary

cal peak performance the performances are partly quite different. The reason is that the computers with best performance have a better relative memory bandwidth because this is the bottleneck. We had expected a superior performance of the Hitachi because this computer has PVP, Pseudo Vector Processing that streams by prefetching data from memory into the cache or into the registers, see [4]. However, the measurement showed that this property of PVP does not improve performance because it does not increase the memory bandwidth. Also translation with COMPAS that combines 8 processors to a unit, gave a poorer performance.

We made several attempts to find a model that allows from the measurement of one computer, in our case the IBM SP WinterHawk-2, to extrapolate in the ratio of the vector triads the performance of another computer. This succeeded only for the 4 computers with quite similar architecture: IBM WinterHawk, Compaq, SGI and SUN and it failed for the other computers. This shows that not only the vector triad which is a measure of the memory bandwidth is decisive but also the complicated interplay of all components of a parallel computer.

Fig. 1: Configurations, properties and measure-

no.	computer	f MHz	theor. peak per proc. MFLOPS	p no. of proc.	theor. peak config. (time correct. factor)	max. perf. for vector triad for data from			max. comm. double ping- pong (inter) MB/sec
						L1- cache (size)	L2- cache (size)	me- mory	
1	IBM SP NightHawk-2 Power3-II proc.	375	1500	16 (2 nodes)	24000	303.0 (64 KB)	163.9 (8 MB)	46.3	40.6 IP ^a
2	IBM SP WinterHawk-2 Power3-II proc.	375	1500	16 (8 nodes)	24000	294.1 (64 KB)	169.5 (8 MB)	48.8	209.7 (74.7)
3	IBM SP Thin120SC	120	480	50	24000	222.2 (128 KB)	—	53.1	53.6
4	Hitachi SR8000-F1 without COMPAS	375	1500	16	24000	537.6 (128 KB)	—	224.2	545.7 PVP ^b (394.1)
5	Hitachi SR8000-F1 with COMPAS	375	1500	16 (2 nodes)	24000	383.9 (128 KB)	—	182.8	394.1 PVP ^b
6	HP Superdome PA8600 proc.	552	2208	12	26496 (1.104)	370.4 (1 MB)	—	34.8	307.2
7	Compaq Wildfire Alpha 21264 proc.	731	1462	16	23392 (0.975)	428.6 (64 KB)	230.8 (4 MB)	13.6	307.2
8	SGI Origin 3000 MIPS R12000 proc.	400	800	30	24000	188.7 (32 KB)	78.1 (8 MB)	33.0	116.3
9	SUN Fire 6800 ^c (prefetch disabled) UltraSPARC-III proc.	750	1500	16	24000	371.7 (64 KB)	94.1 (8 MB)	16.8	89.7
10	CRAY T3E-1200 Alpha 21164 proc.	600	1200	20	24000	345.6 (8 KB)	301.2 (96 KB)	70.8	199
11	Fujitsu VPP300	140	2240	10	22400 (0.933)	—	—	671.5 (vector)	473
12	Fujitsu VPP5000	300	9600	2	19200 (0.800)	—	—	2361.4 (vector)	1420

^a For 8 proc. per node only the slow IP-prot. is possible (HW limitation of adapter).

^b PVP=pseudo vector processing.

^c Only preliminary values because the prefetch was disabled.

ments of the vector triad and communication for the investigated computers.

Is there a simple model to extrapolate performance?

References

- [1] W. Schönauer, T. Adolph, H. Häfner, The same PDE code on many different parallel computers, in G. Joubert, A. Murli, F. Peters, M. Vanneschi (Eds.), *Parallel Computing, Advances and Current Issues*, Proceedings of ParCo2001, Imperial College Press, London, 2002, pp. 362-369.
- [2] W. Schönauer, T. Adolph, *FDEM: The Evolution and Application of the Finite Difference Element Method (FDEM) Program Package for the Solution of Partial Differential Equations*, see www.rz.uni-karlsruhe.de
- [3] rz/docs/FDEM/Literatur/fdem.pdf
- [4] W. Schönauer, *Scientific Supercomputing*, selfedition W. Schönauer, Karlsruhe, 2000, see www.rz.uni-karlsruhe.de/~rx03/book/
- [5] W. Schönauer, *Addendum to Scientific Supercomputing*, Chapter A12, see www.rz.uni-karlsruhe.de/~rx03/addendum/a12/

Acknowledgement

We thank the LRZ for the permission to use the Hitachi and the excellent service.

no.	computer	measured time (corrected time), sec.	
		case 1	case 2
1	IBM SP NightHawk-2	12.12	394.17
2	IBM SP WinterHawk-2	11.04	212.41
3	IBM SP Thin120SC	15.71	491.17
4	Hitachi SR8000-F1 without COMPAS	29.97	299.44
5	Hitachi SR8000-F1 with COMPAS	119.22	1191.98
6	HP Superdome	29.48 (32.55)	1509.69 (1666.7)
7	Compaq Wildfire	52.48 ^a (51.17)	255.13 (248.75)
8	SGI Origin 3000	10.90	220.64
9	SUN Fire 6800 ^b	27.88	457.99
10	CRAY T3E-1200	58.87	496.19
11	Fujitsu VPP300	63.17 (58.94)	—
12	Fujitsu VPP5000	56.08 (44.86)	408.16 (326.53)

^a Needed 2 Newton steps (others need one).

^b Only preliminary values because the prefetch was disabled.

Fig. 2: Results of the measurements for the different computers.

Scalable Mesh-based Simulation on Clusters of Symmetric Multiprocessors (Project MethWerk)

Research Area:

Computer Science

Principal Investigator:

Dr. Peter Luksch

Researchers:

Amitava Gupta, Peter Luksch, Andreas Schmid

Research Institution:

LRR-TUM, Institut für Informatik, TU München

Abstract

In this joint project of LRR-TUM, MTU Aero-Engines, and DLR Institute for Jet Propulsion Technology, methods have been developed to increase scalability of parallel simulations that use mesh-based spatial structures. They have been implemented in a parallel CFD simulation program from DLR. Experimental results obtained on the Hitachi SR8000 and on clusters of workstations have shown significant improvement of load balancing.

Mesh-based Simulations

Many simulations that are used in digital prototyping or in scientific research solve systems of differential equations. Their solution requires discretization in space and time, i.e. the physical property of interest (e.g. pressure or temperature, subsequently referred to as Φ) is computed for certain points in time and space only. The points in space for which the equations are solved typically are given by a mesh.

A common type of mesh are block-structured meshes as displayed in Fig. 1, which shows a straight duct, where the fluid enters from the left front side and leaves via the right back side. Space is divided into blocks that are hexaeders. The mesh can be refined in regions of interest by subdividing a block along the x, y, and/or z-dimension, which results in replacing the block by multiple smaller blocks. The corners of the blocks are the points for which the governing equations will be solved. There are many different algorithms to solve the discretized system of equations. They all have in common that the new Φ value at a given point is computed from its previous value and from the Φ values of its neighbors in the mesh. In some cases, even the neighbors of the neighbors are used in the computation. This process is repeated iteratively until convergence is achieved, i.e. the values change by less than a given threshold value.

The front and back walls in Fig. 1 represent in- and outflow faces. The physical modeling paradigm used in the CFD program by DLR requires that the inlet and the outlet face are not subdivided along the y- and z-direction

Parallel Execution

A natural approach to parallel execution of the solver is to assign to each processor a set of neighboring mesh points for which it will solve the equations. This approach is referred to as the Single Program Multiple Data (SPMD) paradigm, since all processors execute the same program but work on different parts of the data.

Parallel execution is most efficient if all processors have the same amount of work to do (provided all processors work at the same speed). In this case the load is balanced. Communication is minimized if the number of cut edges is minimized. A cut edge is an edge in the mesh that connects mesh points in different partitions. For each cut edge, the Φ values have to be communicated between the processors.

Finding a partitioning (i.e. an assignment of mesh points to processors) that meets both requirements requires an amount of time that grows exponentially with the number of mesh points. Exhaustive search for the optimal partitioning therefore is not possible in practice. Instead, heuristic algorithms are used that are known to generate good, near-optimal mappings of mesh points to processors.

These algorithms fall into two categories, graph matching and graph partitioning. Graph partitioning algorithms generate partitions that have nearly the same size and that have a near-minimal number of cut edges. Graph matching algorithms start with a partial mapping and subsequently map mesh points to

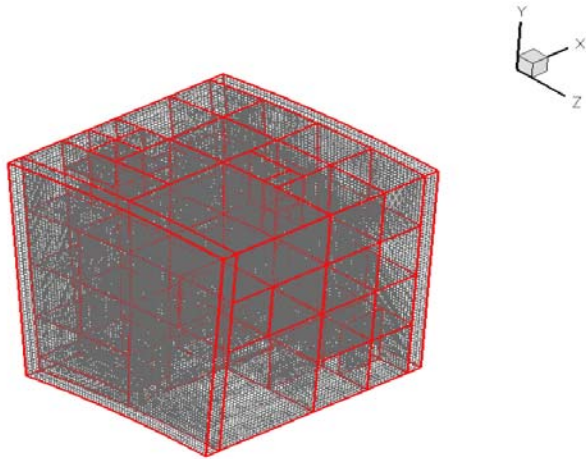


Fig. 1: Block-structured grid (test case)

processors in a way that minimizes a cost function. The definition of the cost function is more flexible than with graph partitioning methods. On a cluster of symmetric multiprocessors, nodes have multiple CPUs that have access to shared memory and a single network interface chip (NIC). Only one CPU at a time can communicate.

Figure 2 illustrates the problem with an example workload. Block A takes five time units to compute (green bar) and 15 time units to communicate results (red bar).

Block B requires 18 units for computation and 2 units for communication, as displayed in the top part of the figure. We assume that the program computes all blocks first and then communicates results. The pseudo-code is given in the upper box on the right hand side of the figure. If blocks A and C are assigned to process P1 and B and D to P2, the load is almost perfectly balanced w.r.t. computation and communication time. The NIC will remain idle until A has computed all its blocks. When B has completed computation of its blocks, it has to wait for the NIC, which still

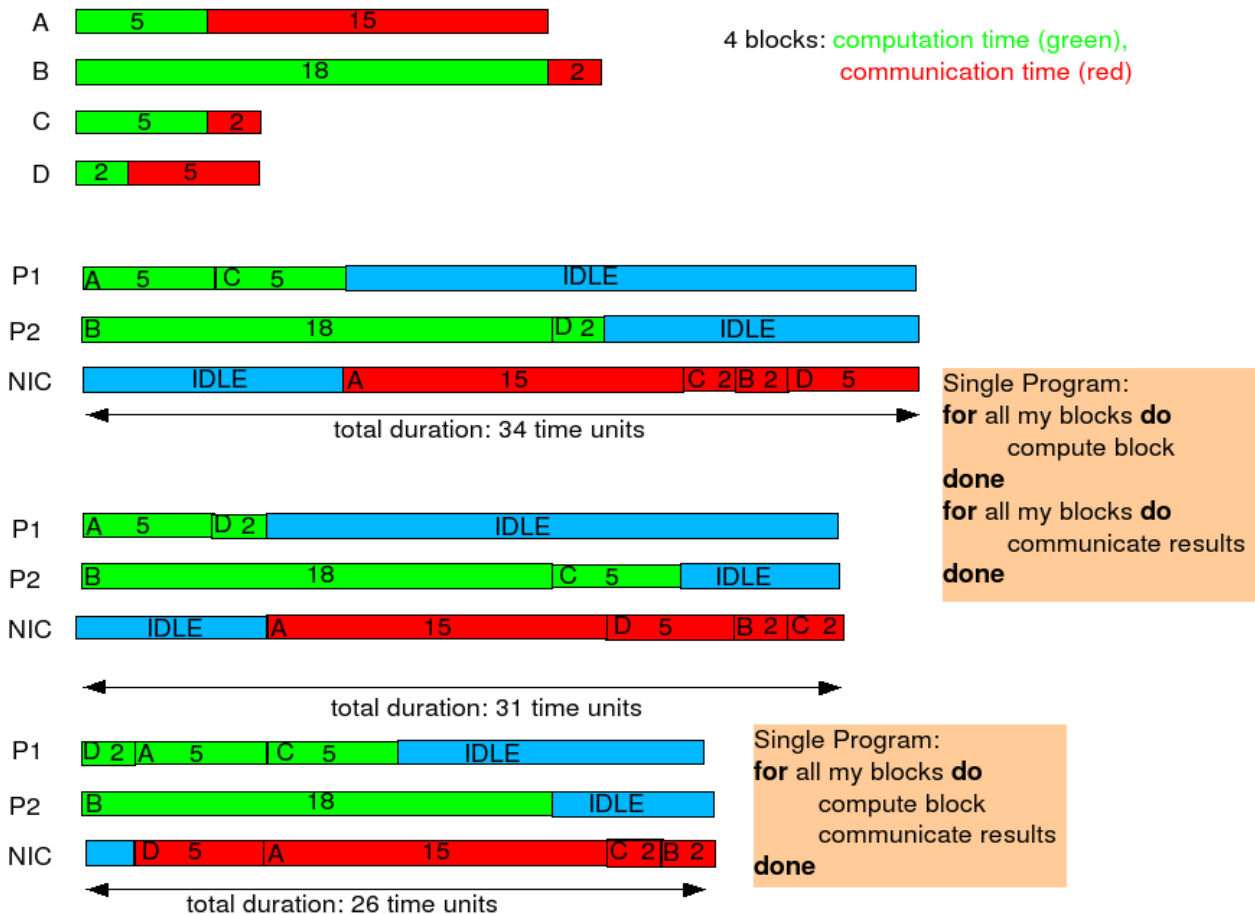


Fig. 2: Optimization for parallel execution

is busy communicating A's results. The total execution time is 34 time units. If we map A and D to P1 and B and C to P2, load balancing is also nearly perfect - each processor has a load of 20 units computation time and communication time. However, P1 completes communication earlier. As a result, the total execution time is only 31 units.

If we change the program as indicated in the second pseudo code box, we can overlap computation and communication. In this case, we only consider computation time for load distribution. On both processors, we proces the block with minimal computation time first so that communication can start as early as possible. This optimization minimizes execution time to 26 units in our example. It will, however, be effective only if the message passing library actually supports asynchronous communication, which is not the case with all MPI implementations.

Experimental Results

Our experimental results have shown that the optimized partitioning on SMP nodes reduces the turnaround time by up to 50%. For load distribution among SMP nodes, we have used the graph partitioning tool Metis. For the mapping of mesh nodes to CPUs within an SMP node, we have developed and used a modified graph matching algorithm that avoids the "state explosion" that makes pure graph matching very slow of large numbers of nodes.

References

- [1] A. Gupta, P.Luksch, A. Schmidt: Meth-Werk: Scalable Mesh-based Simulation on Clusters of SMPs. In: A.Bode and F. Durst (Eds.): High Performance Computing in Science and Engineering, Garching 2004.
- [2] H. Gao, A. Schmidt, A. Gupta, P. Luksch. Load Balancing for Spatial-Grid-Based Parallel Numeric Simulations on Clusters of SMPs . In *Proceedings of the 11th Euromicro Conference on Parallel, Distributed and Network based Processing*, pages 75-82, Genova, Italy, February 2003.

Project Partners:

MTU AeroEngines GmbH, Munich

DLR, Institute of Propulsion Technology, Cologne

Simulation for the Neural Map Formation in the Primary Visual Cortex

Research Institution:

Theoretische Physik T35

Physik Department, Technische Universität München

Research Area:

Computational Neuroscience

Principal Investigator:

Oliver Wenisch

Researchers:

Joachim Noll, Oliver Wenisch, J. Leo van Hemmen

Abstract

Neurons in the primary visual cortex respond selectively for specific features of a visual stimulus such as the orientation of contours or their direction of movement. These response properties of neurons vary systematically across the cortical surface and are arranged in so-called neuronal maps for several types of selectivity, e.g. the orientation and direction preference maps. The maps are believed to develop during early life according to Hebbian learning processes sculpting the synaptic connections between the neurons.

Recently, it was found that learning rules of synaptic connections in the primary visual cortex are dependent on the exact timing of the spiking activity of the corresponding pre- and postsynaptic neuron. To account for these timing effects, the term 'learning window' has been introduced describing the fact that synaptic coupling strength is only changed by a pre- and

postsynaptic spike separation of less than about 150 milliseconds. Moreover, the sign and amount of change is determined by the relative timing of the pre- and postsynaptic spikes.

In this simulation study we investigated how the development of neuronal selectivities depends on the particular form of learning and on correlations in the spiking activity of neighbouring neurons. In a biologically detailed model of primary visual cortex we studied synaptic development through a learning window and its influences on the map-formation process.

The simulations were particularly focused on the development of direction selectivity and its corresponding map. According to a hypothesis at the center of a current debate, a neuron's sensitivity to stimuli moving in a specific direction may be traced back to an asymmetric synaptic coupling pattern to its surrounding cells. By the large-scale computer simulations in this study we have tried to investigate and verify the asymmetry hypothesis by taking into account many biological details involving both the neurons in visual cortex and their underlying learning dynamics. Because modeling the map formation process implies the concurrent simulation of the activities of several thousands of neurons and their synaptic connections, the utilization of the Hitachi SR-8000 high-performance parallel computer has allowed and substantially speed up the necessary simulations and lead to valuable insights from networks with a more realistic size, the data not being marred by boundary effects.

Model Description

As already stated, the learning process depends on the exact timing of spike events in the network. Therefore, we implemented a stochastic spiking neuron model similar to the common integrate-and-fire models and especially optimized for the simulation of large-scale neuronal networks. In this framework the state of a particular neuron is completely determined by its instantaneous membrane potential where inputs from other neurons of a certain circular neighbourhood within the two-dimensional model cortex are integrated. Figure 1 shows a schematic drawing of the interconnections between the two neuron populations that were simulated, i.e., excitatory and inhibitory cells.

These provide, respectively, positive or negative inputs to the membrane potentials of receiving neurons. Spike trains of neurons are realized as inhomogeneous Poisson processes with the membrane potential serving as the rate function. Accordingly, the neuronal network shows spontaneous spiking activity even in the absence of external inputs (cf. Figure 2) - similar to what has been found in neurophysiological experiments.

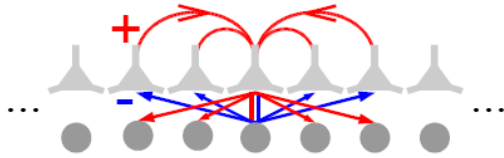


Fig. 1 : One-dimensional schematic of the simulated two-dimensional cortical network: Excitatory (pyramidal shape) and inhibitory neurons have been modelled separately, providing positive (red) or negative (blue) inputs to target cells via the recurrent connections within a certain neighbourhood. Periodic boundary conditions were applied.

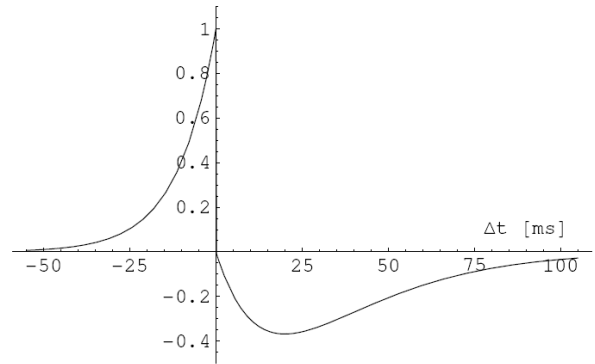


Fig. 3 : Asymmetric learning window showing which relative change in the synaptic coupling strength of two neurons is exerted by a temporal offset Δt between post- and pre-synaptic spike.

Driven by both the intrinsic spontaneous activity and structured external inputs coming from the retina, the coupling strength between two synaptically connected neurons is changed according to a spike-timing dependent learning rule modelled after physiological findings [1]. This implies that only those pre- and postsynaptic spikes contribute significantly to changing the synaptic

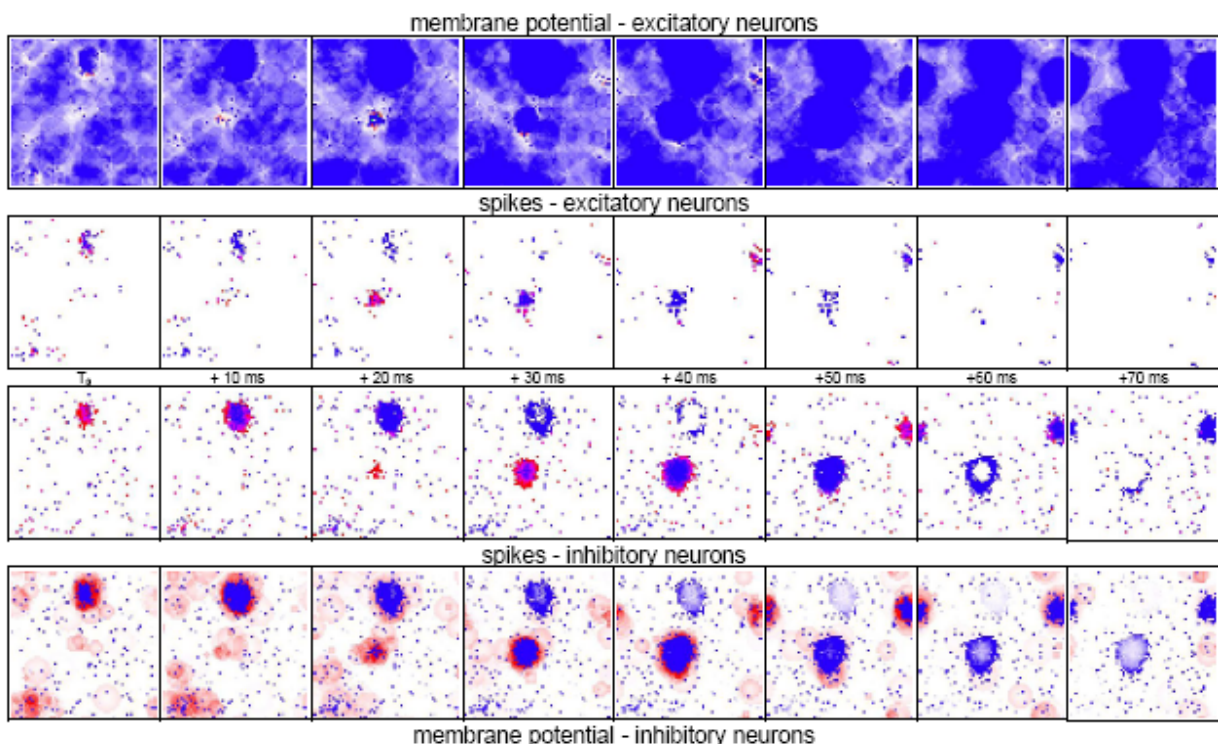


Fig. 2 : Dynamics of spontaneous activity in simulated visual cortex with a grid of 64×64 neurons for both the excitatory and inhibitory population. Middle panels: Blue dots represent inhibitory neuron activity, red denotes excitatory spikes. Top and bottom panels: Dynamics of membrane potential in excitatory and inhibitory cells (elevated voltage levels shown in red, reduced levels in blue). Besides structured external inputs, correlated spontaneous activity can drive the synaptic development.

weight between two neurons that are separated less than approximately 150 milliseconds. Furthermore, the change is facilitating or depressing depending on the temporal order of the spikes. Only if the presynaptic spike preceded the postsynaptic spike, that is, the presynaptic neuron provided correctly timed input to its target that helped driving it to spiking, the connection is strengthened. Otherwise, the synapse is weakened. This characteristic form of the learning rule motivated the term of an asymmetric ‘learning window’ (see Figure 3).

In this way, the learning process encodes temporal causality into the synaptic coupling pattern between neighbouring neurons giving rise to spatially asymmetric weight profiles when learning has settled. This is especially important for the processing of spatiotemporally correlated activity as provided by moving stimuli in that a certain weight asymmetry of the inputs to a given neuron makes the neuron respond preferentially to the stimulus direction that provides the strongest input.

In our simulations we were also able to reproduce the typical arrangement of these direction response preferences in the form of direction selectivity maps as found in experiments ([2, 3], and Figure 4).

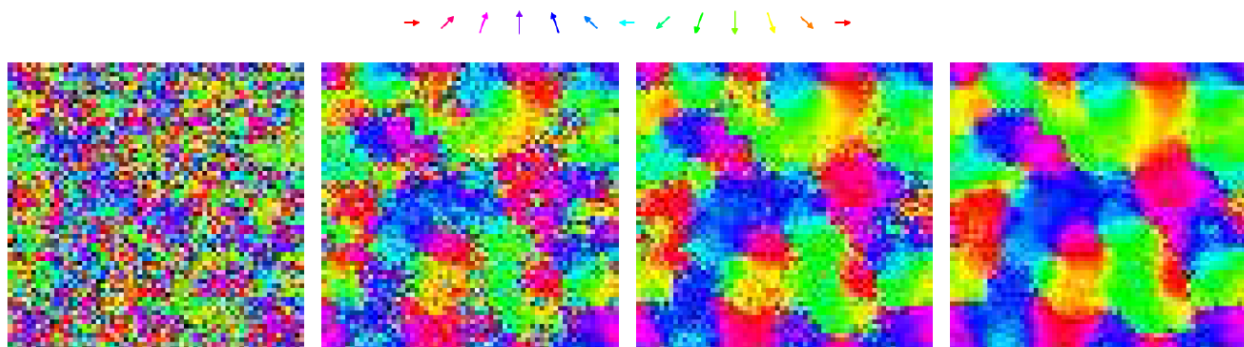


Fig. 4 : This series of snapshots depicts the temporal development of the direction preference map of the simulated cortex over a time span of 10^5 seconds simulated time, i.e., roughly one day real time. The colour maps represent the different preferred stimulus directions for each cortical grid position as shown by the arrows above the maps.

References

- [1] Zhang, L. I., Tao, H. W., Holt, C. E., Harris, W. A., and Poo, M.-M., 1998 : A critical window for cooperation and competition among developing retinotectal synapses. *Nature*, 395:37-44.
- [2] Weliky, M., Bosking, W. H., and Fitzpatrick, D., 1996 : A systematic map of direction preference in primary visual cortex. *Nature*, 379(6567):725-728.
- [3] Wenisch, O., Noll, J., and van Hemmen, J.L., 2005 : Spontaneously emerging direction selectivity maps in visual cortex through STDP. *Biological Cybernetics*, 93(4), 239-247.

Parallelization of Maximum Likelihood based Methods for the Reconstructon of a Tree of Life from Molecular Gene Sequence Alignments (Project ParBaum)

Research Institution:

Lehrstuhl für Rechnertechnik und Rechnerorganisation/ Parallelrechnerarchitektur, Institut für Informatik, Technische Universität München

Research Area:

Bioinformatics

Principal Investigator:

Dr. Harald Meier

Researchers:

Dr. Alexandros Stamatakis, Dipl. Inf. Michael Ott, Dr. Harald Meier

Abstract

The inference of a "tree of life", representing the phylogenetic relationship of all currently known organisms, is supposed to be one of the "grand challenges" in Bioinformatics. Today the most important approach is the reconstruction of evolutionary trees from molecular sequence information of genes or proteins of the respective organisms. Given the large amount of available molecular sequence data and the high computational complexity of the problem, high end software and hardware solutions have to be developed and applied in order to make the grade. In the KONWIHR-project "ParBaum", high performance computer applications for calculating huge phylogenetic trees of organisms from gene sequence information have been developed: RAxML is the currently fastest program for the highly efficient Maximum Likelihood based computational phylogenetic treeing of gene or

protein sequence data. The parallel implementation of RAxML on the HLRB and various other high performance computers led to the fastest phylogenetic analysis system worldwide, on which phylogenetic trees comprising even 10.000 organisms were calculated in a reasonable time. This was a large step forward towards the final goal, to reconstruct a tree of almost 35.000 organisms from a non redundant ssu-rRNA gene sequence alignment. This tree shall serve as a comprehensive visual reference book of evolutionary relationships of organisms as well as a reference tree for the rapid molecular identification of microorganisms such as pathogenic bacteria by additive phylogenetic analyses of sequences of their ssu-rRNA genes.

From Gene Sequences to Phylogenetic Trees

The inference of evolutionary relationships is of fundamental importance for understanding the biology of organisms. Recent years have witnessed a dramatic increase of data and number of methods in this field. Since the awareness that information on the history of organism's evolution is stored within the molecules of life, in particular the genes and proteins, the main activity in evolutionary biology and bioinformatics is to reconstruct trees of organisms by extracting the evolutionary information from protein or DNA sequences. Thereby, each organism is represented by the sequence information of a universal gene or protein or a set of it, only. The required sequence data can nowadays be easily determined by molecular biologists using standard methods.

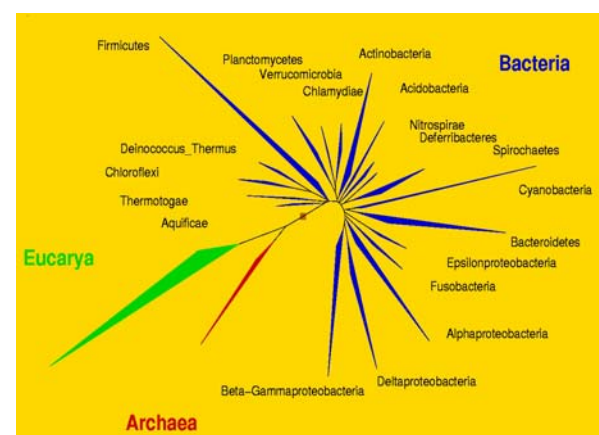


Fig. 1: 10.000 organisms tree with grouped terminal branches based on ssu-rRNA gene sequences

In our study each of the more than 10.000 organisms was represented by a sequence of a single gene, the gene for the small subunit ribosomal RNA (ssu-rRNA). This gene is present in all known organisms and its sequence harbours rich information on the history of an organism's evolutionary relationship. For the tree reconstruction we used multiple sequence alignments (MSA) of the ssu-rRNA genes of different sizes as the input data. From a few hundreds up to ten thousand sequences were arranged in a suitable format for this purpose. The main problem and challenge with the reconstruction of phylogenetic trees of this size is the high computational complexity: The phylogenetic treeing problem is known to be NP-complete. The number of possible tree topologies (trees with differently arranged branches and leaves) increase dramatically with the increasing number of sequences or respective organisms. For 51 sequences only there exist more tree topologies than atoms in the universe. This fact implicates that there is only one correct tree topology within a large forest which has to be found.

Method for Tree Reconstruction

Maximum Likelihood (ML) is the preferred criterion for reconstructing trees from molecular sequence data. ML-based methods allow for the evaluation of a tree's quality once it has been built. A so-called likelihood-value is calculated, which indicates how probable a given tree topology may have led to the given sequence alignment. A ML-based method is superior to other methods as it interprets the given data more precisely and allows an analysis under different assumptions (evolutionary models). Unfortunately the best treeing methods (the phylogenetic analysis methods based on maximum likelihood) include the most computing intensive calculations. Due to high computational complexity and the NP-completeness of the treeing problem heuristics have to be applied – strategies to reduce the search space and allow for finding the best tree without examining every possible tree topology. Nevertheless only very small trees of less than 500 sequences were inferred in the past on standard computers. To calculate a gene tree of life in acceptable time, however, high end software applications on parallel supercomputers have to be applied.

Solutions for the Inference of Large Evolutionary Trees – Technical Optimization and Algorithmic Development

Our work is based on a widely used heuristic implementation of the ML method, fastDNAmL. The program starts with a random 3-branch (=sequence) starting tree. One sequence after the other is inserted as new branch at all possible positions. After every insertion step all new topologies are evaluated. The tree representing the highest likelihood value is optimised in its branches length and used for introducing the next sequence and its respective branch. In the first phase of the project we focused on technical optimization of the sequential code. A performance profile of the program identified the function for calculating the likelihood score of the tree to produce the highest load. Introducing a pre-analysis function of the input data together with a new data structure for efficient caching of commonly used intermediate data, the runtime of the program was reduced by 25 -65 percent depending on the sequence data analysed and the computer architecture used. The resulting program was called AxML [1, 2].

By just technical optimisation the complexity of the method could not be reduced by orders of magnitudes necessary in order to calculate trees consisting of thousands of organisms. Therefore the development and implementation of new heuristics for the tree search took centre stage in the second project phase.

We developed a two step algorithm and implemented it in RAxML. This algorithm quickly creates an initial tree topology, which already includes all sequences to be analysed, using the faster but less accurate Maximum Parsimony method. In the second step the start tree is continuously optimised and thus the likelihood-value of the tree maximized. The improvement of the tree's likelihood-value is mainly achieved by changing the topology by shuffling the branches around within the tree using nearest neighbour interchange as well as subtree pruning and regrafting techniques. RAxML is the currently fastest and most accurate ML-based treeing program, with a speedup of 10.000% compared to initial fastDNAmL. It allows the calculation of trees comprising up to 1000 organisms even on standard computers [2,3,5].

Parallel implementation and performance evaluation

We developed a simple master-worker based parallel version of AxML, called PAXML. Here, a master process builds the tree by stepwise addition and distributes the topologies of each insertion round to the workers. The workers processes evaluate the trees and report the results to the master. It selects the best topology, introduces the new branch and redistributes the topologies to the workers for evaluation. On the HLRB we experienced a runtime improvement of 26% to almost 30% over parallel fastDNAmI depending on the alignment data, thereby. On a cluster of home computers the runtime improvement was even up to 70% [1].

A major breakthrough was achieved by a non-deterministic parallel implementation of RAxML. A master distributes the full starting trees to the workers. In addition each worker receives a list of subtrees, for which he has to find the optimal position within the starting tree received. After each round of optimisations the workers communicate to the master the trees with the highest likelihood. The master process selects the best tree and redistributes it for further optimisation. Performing parallel test runs on HLRB and the RRZE computer cluster we achieved very good, for some alignment data even superlinear speedups [3]. The high performance measured motivated us to initiate reconstruction of a large phylogenetic tree. We succeeded in inferring the phylogeny from a multiple alignment with 10.000 ssu-rRNA gene sequences in one parallel program run within 9500 CPU hours in total using 32-64 processors - the largest tree computed so far[4].

Future Perspectives

Besides further technical and algorithmic optimisations, future work on RAxML will focus on parallelization strategies and the adaption of the program to different HPC architectures. Here, our research touches a hybrid multi-level parallel implementation on supercomputers like the new HLRB2 and other HPC environments like IBM BlueGene or the Cell Broadband Engine. The steadily increasing computational power of HPC systems together with a tailor-made parallel RAxML implementation for these architectures will allow us to make a big step forward to our final goal, the reconstruction of a "Tree of Life".

References

- [1] Stamatakis, A.P., T. Ludwig, H. Meier and M.J. Wolf. Accelerating Parallel Maximum Likelihood-based Phylogenetic Tree Calculations using Subtree Equality Vectors. *In Proceedings of Supercomputing Conference (SC2002)*, Baltimore, Maryland.
- [2] Stamatakis, A. P., T. Ludwig and H. Meier. 2004. The AxML Program Family for Maximum Likelihood-based Phylogenetic Tree Inference. *Concurrency and Computation: Practice and Experience*, 16:975-988.
- [3] Stamatakis, A. P., T. Ludwig and H. Meier. 2005. RAxML-II: A Program for Sequential, Parallel & Distributed Inference of Large Phylogenetic Trees. *Concurrency and Computation: Practice and Experience*, 17(14):1705-1723.
- [4] Stamatakis A., T. Ludwig, and H. Meier. 2004. Parallel Inference of a 10.000-taxon Phylogeny with Maximum Likelihood. *Lecture Notes in Computer Science*, 3149:997-1004.
- [5] Stamatakis A., T. Ludwig, and H. Meier. 2005. RAxML-III: A Fast Program for Maximum Likelihood-based Inference of Large Phylogenetic Trees. *Bioinformatics*, 21(4): 456-463.

Links:

<http://www.lrr.in.tum.de/zope/groups/abiot/project/parbaum>

<http://icwww.epfl.ch/~stamatak/>

Project Partners:

Department for Microbiology, TU München

Department for Microbial Ecology, University Vienna

Electronic Properties of DNA

Research Institution:

CSCS (Centro Svizzero di Calcolo Scientifico)

Research Area:

Computational Biochemistry

Principal Investigator:

Ari Paavo Seitsonen

Researchers:

Dr. Karine Costuas, Prof. Mauro Boero, Dr. Francesco Luigi Gervasio, Dr. Ari Paavo Seitsonen, Dr. Walter Silvestri

Abstract

The electronic structure of DNA strands has recently received considerable attention due to appealing potential applications of DNA as a molecular wire. Furthermore increasing use of DNA strands is being made in nanotechnology as connectors and in the development of biochips. The difficulty of performing reliable and reproducible experiments calls for high level theoretical studies and simulations. However, until recently the calculations of DNA electronic properties were restricted to the study of small fragments, which did not include the solvation water and the counter-ions.

In our project we have addressed the issue of the electronic properties of DNA by executing the first, state of the art electronic structure calculations on a full DNA including the solvent water and counter-ions. These studies lead us to an improved understanding of the electronic structure of DNA, and we have subsequently extended the studies to the conduction mechanism in DNA. The quantum problem in our simulations scheme is solved within density functional theory in the Car-Parrinello scheme, using a gradient corrected exchange-correlation functional and a plane wave basis set. In the last 15 years this methodology has been applied

successfully to investigation of structure, dynamical and electronic properties of a large variety of systems, including those of biological interest.

Electronic structure of pure DNA

Charge transfer processes in DNA play an important role in oxidative damage and possibly in related repairing mechanisms. Furthermore, if conductive, DNA could find applications in nanoelectronic devices. Even after a vast number of experiments has been performed, the details of the electronic structure of DNA still provides surprises, contradictory outcomes and its knowledge turns out incomplete.

Our goal is to provide an insight into important quantitative details of the DNA structure, its hydration and electronic structure, and conduction mechanism. In particular, the system we chose as the starting point, the decamer double strand $d(GpCpGpCpGpCpGpCpGpCp)$, has been synthesized in the laboratory, and its crystalline structure has been determined recently [Figure 1]. The molecular formula is $C_{228}N_{96}O_{144}P_{24}Na_{24}H_{264} \cdot 138(H_2O)$. This Z-DNA crystal contains both the solution waters and counter-ions, and the infinitely repeated strand is a much better approximation to biological DNA than small fragments where boundary conditions dominate.

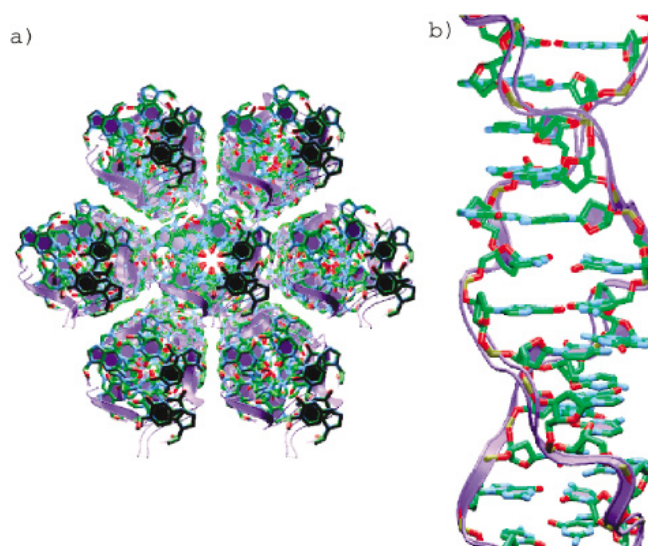


Fig. 1: View of the three-dimensional structure of the Gua:Cyt decamer (a) along and (b) perpendicular to the c axis. Water molecules, counter-ions and hydrogens are omitted for clarity. The sugar-phosphate backbone is represented as ribbons.

Calculational method

We have employed density functional theory to explicitly solve the electronic structure of the whole system. This makes the computational effort extremely demanding, and at the time of the project, when the Hitachi SR8000-F1 arrived, it was by far the only machine available which could enable us to start the project. Our computational cell was hexagonal with lattice constants $a = 18.08 \text{ \AA}$ and $c = 43.10 \text{ \AA}$. The core electrons were described by pseudopotentials, but still 1980 valence orbitals had to be treated explicitly. In total we had to propagate 808.311.240 plane wave coefficient for the electronic degrees of freedom at each ionic time step. The starting configuration of the optimization procedure is the X-ray structure, complemented by an educated guess for the hydrogen atoms. We relaxed the atomic structure by simulated annealing method within the Car-Parrinello scheme.

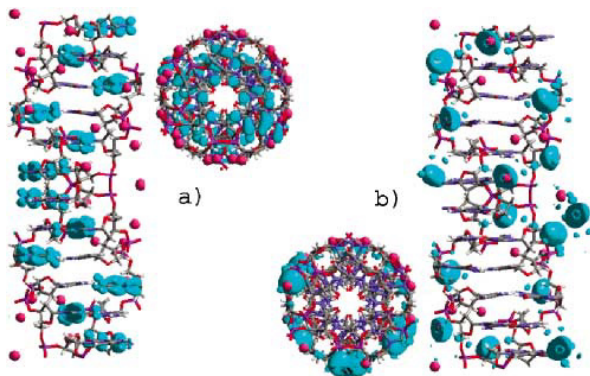


Fig. 2: Isosurface (in cyan) of the electron density manifold due to the 12 (a) highest occupied (valence band) and (b) lowest unoccupied (conduction band) electronic states. Whereas (a) is localised on the guanine base pairs, (b) is a charge transfer state on the Na^+ counter-ions and PO_4^- groups.

Electronic structure of pure DNA

The highest occupied molecular orbitals, shown in Figure 2a), are formed by a manifold of 12 orbitals of the guanine base [Gervasio *et al*, 2002]. The band gap turned out to be 1.28 eV in our calculations, and even accounting for the systematic underestimation of this kind of calculations we expect the true gap to be not larger than 2 eV. This small value is explained by the lowest unoccupied molecular orbital in Figure 2b, which reside on the counter-ions and

the backbone. Thus a reliable determination of the electronic structure of DNA demands for the inclusion of the counter-ions.

The dipole moment of the water molecules ranges from 1.7 D inside the helix to 3.8 D in the water droplets. This variance makes it difficult if not even impossible to describe the structure without an explicitly polarisable water model, again demonstrating how important the electronic structure calculations are for an adequate description of such complicated systems.

Charge localisation and hopping in DNA

Motivated by these studies we have tackled the problem of the detailed charge transfer mechanism along the axis of DNA. First we found that simply removing an electron to create a hole in the highest occupied molecular orbital was not sufficient to localise the hole, and we could also exclude distortion of the helix as a possible candidate.

A more promising reaction scenario involves a double proton transfer shown in Figure 3 [Gervasio *et al*, 2006]. We calculated a reaction barrier for this phenomenon to be 9 kcal/mol (0.37 eV; Fig. 3B). Once this reaction step has occurred, the oxygen on the guanine becomes an acid pair, trapping a hole from elsewhere in the DNA and thus leading to charge transfer along the double helix. After this the hydrogen ^1H is transferred back to the cytosine for the final state.

For these studies we have used the QM/MM technique, where only the central part of the system is described with the electronic structure method and the surroundings with a classical potential field. This way we have been able to make molecular dynamics calculations feasible even for the 38-base pair B-DNA system $d(5'ACGCACGTCGCATAATATTACGTGGGTTATATTAGC-3')$ [Boero *et al*, 2006].

Summary

Using the Hitachi SR8000-F1 installed at Leibniz Rechenzentrum we were able to start a series of exhaustive but also very rewarding investigations of the electronic structure and the intrinsic conduction mechanism in DNA. The manifold of highest occupied molecular orbitals are localised at the base pairs, and the inclusion of counter-ions and water molecules is essential in

order to describe the electronic structure reliably. More recently we have managed to pinpoint the conduction of holes to occur via double hydrogen exchange, which allows the hole to hop and localise on a base along the double strand.

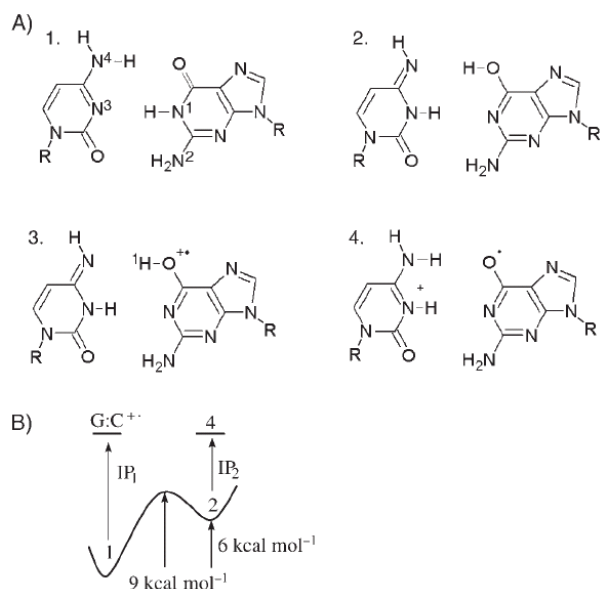


Fig. 3: Mechanism for the charge transfer by localisation of a hole on a guanine base (on the right). A) 1. Initially the G has a neutral Watson-Crick pair character, 2. the reaction initiates with a double proton transfer, 3. the hole (radical cation) is transferred to the guanine and 4. the final state, where the hole is localised on the guanine and the oxygen of cytosine is a radical. B) Free-energy diagram for the double proton transfer reaction. The ionisation potentials IP_1 and IP_2 have been calculated to verify the mechanism.

References

- [1] Gervasio, F. L., Carloni P. and Parrinello M., 2002 : "Electronic structure of wet DNA". *Phys. Rev. Lett.* 89, 108102 <http://dx.doi.org/10.1103/PhysRevLett.89.108102>
- [2] Boero, M., Gervasio, F. L. and Parrinello, M., 2006 : "Charge localisation and hopping in DNA". *Molec. Simul.* in press
- [3] Gervasio, F. L., Boero, M. and Parrinello, M., 2006 : "Double proton coupled transfer in DNA". *Angew. Chem.* 118, 5734 <http://dx.doi.org/10.1002/ange.200602106>

Links

<http://www.cpmc.org/>

Project Partners:

Max-Planck-Institut für Festkörperforschung, Stuttgart

Eidgenössische Technische Hochschule Zürich (ETHZ)

Centre for Computational Sciences, University of Tsukuba

Multi-Dimensional Quantum Dynamics of Chemical Reaction Processes

Research Institution:

Theoretische Chemie, TU München

Theoretische Chemie, Univ. Bielefeld

Research Area:

Theoretical Chemistry

Principal Investigator:

Prof. Dr. Uwe Manthe

Researchers:

Dr. Alexandra Viel,

Dr. Tao Wu,

Dr. Fermin Huarte-Larranaga,

Dr. Rob van Harreveld,

Dr. Mauricio Coutinho-Neto,

Prof. Dr. Uwe Manthe

Abstract

Quantum effects have to be considered for the study of many chemical phenomena: Tunneling increases the rate of chemical reactions when hydrogen atoms or protons are transferred. The course of photochemical reactions, i.e. chemical reactions resulting from interaction with light, is often determined by vibronic coupling due to conical intersections of excited electronic potential energy surfaces. Zero point energy effects have a strong impact on the structure and dissociation dynamics of many van der Waals clusters. The quantum-mechanical simulation of chemical processes provide here theoretical insight but are a challenging task since the computational costs increase dramatically with increasing size of the molecules involved. Special com-

putational methods must therefore be developed and applied.

Simulating the tunneling of a proton along a hydrogen bond within a single molecule, rigorous full quantum dynamics calculations for the tunneling splitting on malonaldehyde using all 21 internal degrees of freedom could be performed. For the calculation of the tunneling splitting we use two completely independent methodologies: the MCTDH method and the POITSE QMC based method. These two approaches are based on very distinct frameworks. The MCTDH method uses a time dependent basis set expansion approach while the POITSE uses a stochastic approach for the solution of the Schrödinger equation. Extensions to the calculation of tunneling splitting of excited vibrational states as well as the study of the impact of the use of linearized normal modes are planned.

Prototypical examples of photoinduced reaction processes occurring on a femtosecond time scale are also studied. The photoisomerization of polyenes (like ethylene) and the photoionisation of ammonia are examples of a process which involve vibronic coupling, i.e. a strong coupling of nuclear (vibrational) and electronic motion. Electronic potential energy surfaces of these systems show conical intersections which can direct the course of the process. These potential energy surfaces have been constructed based on (ab initio) quantum chemical calculations and quantum dynamical simulation including 6 coordinates have been performed. In these systems vibronic coupling strongly influences the dynamics.

Tunnelling splitting in malonaldehyde

The 9-atom malonaldehyde molecule (see Fig.1) is a popular system for the study of intramolecular proton transfer of the hydrogen atom involved in the strong intra-molecular hydrogen bond. The tunnelling of the proton between the two equivalent configurations induces a splitting of the vibrational levels which have been measured experimentally with high precision. From the theoretical point of view, the accurate determination of the tunnelling splitting for this system with 21 internal degrees of freedom represents a challenge for quantum mechanical studies. The central result obtained in 2004 was the computation of an accurate quantum value for the ground tunnelling splitting of malonaldehyde

considering the 21 Cartesian normal modes and using a full dimensional potential energy surface published in 2001. To our knowledge this was the first rigorous full dimensional calculation studying tunnelling splittings in a molecule with more than a handful of atoms.

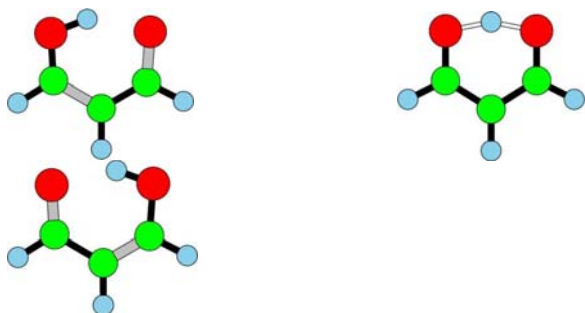


Fig.1: Two equivalent configurations of the malonaldehyde molecule (left, right) and the transition state geometry (centred) for the proton transfer reaction. Colour scheme: C=green, O=red, H=blue

Two completely independent exact quantum methods have been used: MCTDH and POITSE. The MCTDH calculation yields a value of 25 cm^{-1} with 10% accuracy and the POITSE calculation a value of $25.7 \pm 0.3 \text{ cm}^{-1}$. We have recently determined the tunnelling for the deuterium isotope as being $3.21 \pm 0.1 \text{ cm}^{-1}$. These theoretical values are respectively 20% and 10% above the experimental values of 21.6 cm^{-1} for H and 2.9 cm^{-1} for D.

Photo-ionization induced femtosecond dynamics of ammonia

The photoelectron spectrum of ammonia (NH_3) and the associated dynamics of the NH_3^+ cation has been a topic of interest for decades. The cation is a typical example of vibronic coupling which means that coupling between the light electrons and the heavy atoms can not be neglected anymore. For this typical pseudo Jahn-Teller system, the three lowest electronic states and 6 nuclear coordinates participate the dynamics induced by the photoionisation. We have been able to build a full-dimensional anharmonic analytical representation of these three coupled electronic states of the cation based on high quality ab initio computations. The dynamics after ionization has been investigated by

means of time-dependent wave packet propagation making use of the MCTDH method to tackle this 6-dimensional problem.

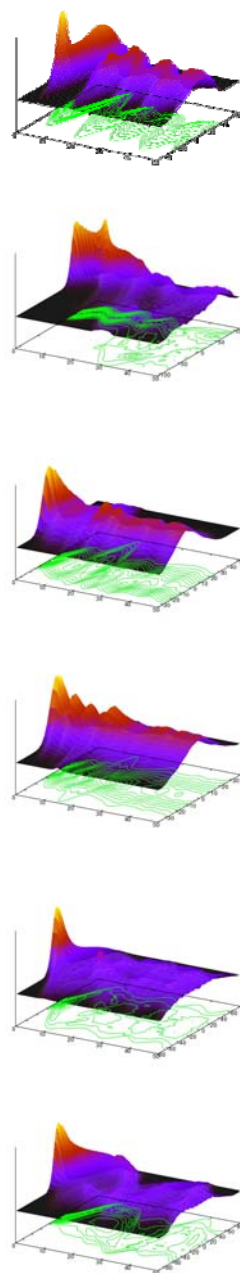


Fig. 2: Probabilities for the six coordinates (q_1 to q_6 , from top left to bottom right) as a function of time in femtoseconds after ionization to the excited state. a.u. have been used for the mass weighted normal modes q_i .

Fig.2 presents the time evolution up to 50 femtoseconds of the probability densities for each of the six vibrational coordinates monitoring the evolution after ionization to the cation excited state. A quasiperiodic oscillatory motion along

the symmetric stretch q_1 with a frequency of 12-13 fs is rapidly damped due to intrinsic nonseparability of the potential surface. In about 20 fs, the molecule reaches planarity ($q_2=0$). Spreading and damping are observed for the 4 asymmetric modes (q_3 to q_6). The photoelectron spectrum computed using the time evolution of the wavepacket is in good agreement with the experimental spectrum. The low energy band presents a well resolved progression due to the umbrella inversion mode, while the high energy one is congested and no resolved progression can be identified which is typical of strong vibronic coupling. This coupling is responsible for a very rapid radiation-less decay of the excited state illustrated on Fig.3. The evolution of the adiabatic electronic populations shows the presence of three time scales in the system: i) a ultra-fast Jahn-Teller dynamics of the two excited states which occurs in 5 fs, ii) a 20 fs time scale for a incomplete internal conversion to the ground state, and iii) a more than 100 fs for the decay of the remaining excited state population.

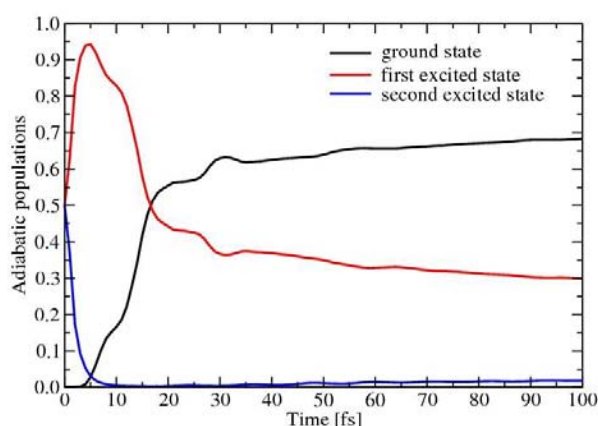


Fig.3: Adiabatic electronic populations as a function of time in fs.

Photoinduced dynamics of ethylene

This work constitutes the first step to better understand the photodynamics (and photoisomerization) of polyenes for which the dynamics near conical intersections should have a determinant effect. Within the project, important progress in the understanding of the photodynamics in ethylene has been achieved. Similarly to the ammonia cation case, non-adiabatic couplings play an important role in the dynamics. We proposed a 3-sheeted 6-dimensional potential energy surface for the three lowest valence state of ethyl-

ene which includes the scissoring coordinates. The dynamics, studied by MCTDH based wavepacket propagation demonstrates a relatively unimportant role of the pyramidalization coordinate at very short time, contrary to previously thought, but it reveals the necessity to include the scissors in this reduced dimensionality study.

References

- [1] M.D. Coutinho-Neto, A. Viel and U. Manthe, 2004: The ground state tunneling splitting of malonaldehyde: Accurate full dimensional quantum dynamics calculations, *J. Chem. Phys.* **121**, 9207-9210
- [2] Viel, R. Krawczyk, U. Manthe and W. Domcke, 2004: Photoinduced dynamics of ethene in the N, V, and Z valence states A six dimensional nonadiabatic quantum dynamic investigation, *J. Chem. Phys.* **120**, 11000-11010
- [3] A. Viel, W. Eisfeld, S. Neumann, W. Domcke, and U. Manthe, 2006: Photoionization induced dynamics of ammonia: Ab initio potential energy surfaces and time-dependent wave-packet calculation for the ammonia cation. *J. Chem. Phys.* **124**, 214306[16]
- [4] Viel, M.D. Coutinho-Neto and U. Manthe, 2006: The ground state tunneling splitting and zero point energy of malonaldehyde: a quantum Monte Carlo determination, to be submitted to *J. Chem. Phys.*

Collaborators

Prof. Dr. Wolfgang Domcke (TU München)

Dr. Wolfgang Eisfeld (TU München)

Reactivity of RuO₂: Oxidation of carbon monoxide

Research Institution:

Justus-Liebig-Universität Gießen

Research Area:

Chemistry

Principal Investigator:

Prof. Herbert Over

Researchers:

Dr Ari Paavo Seitsonen, Jan Philipp Hofmann

oxidation reaction, yet ruthenium dioxide is an excellent catalyst. We have explained this to result from the undercoordinated atomic species at the surfaces of the oxide [Over *et al*, 2000. Science **287**, 1474-1476]. These calculations yield support, explanations and inspiration for the experiments performed in the "model catalysis & surface chemistry" group at the Justus-Liebig-Universität Gießen. Our calculations provide the adsorption structures, reaction paths with energetics and entropic contributions with all the relevant structure and intermediate states of the reactions.

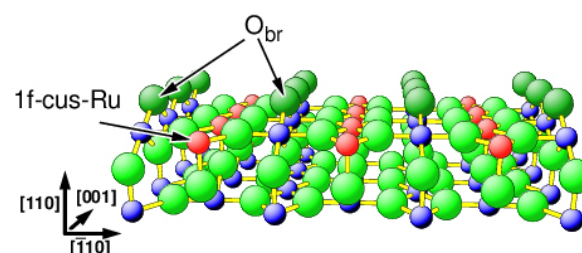


Fig. 1 : The atomic structure using a ball-and-sticks representation of the RuO₂(110) surface, facing upwards. The blue and light green balls denote fully coordinated ruthenium and oxygen atoms. The red atoms denote the 1f-cus-Ru, singly undercoordinated ruthenium atoms, and the 2-fold coordinated oxygen atoms are O_{br}.

Abstract

Heterogeneous catalysis is one of the key technologies in chemical industry. Due to the huge quantities produced the optimisation of the reaction conditions and catalyst materials is a highly rewarding goal. A systematic approach by understanding the microscopic mechanisms governing the reactivity can lead to rational "catalyst design".

We use density-functional theory (DFT) to investigate the atomistic reaction mechanism and reactivity of surfaces of RuO₂, a promising candidate for a catalyst material, at the atomic scale. DFT can provide the energy landscape along reaction paths and reaction rates without empirical parameters since the electronic structure is solved explicitly at each atomic configuration. Recently we have studied the properties of stoichiometric, reduced and oxidised RuO₂(110) and RuO₂(100) surfaces, and the oxidation reaction of carbon monoxide (CO) into carbon dioxide (CO₂) on the Hitachi SR8000-F1 supercomputer installed at Leibniz-Rechenzentrum (LRZ). The clean surface of metallic ruthenium is a poor catalyst for the CO

Surface chemistry of ruthenium dioxide

Ruthenium dioxide (RuO₂) grows in the rutile structure familiar from TiO₂, but RuO₂ is a metallic oxide. The catalytic activity of RuO₂ sets in at relatively low temperatures, leading potentially to massive savings in the energy requirements during the operation of the catalyst for air purification.

Figure 1 shows the surface structure of RuO₂ (110), the most common surface orientation of ruthenium oxide. The stoichiometric surface exposes two kinds of *coordinatively undercoordinated sites* (cus), *i.e.* atoms at the surface with a coordination lower than in the bulk. This makes them highly reactive, and they are the candidates for the reaction steps to start from in the Langmuir-Hinshelwood reaction mechanism. The surface termination can be reduced by heating the surface or reacting the bridging oxygens O_{br} away, or oxidised with a surplus exposure in molecular oxygen, leading to singly-coordinated (or 2-fold undercoordinated) on-top oxygen O_{ot} atoms.

Computational method

We use DFT to solve the electronic structure explicitly in the calculation. This describes also the interaction of atoms with each other. In our case the inclusion of the electronic structure is particularly important, because in the course of the reactions covalent bonds are formed and broken. We expand the electronic orbitals in plane waves, and describe the core-valence interaction either using pseudo potentials. For the exchange-correlation term we employ the generalised gradient approximation (GGA). In order to investigate the surfaces the unit cell is repeated periodically along the surfaces, and vacuum is used to separate the neighbouring cells. This is the so-called slab geometry.

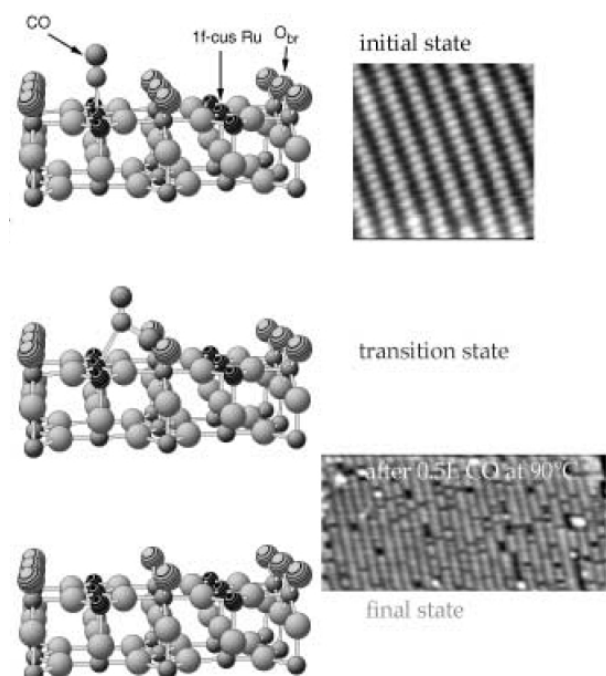


Fig. 2: CO oxidation reaction mechanism on stoichiometric $\text{RuO}_2(110)$ surface. On the left the atomic the atomic geometry and on the right the experimental scanning tunnelling microscope image of the surface before (initial) and after (final) the reaction. The removed bridging oxygen atoms appear as holes in the rows. The transition state shows the activation barrier.

Adsorption and oxidation of carbon monoxide

Carbon monoxide adsorbs on the stoichiometric $\text{RuO}_2(110)$ and $\text{RuO}_2(100)$ surfaces at the 1f-cus-Ru sites. It can then react with the 2f-oxygen O_{br} in the bridging rows. The energy change, or

potential energy surface, as a function of the forced distance between the carbon and the reacting oxygen on $\text{RuO}_2(110)$ is shown in Figure 3. Behind the reaction barrier (distances smaller than at the transition state in our case) the energy decreases monotonously, forming carbon dioxide, which then desorbs at the experimental temperatures. The energy barrier for this reaction is 0.70 eV; this value is 50 % lower than on the metallic $\text{Ru}(0001)$ surface, explaining the higher reactivity of the oxide. From the analysis of the components of the activation we have concluded the lower barrier to result from a lower energy required to activate the oxygen.

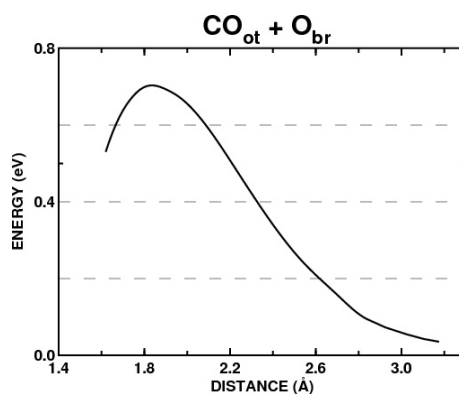


Fig. 3: Energy along the reaction path shown in Figure 2. The reaction coordinate is the distance between the carbon of CO and the reaction O_{br} .

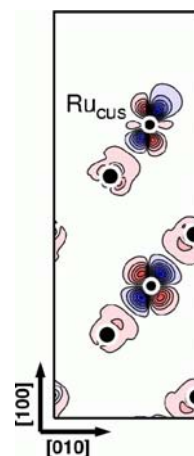


Fig. 4: Density difference of the self-consistent minus the atomic densities on $\text{RuO}_2(100)$ surface. The 1f-cus-Ru atom shows a “dangling bond”, i.e. a magnified lobe of reduced density pointing above the surface.

After this reaction the surface is reduced, unless further oxygen is provided to the surface. We have studied the subsequent adsorption and oxidation reactions of CO on the surface. First CO adsorbs on the bridging 2f-cus-Ru sites left empty by the reacted O_{br} . From there it can react with the neighbouring O_{br} . Finally, CO covers all the bridging sites, and they can be reacted away by on-top oxygen (cf. Over *et al*, 2002).

On $RuO_2(100)$ the reaction mechanism is very similar, as the surface termination provides similar undercoordinated sites as on $RuO_2(110)$. As example of the reactive site on the surface we show the density difference at $RuO_2(100)$ in Figure 4, showing the *dangling bond* at the 1f-cus-Ru atom.

Conclusions

The computing time provided by the Hitachi SR8000-F1 has enabled us to study the atomic and electronic structure, and chemical reactions on the ruthenium dioxide (110) and (100) surfaces. The assignment of species seen in core level spectroscopy and in scanning tunnelling microscopy requires quantification from the theoretical calculations. This insight let us support and sometimes also predict the experiments performed in close collaboration with the theoretical calculations.

We conclude the high activity of ruthenium dioxide compared to the surfaces of clean Ru metal to originate from the weaker bonding of the oxygen to the surface. Thus the reactivity of the ruthenium oxide surfaces is dictated by the undercoordinated surface sites.

References

- [1] Over, H; Seitsonen, A P; Lundgren, E; Schmid, M; Varga, P : 2001, *Direct imaging of catalytically important processes in the oxidation of CO over $RuO_2(110)$* . J Am Chem Soc **123**, 11807-11808
- [2] Seitsonen, A P; Over, H; 2002 : *Ruthenium dioxide, a versatile oxidation catalyst: First principle analysis*, in: Proceedings of the Conference on High Performance Computing in Science and Engineering, Springer, Berlin, pp. 171-180
- [3] Over, H; Seitsonen, A; 2003 : *Oxidation of metal surfaces*. Science **297**, 2003-2004
- [4] Over, H; Knapp, M; Lundgren, E; Seitsonen, A P; Schmid, M; Varga, P; 2004 : *Visualisation of atomic processes on ruthenium dioxide using scanning tunnelling microscopy*, ChemPhysChem **5**, 167-174 (Minireview)
- [5] For a full list of publications achieved in LRZ/Hitachi please refer to the web pages listed below.

Links

<http://www.chemie.uni-giessen.de/home/Over/>

<http://www.iki.fi/~apsi/Science/Projects/RuO2/>

Density Functional Investigations of Complex Chemical Systems

Research Institution:

Fachgebiet Theoretische Chemie, Technische Universität München

Research Area:

Theoretical Chemistry
Computational Chemistry

Principal Investigators:

Prof. Dr. N. Rösch, Dr. Sven Krüger

Researchers:

Dr. Zhao-Xu Chen, Dr. Parawan Chuichay, Dr. Ramesh Deka, Alexander Genest, Dr. Chan Inntam, Dr. Grzegorz Jezierski, Alena Kremleva, Dr. Kok-Hwa Lim, Dr. Alexey Matveev, Amjad Basha Mohammad, Dr. Lyudmila Moskaleva, Dr. Valdimir Nasluzov, Dr. Konstantin Neyman, Shyama Ray, Dr. Florian Schlosser, Dr. Aleksey Shor, Dr. Elena Ivanova Shor, Dr. Katcharin Siriwong, Egor Vladimirov, Mathias Winkler, Dr. Ilya Yudanov

Abstract

Modern density functional (DF) methods as implemented in the parallel program PARAGAUSS have been applied to determine the geometric and the electronic structure of complex chemical systems. The studies focused on transition metal species at oxide surfaces, problems of heterogeneous catalysis, and the chemistry of actinide complexes in solution and at mineral surfaces. In this report we discuss aspects of chemical complexity beyond the pure

size of a molecular system and how they affect the computational requirements of such modeling. Examples will be drawn from our recent work, carried out on the Hitachi SR8000 at the Leibniz Rechenzentrum München

Complexity in Chemistry

Envisaging complexity in chemistry, one commonly thinks of large and complicated molecules of biochemistry, like enzymes or DNA, or composite materials in technology or more involved classes of minerals. This notion is mainly concerned with compositional and structural complexity of materials or pure size of molecules. Another important example of chemical complexity are systems comprising a variety of molecules and reactions that are taking place between them. Again such systems are common in biochemistry, like the chemistry of cells, but also in the geosphere, e.g. in soils or in the weathering zone of rocks.

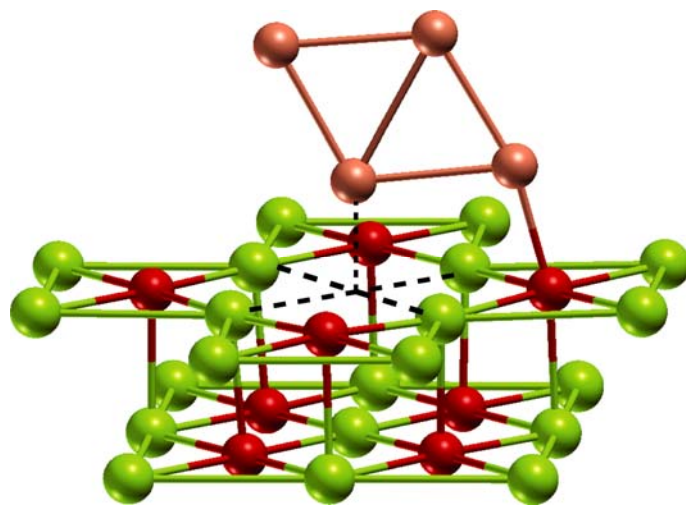


Fig. 1: Cluster model of a Cu_4 particle adsorbed at an oxygen vacancy at the $\text{MgO}(001)$ surface.

Heterogeneous catalysis provides many technologically important examples. In addition to the catalytically active material, such systems comprise a support as well as a mixture of reactants, intermediate species, and products. The interaction of all these components leads to a complex chemical system, structurally as well as with respect to reaction paths and dynamics. Another class of complex chemical systems, often overlooked, are molecules or materials including heavy transition metal or actinide elements.

Here, the complexity results from many chemically “active” electrons in the valence shell. This leads to an increased chemical variability of these elements, which is manifest in several accessible oxidation states, many close lying electronic states, magnetic phenomena, complex spectral signatures, and other peculiarities. Computational modelling of compounds of such elements, with emphasis on heterogeneous catalysis and environmental chemistry, was a focus area of our project. However, biophysical problems have also been treated.

Computational approaches to electronically complex chemical systems

Many properties of elementary chemical systems like hydrocarbons, which are mainly determined by covalent bonding, can nowadays be accurately calculated with readily available methods. The computational effort increases with molecular size, but even species with 100 (light) atoms can reliably be treated on a PC. This is different for systems involving heavy elements.

First of all, heavy element compounds are more cumbersome due to the large number of electrons. Their properties often depend crucially on “correlation” effects in the electron-electron interaction. An accurate treatment of electron correlation, particularly important for elements with many valence electrons like transition metals and actinides, considerably increases the computational effort. Starting from the second row of transition metals, also relativistic effects become noticeable as electrons close to the atomic nucleus move sufficiently fast. Thus, the common quantum mechanical approach based on the Schrödinger equation has to be replaced by many-electron methods based on the fundamental equation of relativistic quantum mechanics, the Dirac equation. We developed such methods in the framework of density functional theory. At such a level, small molecules with one or two heavy atoms still can be treated on a PC, more involved systems of current interest require high-performance computing facilities. These are nowadays not provided by fast processors, but mainly by large ensembles of processors.

An efficient use of this architectures implies a suitable partitioning of the problem and parallel solution of many tasks. The following examples will provide an impression of typical problems in modern computational chemistry. They have

been computed with our density functional software ParaGauss for parallel computers at the Hitachi SR8000 of Leibniz Rechenzentrum München

Examples: Heterogeneous Catalysts and Actinide Complexes in the Environment

Small transition metal clusters, i. e. particles consisting of few atoms up to the size of a several nanometers, are of special interest due to their catalytic abilities. As these particles are very reactive, they are stabilized at a solid support. Computational modeling of heterogeneous catalysis involves the particles itself, their binding to the support (often an oxide), as well as the interaction with reactants, intermediate species and products. Thus, a complex chemical system with many mutually interacting components has to be modeled. One strategy for describing a single metal particle deposited on a substrate treats the particle and its intimate surrounding at an accurate quantum mechanical level (Fig. 1) while the distant environment of the substrate surface is represented by a more approximate method. For such an “embedding” of a quantum mechanical system, we developed an approach where distant surface regions are treated as elastically deformable solid, composed of polarizable ions. This type of modeling of the environment of the particle of chemical interest accounts for the effect of the long-range electrostatic fields present at oxide surfaces and admits a relaxation of the substrate in response to the interaction with the metal particle. With such models, we calculated the interaction of transition metal atoms and small particles with well ordered as well as defective oxide surfaces. In agreement with experiment we were able to show that metal particles bind preferentially to oxygen vacancies. The chemical properties of small supported clusters are affected by the substrate and vary considerably with particle size. In this way, one can also describe their growth mechanism at oxide surfaces.

Another active area of our research is the computational modeling of actinide complexation in solution. The study of the complexation of actinide ions by various inorganic and organic species present in natural waters or at mineral surfaces is crucial in environmental chemistry to understand the chemical state as well as the distribution of actinides in nature. It is not sufficient to calculate the interaction with complexing ligands, like carbonates, hydroxides or vari-

ous functional groups present in natural organic matter; one has to treat also the interaction with water molecules of the solvation environment. As water molecules of the first shell around an actinide ion interact chemically like other ligands, they have to be treated explicitly and quantum mechanically. More distant water molecules can be represented at a simpler level, e.g. using a force field. To account for long-range polarization of the solution, the complex together with explicitly treated water molecules is immersed in a polarizable continuum model which reacts to changes of structure and charge distribution in the complex. With such a modeling, we studied complexes of uranyl UO_2^{2+} with small organic acids and alcohols. These ligands also serve as models of functional groups of larger natural organic species like humic substances. Our calculations of bond distances in these complexes lead to a new interpretation of previous structure determinations by X-ray absorption fine structure. Spectroscopically observed changes of distances between uranyl and its ligands have previously been assigned to different complex shapes. Our calculations showed that the number of ligands of a uranyl ion is more important. As consequence, we were able to rationalize also experimental results for geometrical parameters of uranyl complexes with humic acids.

Links

<http://www.theochem.tu-muenchen.de>

References

- [1] Rösch, N., Matveev, A. V., Nasluzov, V. A., Neyman, K. M., Moskaleva, L. V, and Krüger, S., 2004: Quantum Chemistry with the Douglas-Kroll-Hess Approach to Relativistic Density Functional Theory: Efficient Methods for Molecules and Materials, in: Relativistic Electronic Structure Theory - Applications, Schwerdtfeger, P. (Ed.), Theoretical and Computational Chemistry Series, Vol.14, Elsevier, Amsterdam, 2004, 656-722.
- [2] Rösch, N., Nasluzov, V. A., Neyman, K. M., Pacchioni, G. , and Vayssilov, G. N., 2004: Supported Metal Species and Adsorption Complexes on Metal Oxides and in Zeolites: Density Functional Cluster Model Studies, in: Computational Material Science, Leszczynski, J. (Ed.), Theoretical and Computational Chemistry Series, Vol. 15, Elsevier, Amsterdam, 367-450.
- [3] Schlosser, F, Krüger, S., and Rösch, N., 2006: A Density Functional Study of Uranyl Monocarboxylates, *Inorg. Chem.* 45, 1480-1490

Project Partners:

Institute of Chemistry and Chemical Technology, Krasnojarsk; Dipartimento di Scienza dei Materiali, Università degli Studi di Milano-Bicocca; Departament de Química Física, Universitat de Barzelona; Faculty of Chemistry, University of Sofia; Department of Chemical Engineering, University of California at Davis; Fritz-Haber Institut, Berlin; Institut für Physikalische und Theoretische Chemie, Universität Nürnberg-Erlangen

Theoretical Studies of Structures of Vanadate Complexes in Aqueous Solution

Research Institution:

Max-Planck-Institut für Kohlenforschung

Research Area:

Computational Chemistry

Principal Investigator:

Dr. Michael Bühl

Researchers:

Dr. Michael Bühl, Dr. Rachel Schurhammer, Dr. Petra Imhof

Abstract

The Car-Parrinello Molecular-Dynamics method was applied to study structures and properties of vanadium complexes. For a peroxo-imidazol complex, a biomimetic model for haloperoxidases, a plausible catalytic cycle for olefin epoxidation was studied computationally. Several intermediates in this cycle have been characterized computationally, both in the gas phase and in aqueous solution, and the rate-limiting step has been identified. In order to obtain a better reference value for ^{51}V NMR chemical shift computations, the standard, VOCl_3 , which had only been computed in the gas phase so far, was modeled as the neat liquid used in the experiments.

Introduction

Vanadium-dependent haloperoxidases are a class of enzymes used by marine organisms to oxidize chloride or bromide into ClO or BrO ions, which are then employed for subsequent functionalization of various substrates. In vitro, these enzymes also catalyze other oxygen-transfer reactions, making them potentially interesting for synthetic purposes.

The imidazole-containing peroxo complex **1** (see left-hand side of Fig. 1) had been proposed as a structural model for these peroxidases, as it contains a similar ligand environment about vanadium. We have become interested to probe with computational methods if compounds derived from **1** could also be functional enzyme models, that is, if they could be used as oxygen-transfer catalysts. As an attractive synthetic application we investigated their potential use in olefin epoxidation with the “green” (environmentally benign) oxidant H_2O_2 . We also computed the principal characteristic of a particularly useful spectroscopic method, ^{51}V NMR spectroscopy, and the potential use of its key parameter to identify potent catalysts.

Results

We have computed several possible catalytic cycles with the modern tools of density functional theory (DFT), and have identified oxygen transfer from the catalyst **1** to the model substrate ethylene as the rate-determining step (that is, the one with the highest activation barrier), see right-hand side of Fig. 1 for a plot of the corresponding transition state (Bühl 2004a). When probing computationally how this barrier can be tuned by replacing the imidazole ligand with other N-donors, it turned out that deprotonation of that ligand at the free NH group should be particularly beneficial. An increase of the catalytic activity is also predicted when this NH moiety is involved in a strong hydrogen bridge, for instance to a carboxylate group. Interestingly, such a structural motif is also found in the native enzyme, and may thus be instrumental for its activity.

According to DFT-based molecular dynamics simulations, the imidazole group in **1** is quite flexible and can show large torsional amplitudes or even free rotation about the V-N bond. This can have a noticeable effect on the computed ^{51}V chemical shift, a key NMR spectroscopic parameter of this species. An even stronger impact

on this property is exerted by the V-N distance, which is indicated to decrease significantly upon going from the gas phase into aqueous solution.

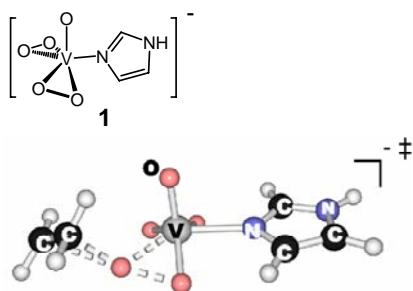


Fig. 1 : Left: Schematic structure of complex **1**; right: Transition state for ethylene epoxidation, as obtained from density functional computations.

A small systematic error is apparent for the theoretical ^{51}V chemical shifts when they are referenced to gaseous VOCl_3 , a deviation that is not improved when the latter compound is modeled as the bulk liquid (Bühl 2004b) that is used experimentally.

Conclusions

We have presented computational evidence that complexes derived from model compound **1** could be functional mimics of haloperoxidases, that is, they could be active catalysts for oxygen-transfer reactions such as olefin epoxidation. These predictions can be tested experimentally. Conceptually, the combination of molecular dynamics simulations and NMR chemical shift calculations presents itself as a promising computational tool to study structures and properties of transition metal complexes under realistic conditions, that is, at ambient temperature and in solution.

References

- [1] Bühl, M., Schurhammer, R., and Imhof, P., 2004a: Peroxovanadate Imidazole Complexes as Catalysts for Olefin Epoxidation: Density Functional Study of Dynamics, ^{51}V NMR Chemical Shifts, and Mechanism. *J. Am. Chem. Soc.* 126, 3310-3320.
- [2] Bühl, M., Schurhammer, R., and Imhof, P., 2004b: Theoretical Studies of Vanadium Complexes: Reactivities and ^{51}V NMR Chemical Shifts in Solution. in: *High Performance Computing in Science and Engineering, Munich 2004* (Eds.: Wagner, S., Hanke, W., Bode, A., and Durst, F.), Springer Verlag, Berlin, pp.189-198.

Links

http://www.mpi-muelheim.mpg.de/mpikofo_buehl.html

Polyoxometallates

Research Institution:

Theoretische Chemie, Fakultät für Chemie, Universität Bielefeld

Research Areas:

Computational Chemistry
Molecular Dynamics

Principal Investigator:

Priv.-Doz. Dr. Dirk Andrae

Researchers:

Dipl.-Chem. Ralf Brodbeck
Priv.-Doz. Dr. Dirk Andrae

Abstract

Quantum chemical methods have been applied to calculate the molecular structure and properties of a series of molybdenum and tungsten polyoxometallates. These were of the Lindqvist, Keggin, Wells–Dawson, and Preyssler type, respectively. Force field parameters for tungsten polyoxometallates were derived from the obtained data, compatible with the AMBER force field. Molecular dynamics simulations, which are based on classical mechanics, were then performed for tungsten polyoxometallates encapsulated with dendrimeric amphiphilic cations, in trichloromethane as solvent. The term ‘dendrzymes’ has been introduced for such dendrimer-encapsulated polyoxometallates, since they may serve in the future as homogeneous redox catalysts with enzyme-like substrate specificity, regioselectivity and stereospecificity.

Quantum chemical study of polyoxometallates

Many chemical and physical properties of molecular systems can be understood from their electron density distributions. Nowadays, good to excellent approximations to such distributions can be calculated with various software tools, all of which apply quantum mechanical methods. In *ab initio* methods, an approximate wave function is calculated, from which the electron density distribution is easily obtained, whereas methods relying on density functional theory (DFT) give this distribution in a more direct way. Both kinds of approach can be combined with effective core potentials, so that the atomic cores (and a corresponding number of electrons) can be removed from the explicit calculation, and all efforts can thus be focused on the determination of only a valence part of the electron density distribution. In this project, density functional methods were applied to calculate properties of molybdenum and tungsten polyoxometallates of the following types (the highest possible symmetry group is indicated in parentheses; see also figure 1):

the Lindqvist type $[(O)M_6O_{18}]^{2-}$ (O_h ; $M = Mo$ or W), the α -Keggin type $[(XO_4)M_{12}O_{36}]^{q-}$ (T_d ; $M = Mo$ or W ; $q = 3$ for $X = P$, or $q = 6$ for $X = Zn$), the α -Wells–Dawson type $[(XO_4)_2M_{18}O_{54}]^{6-}$ (D_{3h} ; $M = Mo$ or W ; $X = P$), and the Preyssler type $[(XO_4)_5M_{30}O_{90}]^{15-}$ (D_{5h} ; $M = W$; $X = P$). All species of these types can be understood formally as being built up from central anions (determining the total charge) surrounded by a neutral polyoxometallate cage, but this point of view has no physical basis. Direct results from the quantum chemical calculations are, e.g., optimized molecular structures (also known as equilibrium structures, i.e. the spatial arrangement of the atomic nuclei giving the lowest value for the total energy) together with the associated electron density distribution. From these results, other quantities, like partial atomic charges (located at the positions of the atomic nuclei) or the molecular electrostatic potential, have been calculated. Molecular structures and molecular electrostatic potentials served as ingredients for the next step, the derivation of force field parameters.

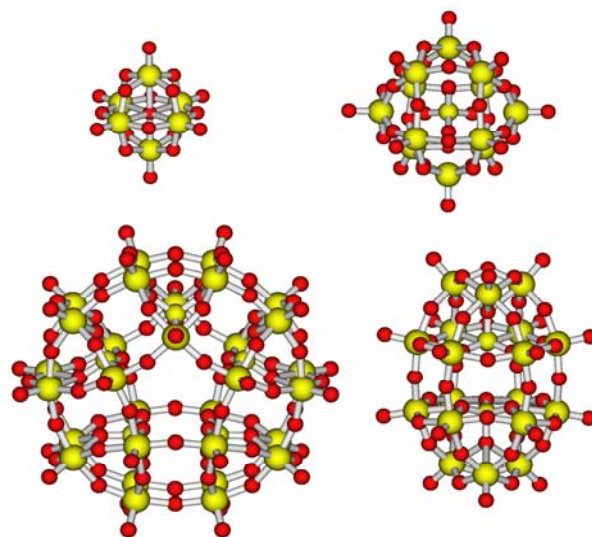


Fig. 1: Molecular structures of the studied polyoxometallate types (clockwise, from the upper left corner: Lindqvist, α -Keggin, α -Wells–Dawson, and Preyssler type; oxygen in red, other atoms in yellow).

Derivation of force field parameters for polyoxotungstates

A force field for molecular dynamics (MD) simulations represents the potential energy of a molecular system as a sum of classical terms for the various degrees of freedom (changes of bond lengths, bond angles, etc.), and terms for van-der-Waals and electrostatic interactions. Every term depends on some empirical parameters, like force constants and equilibrium values of coordinates, which must be de-

terminated before the force field can be used. This has to be done for all atom types, pairs of atom types, etc., involved in the force field to be used. In this project, the so-called 'generalized AMBER force field' (GAFF) was to be used in MD simulations of dendrimer-encapsulated α -Keggin ions ($M = W$) in trichloromethane solution (see below), since parameters for the organic molecules, the dendrimers and the solvent molecules, are already available. Hence, force field parameters for the α -Keggin ions were required. These were generated from the results previously obtained for the series of polyoxotungstates, so that equilibrium structures, molecular electrostatic potentials, and normal mode frequencies from the force field are in good to reasonable agreement with the corresponding results from quantum chemical calculations. During this process, emphasis was laid on the α -Keggin type of ions, since it is involved in the final part of this work. But the other polyoxometallates (Lindqvist, Wells–Dawson, and Preyssler) were nevertheless kept in the set, in the hope to make the resulting force field more robust and perhaps more widely applicable (within the series of polyoxotungstates).

Molecular dynamics simulations of dendrzyme model systems

From the previous part, a complete set of parameters (compatible with the GAFF format) for all required atom types was at hand. This set was used now in the last part of this project for MD simulations of dendrzyme model systems. Two of the model systems studied in this project are presented in figure 2 (hydrogen atoms are not shown): The α -Keggin ion $[(\text{PO}_4)\text{W}_{12}\text{O}_{36}]^{3-}$ surrounded by three dendrimers derived from the bis(3,5-dimethoxybenzyl)dimethylammonium ion, $[\text{C}_{52}\text{H}_{60}\text{NO}_{12}]^+$ (upper part), and the α -Keggin ion $[(\text{ZnO}_4)\text{W}_{12}\text{O}_{36}]^{6-}$ surrounded by six *N*-methyl-3,5-bis(3,5-di-*tert*-butylphenyl)pyridinium ions, $[\text{C}_{34}\text{H}_{48}\text{N}]^+$ (lower part). The MD simulations were done for trichloromethane solutions of these ion clusters (with concentrations about 10 mmol/l in the former case and 20 mmol/l in the latter case, respectively). An *NVE* ensemble with periodic boundary conditions was imposed (keeping constant the particle number, the cell volume and the total energy). Such MD simulations, where the content of the cell (ion cluster and solvens molecules in our case) is allowed to evolve according to the laws of classical mechanics, primarily yield a set of positions in space as function of time ('trajectories') for every atom in the simulation cell. Methods from statistical mechanics and statistical thermodynamics can be used then to analyze these trajectories. An enzyme-like substrate specificity, that has already been seen in experiments with dendrzyme model systems based on redox-active polyoxometallates, can partially be

supported by our results: Whether a substrate is able to approach the central polyoxometallate or not depends (i) on the fraction of polyoxometallate surface covered by the dendrimers, and (ii) on the spatial requirements of the dendrimer molecules (steric hindrance of substrate access).

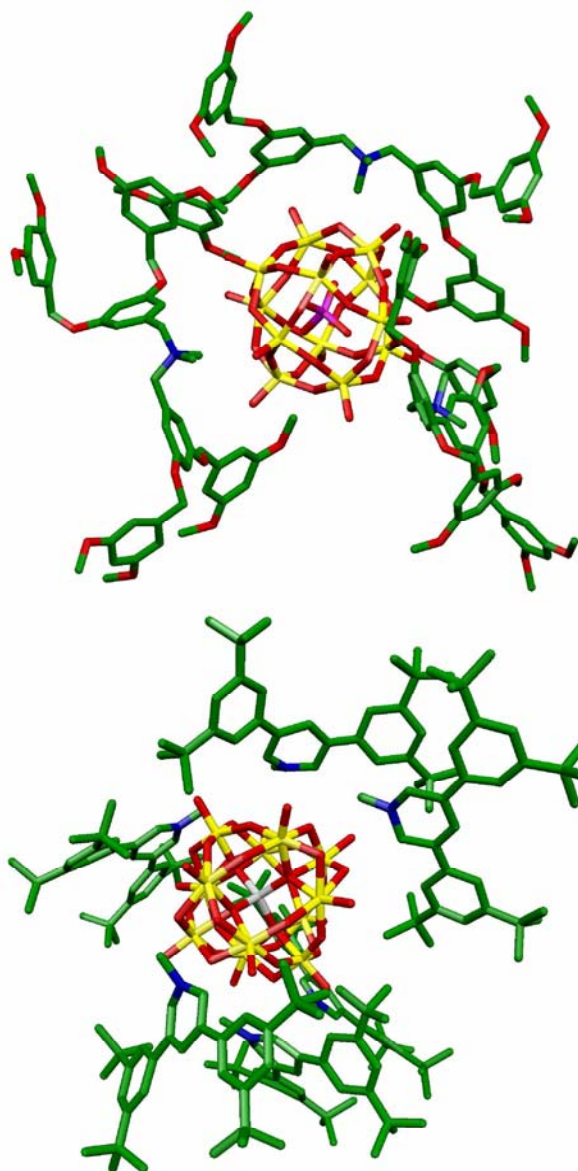


Fig. 2: Molecular structures of dendrimer-encapsulated α -Keggin ions (from snapshots of the molecular dynamics simulations; solvens molecules and hydrogen atoms of the dendrimers are not shown; see text for further details).

References

Volkmer, D. *et al.* (2002) *J. Am. Chem. Soc.* 124, 10489–10496

Project Partners:

Prof. Dr. Dirk Volkmer (Ulm)

Prof. Dr. Bernt Krebs (Münster)

Priv.-Doz. Dr. Dirk G. Kurth (Potsdam)